UNIVERSITY OF PADUA

ICEA DEPARTMENT

MASTER SCIENCE DEGREE

IN

ENVIRONMENTAL ENGINEERING

Laboratory experiments on the saltwater intrusion process

SUPERVISOR:
Prof. Paolo Salandin

COADVISORS:
Prof. Roberta Bertani
Dr. Elena Crestani
Dr. Enrica Belluco

STUDENT:
Erika Bertorelle

Academic year 2013/14

Desidero ringraziare tutti quelli che mi hanno aiutata a raggiungere questo traguardo importante che è la laurea.

Grazie al Prof. Salandin, che con la passione per il suo lavoro in questi anni mi ha insegnato molto di più delle nozioni.

Grazie alla Prof. Bertani, ad Elena ed Enrica, per l'aiuto costante, preciso e puntuale, e anche per avere reso piacevoli le giornate in laboratorio.

Grazie alla mamma e al papà per avermi dato la possibilità di proseguire gli studi. Grazie a mia sorella e alla mia nipotina per avermi sempre supportata e a volte sopportata nei momenti difficili.

Grazie alle mie colleghe e colleghi, alla Cinzia soprattutto, che mi aiuta sempre senza chiedermi mai niente in cambio.

Grazie a tutti i miei amici e a chi mi vuole bene, a Isabella in particolare, con cui ho condiviso i momenti più belli e più brutti della vita.

A tutte queste persone voglio dedicare il mio lavoro, e al mio migliore amico, che anche se non c'è più so esattamente cosa mi direbbe in questo momento: "Eri sono orgoglioso di te".

Summary

Saltwater intrusion is the movement of saline water into freshwater aquifers, which can lead to contamination of drinking water resources. Salt is the most common pollutant of fresh groundwater that affects many aquifers in the Mediterranean coasts, as well as many other areas including North Africa, the Middle East, China, Mexico, the Atlantic and Gulf Coasts of the United States, and Southern California.

This contamination process mainly results from the high demand of water resources during the summer months. Once saltwater intrusion has begun, the continued irrigation of crops using water with high salt content produces a progressively higher residue of salt in soil, that is not eliminated when aquifers are recharged and which helps to accelerate the desertification of soils.

The aim of this work is to reproduce an experimental model representing the terminal part of an idealized aquifer, where the material is uniform. The device consists of a sand-box suitable designed, through which it will be possible to evaluate the rising of the salt wedge and the efficiency of mobile barrages in limiting it, as well as the effects of a freshwater recharge by infiltration.

Preliminary experimental tests were developed in order to point out the best type of tracer to visualize saltwater intrusion in the sand-box device. Although different measurement techniques will be employed, a special attention was devoted in the sampling of saltwater and in the colorimetric analysis. It was verified that conducibilities and absorbances have the same trend for the chosen dye. Other tests were done to verify the influence of different types of needles in the upconing of saltwater. Moreover it was analyzed the possibility to dilute samples in order to reduce the sampling volume and, consequentely, upconing.

The location of the saltwater toe and the thickness of the mixing zone under different conditions were preliminary reproduced by the finite elements, density dependent flow and transport code SUTRA (Voss and Provost, 2010) [48]. The numerical results obtained showed the dependence of saltwater intrusion from dispersion and hydraulic conductivity, revealed the pumping rate at which hypotetically upconing occurs, showed that the best position for a subsurface barrier in order to limit saltwater rise is near the coast rather than far from it, the effects of a freshwater recharge and of a non-uniform soil.

A 24 hours experiment in the sand-box facility was finally completed and the numerical results were compared with the physical ones.

Contents

List of Tables

List of Figures

Part I

Saltwater intrusion process

Chapter 1

Introduction

Saline water is the most common pollutant in fresh groundwater. Because saltwater has a higher mineral content than freshwater, it is denser and has a higher water pressure. As a result, saltwater can push inland beneath freshwater. Intrusion of saline water occurs where saline water displaces or mixes with freshwater in an aquifer.

The boundary between saltwater and freshwater is not distinct; the zone of dispersion and molecular diffusion, transition zone, or saltwater interface is brackish with saltwater and freshwater mixing. Mixing by dispersion is caused by spatial variations (heterogeneities) in the geologic structure and the hydraulic properties of an aquifer and by dynamic forces that operate over a range of time scales, including daily fluctuations in tide stages, seasonal and annual variations in groundwater recharge rates, and long-term changes in sea-level position. These dynamic forces cause the freshwater and saltwater zones to move seaward at times and landward at times.

The mechanisms responsible for saline water intrusion generally fall into three categories (Todd, 1976) [45].

Groundwater extraction is the primary cause of saltwater intrusion. Under baseline conditions, the inland extent of saltwater is limited by higher pressure exerted by the freshwater column, owing to its higher elevation. Groundwater extraction can lower the level of the freshwater table, reducing the pressure exerted by the freshwater column and allowing denser saline water to displace fresh water. This situation commonly occurs in coastal aquifers in hydraulic continuity with the sea when pumping of wells disturbs the natural hydrodynamic balance.

The second category concerns the alteration of natural barriers that separate fresh and saline waters. An example would be the construction of navigation channels or agricultural and drainage channels, which provide conduits for saltwater to move inland, and sea level rise.

The third mechanism deals with the subsurface disposal of waste saline water, such as into disposal wells, landfills and other waste repositories.

Saltwater intrusion can also be worsened by extreme meteorological events.

1.1 Chemical characteristics and sources of saltwater

All water contains dissolved chemical materials called "salts". When the concentration of these dissolved materials becomes great, the water is referred to as "saltwater". This term can be confusing because it can mean different things to different people. As a result, different classification methods have been developed to differentiate between freshwater and saltwater

and to define the degree of salinity (that is, the total dissolved-solids concentration) of the water.

With reference to the circular 1262 of the USGS water can be defined as "freshwater" when having a total dissolved-solids concentration of less than 1000 mg/l; waters with a total dissolved-solids concentration greater than 1000 mg/l are considered to be saltwater (or saline). This arbitrary upper limit of freshwater is based on the suitability of the water for human consumption.

Although waters with total dissolved-solids concentrations greater than 1000 mg/l have been used for domestic supply in some areas of the United States where water of lower dissolved-solids concentration is not available, water containing more than 2000 to 3000 mg/l of total dissolved solids is generally too salty to drink (Freeze R. A., Cherry J. A., 1979) [22].

"Brackish waters" can be defined as those having a total dissolved-solids concentration of 1000 to 35000 mg/l. The upper concentration limit for brackish water is set at the approximate concentration of seawater (35 g/l).
Water with a dissolved-solids concentration exceeding that of seawater is called a "brine".

The average concentrations of major dissolved constituents of seawater are reported in Table 1.1 (Chow V. T., 1964) [13].

Table 1.1. Composition of dissolved solids in seawater and amount of major ions of "average" seawater in parts per million

Ion	Percent composition	Amount in $average$ seawater [ppm]
chloride	55.04	18980
sodium	30.61	10556
sulfate	7.68	2649
magnesium	3.69	1727
calcium	1.16	400
potassium	1.10	380
bicarbonate	0.41	140
bromide	0.19	65
boric acid	0.07	26
strontium	0.04	13
others	0.01	2
total	100.00	34483

Two additional characteristics of water that are important in groundwater systems are density and viscosity, both of which are dependent on the type and amount of solutes dissolved in the water. Density is important because it is part of the driving force that defines the direction and rate of fluid movement through a ground-water system; moreover, density and viscosity of water affect the hydraulic transmitting properties (permeability and hydraulic conductivity) of the groundwater system, which influence the rate of fluid movement.

The variation of these and other properties depending on the water salinity are reported in Table 1.2 (Reilly T. E., Goodman A. S., 1985) [41].

Table 1.2. Properties of various concentrations of seawater. Salinity and chorinity are given in parts per thousand

Solute mass fraction [%]	Salinity [ppt]	Chlorinity [ppt]	ρ [kg/m^3]	μ [kg/(m · s)]	ν [m^2/s]
0.00	0.00	0.00	0.9982	1.002	1.004
0.50	4.94	2.72	1.0019	1.010	1.008
1.00	9.92	5.48	1.0057	1.018	1.012
2.00	19.89	11.00	1.0132	1.036	1.022
3.00	29.86	16.53	1.0207	1.057	1.036
3.50	34.84	19.29	1.0245	1.070	1.044
4.00	39.82	22.05	1.0283	1.080	1.050
5.00	49.79	27.57	1.0358	1.103	1.065
10.00	99.63	55.18	1.0738	-	-

Density and concentration are related through the relation reported in Equation 1.1 (Voss C. I., Provost A. M., 2010) [48]

$$\rho = \rho(C) \simeq \rho_0 + \frac{\partial \rho}{\partial C} \cdot (C - C_0) \tag{1.1}$$

where ρ_0 is the base fluid density at base concentration C_0. The factor $\frac{\partial \rho}{\partial C}$ is a constant value of density change with concentration. For mixture of freshwater and seawater at 20 °C, when C is the mass fraction of total dissolved solids, C_0 = 0 and ρ_0 = 998.2 kg/m^3, then the factor $\frac{\partial \rho}{\partial C}$ is approximately 700 [kg(seawater)]^2 / [kg(dissolved solids) · m^3].

A number of other sources can affect coastal groundwater quality (Barlow P. M., 2003) [4]. These sources include:

- **precipitation:** sodium and chloride are the most abundant ions in air masses over the sea. Chloride and sodium concentrations, therefore, are high in air masses near sea coasts but decrease rapidly with increasing distance inland. These airborne salts are delivered to coastal watersheds by precipitation. Chloride concentrations in precipitation, however, are relatively small compared to seawater. Concentrations of sodium and chloride can be increased in soils, shallow surface waters (such as tidal lagoons), and groundwater by evaporation and evapotranspiration;

- **sea-spray accumulation, tides, and storm surges:** they can be local sources that increase groundwater salinity in low-lying coastal areas;

- **entrapped fossil seawater in unflushed parts of an aquifer:** such water either was trapped in sedimentary formations when they were deposited or flowed into the formations during periods of relatively high sea levels when seawater flooded low-lying coastal areas;

- **dissolution of evaporitic deposits such as halite (rock salt), anhydrite, and gypsum;**

- **pollution from various anthropogenic sources including sewage and some industrial effluents, oil- and gas-field brines brought to the land surface during exploration and production, road deicing salts, and return flows of irrigation water.**

The freshwater and saltwater zones within coastal aquifers are separated by the transition zone (sometimes referred to as the zone of dispersion) within which there is mixing between freshwater and saltwater. The transition zone is characterized most commonly by measurements of either the total dissolved-solids concentration or of the chloride concentration of groundwater sampled at observation wells. Although there are no standard practices for defining the transition zone, concentrations of total dissolved solids ranging from about 1000 to 35000 mg/l and of chloride ranging from about 250 to 19000 mg/l are common indicators of the zone (Barlow P. M., 2003) [4].

The Italian Law, with the Legislative Decree 31/2001 (concerning the quality of waters aimed to human consumption), establishes for the chemical constituents and the diffuse microbiological agents the guideline concentrations in order to guarantee a water of optimal quality and the maximum allowed concentrations. For chloride the maximum limit is set equal to 250 mg/l (Legislative Decree 31/2001) [17].

Concerning waters aimed to agriculture use there are not specific dispositions in Italy. Their chemical and physical characteristics to be usable in specific contents are subjected to the disposals of the Legislative Decree 152/2006 [18] ("Testo Unico Ambientale"). An important approach to evaluate the water quality for agricolture is given by FAO [2] that, with a series of dispositions (not Laws), sets the guidelines for interpretation of water quality for irrigation.

1.2 Consequences of saltwater intrusion and some example in Italy

Contamination by salts strongly deteriorates water quality making freshwater unsuitable for human consumption and for irrigation. Even a small concentration of chlorides in fact deteriorates water quality. For this reason saltwater intrusion induces the interruption of water diversion for agricolture. If, when diverted, water has values of salinity greater than 1.5-2 permil, it is dangerous to irrigate (only rice crops can slight tolerate these values of salinity). Other problems can be the interrumption of supply for aqueducts, the salinization of groundwater, the dry-up of coastal areas and desertification of soils.

Figure 1.1. Desertification of soil in the Mediterranean Sea area [55]

These problems could theoretically be solved by desalting. However this is expensive and therefore desalting should only be considered as an ultimate solution in cases where the cheaper conventional groundwater resources are insufficient (Dam J. C. van, 1999) [9].

Moreover a by-product of desalting is brine, that is difficult to dispose off. In fact disposal in fresh surface waters will certainly not be tolerated while transport and discharge into saline surface water as estuaries and seas and injection of the brine into deep aquifers, if feasible and acceptable from the hydrogeological point of view, adds also to the costs.

Even for cooling purposes saline and brackish groundwater is not attractive. First of all salinity might cause damage to the installations, by corrosion and, secondly, the same problems described for brine are encountered for the disposal of saline and brackish water after its use for cooling purposes.

Another activity that can cause serious problems is the control (mostly lowering) of the groundwater table by means of artificial control of the surface water in an area or land drainage. This applies in particular in land reclamation projects. In the case of land reclamation in lagoons, tidal inlets or lakes, the lowering of the water table can even be several meters. Such great lowering over sometimes very large areas must have considerable effect on the regional groundwater flow system and can cause an unfavorable redistribution of fresh, brackish and saline groundwater. Artificial lowering of the groundwater table in an area induces seepage or increase of seepage in that area. The seepage water may be or become brackish or saline.

An interesting example of saltwater intrusion in Italy concerns the Venice watershed. The saltwater contamination process in the Venice watershed between the southern edge of the lagoon of Venice and the Adige River was investigated through hydrogeological and geophysical surveys and a new monitoring network of surface water and shallow groundwater (ISES Network). The results showed that the presence of saline water extends up to 20 km inland from the coast; the depth of the fresh-salt water interface varies from 2 to 30 m below the ground level and exhibits a significant, mainly seasonal, time variation; the bottom of the contaminant plume penetrates from 10 even to 100 m depth in the subsoil (Gasparetto Stori G. et al., 2005) [12].

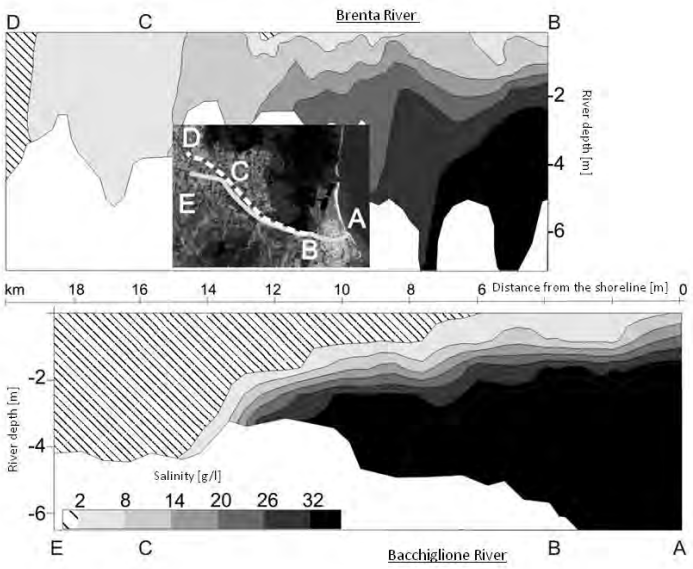

Figure 1.2. Saltwater encroachment along the Brenta and Bacchiglione rivers in Summer 2003: modified from (Gasparetto Stori G. et al., 2005) [12]

Another important case of saltwater intrusion in Italy deals with Po River. The report of the "Consorzio di Bonifica Delta Po-Adige, concerning the construction in the Po River at Porto Tolle (Ro) of a freshwater reservoir to be used for irrigation in periods of emergencies" [16], refers some data for the seawater intrusion in this area. According to this report, streamflows at Pontelagoscuro (Ferrara) between 250 and 300 m^3/s imply the ingression of the saltwedge up to Po della Donzella inlet (moreless 20 km from the coastline) with the consequent impossibility to irrigate Porto Tolle and a part of Ariano Island. For streamflows between 189 and 200 m^3/s the ingression of the salt wedge can reach 30 km from the coastline implying the impossibility to irrigate all Arian Island up to the Romea Road and Porto Viero in the South part of the Po-Polesano collector [16].

Some works have been done to solve the problems, for example the construction of three saltwater barrages respectively at Po della Donzella, Po di Tolle, and Adige outfalls. Another work is the realization of a storage basin in the Volta Vaccari river bend. Here, in the 80's, the "Magistrato per il Po" realized the straightening of the river bend in order to increase the waterfow in Po di Pila River. The old watercourse became suitable to be used as a freshwater reservoir for agriculture use in dry periods.

Figure 1.3. View, from the left bank, of the saltwater barrage at the outfall of Adige River (Bogoni M., 2013) [11]

Figure 1.4. Storage basin realized at Volta Vaccari (Porto Tolle, Ro) [16]

1.3 Control of seawater intrusion

Todd, 1976 [45] summarized several methods to control intrusion that vary widely depending on the source of the saline water, the extent of the intrusion, local geology, water use, and economic factors.

- **Extraction barriers:** this control program is a line of wells that are constructed adjacent to the coast and pumped to form a trough at the ground water level.

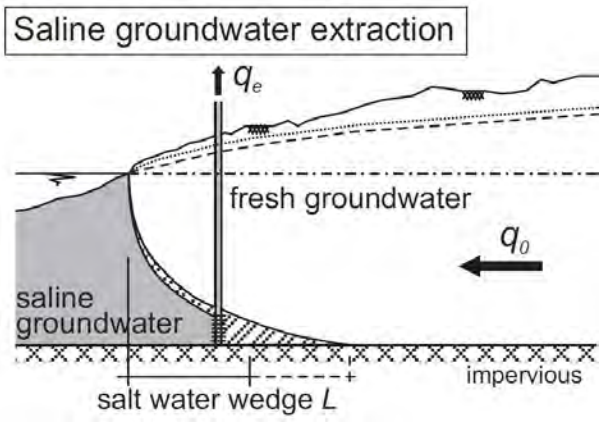

Figure 1.5. Extraction barrier (Gualbert H.P., 2001) [28]

Seawater flows inland from the ocean to the trough, while freshwater within the basin flows seaward toward the trough. The water pumped is brackish and normally is discharged into the sea;

- **Surface and subsurface barriers:** construction of a surface or subsurface barrier parallel to the coast and through the vertical extent of the aquifer can effectively prevent the inflow of seawater into the basin.

Figure 1.6. Saltwater barrage designed on Brenta River [15]

- **Injection barrier:** this method maintains a pressure ridge along the coast by a line of recharging wells. Injected freshwater flows both seaward and landward. High quality imported water is required for recharge into wells. A combination of injection and extraction barriers is feasible; this reduces both recharge and extraction rates but requires a larger number of wells.

- **Modification of pumping pattern:** the pumping pattern disturbs the hydraulic gradient whereby it causes landward migration of seawater. It therefore necessitates that the location of pumping wells be changed/shifted. In a confined groundwater a more inland position of the abstraction works is more favourable than a more seaward position. This is because in inland direction the thickness of the freshwater lens increases, and the danger of upconing of saltwater decreases accordingly.

  A more inland position of the abstraction works allows also for a further inland penetration of the saltwater wedge in its permanent ultimate position. With a further inland position of the salwater wedge, less fresh groundwater will be lost by outflow due to a smaller gradient of the piezometric level of the outflowing fresh groundwater. So, in defining the ultimate position of the salwater wedge, a choice have to be made between a greater rate of continuous and constant abstraction of fresh groundwater with an higher risk of pumping saline water under extreme conditions versus the opposite combination of the two (Bear et. al., 1999) [10].

  In phreatic groundwater in islands and in sand dunes along a coast, the abstraction works should be located at a short distance from the coastline that the largest possible frations of the recharge can be recovered before it is lost by outflow under the coastline. On the other hand this distance should not be too small as the thickness of the freshwater lens decreases towards the coastline, and this thickness must still be great enough under the abstraction works so that, even under extreme stuations of temporary overdraft, no upconing of saltwater will occur. A more inland position of the abstraction works leads however to a smaller volume of fresh groundwater for strategic reserve (Bear et. al., 1999) [10].

- **Aquifer storage and recovery (ASR):** this technique is used successfully in the United States (Barlow et al., 2010) [5]. It is a particular type of artificial recharge whereby freshwater is injected into the aquifer (through a well) during high-supply seasons (winter, spring) and then recovered (pumped to the surface) during low-supply seasons (summer, early fall).

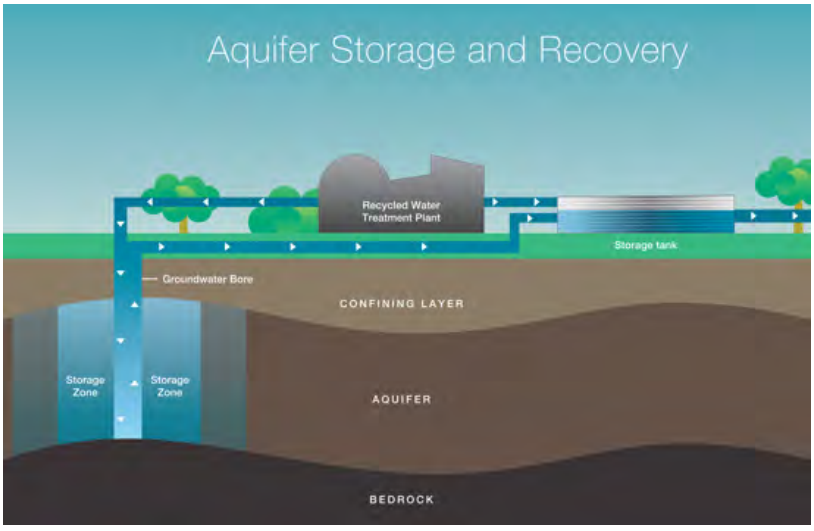

Figure 1.7. Aquifer storage scheme [53]

- **Artificial recharge:** groundwater levels can be raised and maintained by artificial recharge. This necessitates development of a supplemental water source. Artificial

recharge of groundwater is applied for many reasons, such as to increase the sustainable yield, to control the groundwater table or the piezometric level, to increase the volume of fresh groundwater available for emergencies, and/or as a barrier against inflow of saline water. Artificial recharge can be realized by increasing infiltration at the land surface or in surface waters, or by means of recharge wells with well screens in aquifers at any desired depth.

Figure 1.8. Infiltration well for artificial recharge situated at Cornedo Vicentino (Vi) [57]

For the recharge of phreatic groundwater both the techniques can be applied. Confined and semi-confined groundwater in aquifers at some depth an not be recharged from the land surface or surface waters due to high hydraulic resistance between the land and water surface. A special form of artificial recharge is the already mentioned induced recharge, combined with the abstraction of water, where groundwater is abstracted at short distance from rivers.

If the rate of abstraction exceeds the rate of natural flow of groundwater towards the river, inflow of river water is induced, and the abstracted groundwater consists partly of river water. This affects the quality of the abstracted groundwater. In the most downstream reaches of rivers and in estuaries the inflowing groundwater may be brackish or even saline, depending on the tidal regime and on the magnitude of the river flow. This implies a proper treatment after the extraction.

Surface water can be taken from rivers and estuaries and should be transported either by canals or by pipelines. The intakes should be beyond the reach of saltwater intrusion in the river and estuaries, or the estuaries should be provided with dams and sluices. The quality of the water at the source should satisfy certain standards. Such standards depend mainly on the use of the water after recharge and subsequent recovery but also the requirements for transport and consequent recharge. These two latter aspects in itself may already require some pretreatment. This hold in particular for recharge by means of recharge wells, in order to avoid clogging of these wells. Apart from pretreatment of the water for recharge, the rate of recharge per well should be limited. Despite pre-treatment of the water the capacity of the recharge wells decreases during this operation. Therefore regeneration of the reharge wells is needed from time to time. The longer the residence time of the infiltrated water the greater also the smoothing out of the fluctuations in the quality of the infiltrated water. Fluctuations can even more be flattened by applying variable distances between the lines of recharge works and abstraction works respectively.

Another consideration is whether to locate a line of abstraction works, in between two lines of recharge works or, the other way round, the line of recharge works surrounded by two lines or a more or less elliptic configuration of abstraction works. The latter

layout has the advantage that the phreatic groundwater tables will be higher and, accordingly, the depths to the interface greater. This implies the availability of a larger volume of freshwater for emergencies. Moreover, due to the greater thickness the residence times will be somewhat longer and somewhat more spread out. The regime of desired or accepted groundwater tables should not be judged in relation to the topography and the ecological features of the terrain. Depending on the variation of the water requirements over time, as determined by the climate and weather, and on the availability of water of good quality for artificial recharge, the actual rates of abstraction and artificial recharge of groundwater may vary with time, periodically and incidentally. So the volume of fresh groundwater will also vary with time, and the boundary between fresh and saline groundwater will not only move up and down, but also the transition between fresh and saline will become less sharp due to the effects of dispersion and retardations.

Attention should also be paid to the question where the displaced brackish and saline groundwater goes and what effects it has on the surroundings. So, for instance, increased seepage of brackish or saline groundwater in adjacent areas will generally not be appreciated. Therefore the effects of the combined system of abstraction and recharge in the wider surroundings must be forseen, predicted and judged before undertaking any artificial recharge project (Bear et. al., 1999) [10].

- **ADR:** an optimization methology called ADR to control seawater intrusion process was also proposed by Abd-Elhamid and Javadi (2011) [32]. It consists on three phases: the first one (A) is the abstraction of the brackish water; the second one (D) is the desalinization of the brackish water using a reverse-osmosis membrane; the third phase (R) consists to recharge the aquifer with the desalinated brackish water. ADR methodology is considered an economical solution and has a low environmental impact, because desalinizating brackish water using RO treatment process involves lower energy consumption, lower cost, lower pollution and carbon emissions as compared with conventional methods for saltwater desalination and waste water treatment. It also provides fresh water for recharge using the treated brackish water and proposes a solution for the disposal of brine by increasing the outfall to the shore. It is also an efficient method to control seawater intrusion because it increases the volume of freshwater and decreases the volume of seawater, while considering economical aspects, environmental impacts and sustainable development of water resource (Alshawabkeh et. al., 2008) [3].

Chapter 2

Analytical solutions for steady saltwater-freshwater interface

2.1 The sharp-interface approximation

Coastal aquifers have, in general, an hydraulic gradient towards the sea, that is the recipient of their excess fresh water (replenishment minus pumpage). The presence of seawater in the aquifer formation under the sea bottom involves a zone of contact between the lighter freshwater flowing to the sea, and the denser underlying saltwater. Freshwater and saltwater are miscible fluids and therefore the zone of contact between them takes the form of a transition zone caused by hydrodinamic dispersion. Across this zone the density of the mixed water varies from that of freshwater to that of seawater. In many cases of pratical interest, the transition zone in the case of miscible fluids is narrow relative to the size of the flow domain such that for practical purposes a fictitious sharp-interface (a continuous surface completely separating the two fluids) may be assumed. However an abrupt interface between two fluids in a macroscopic sense cannot exist (it is a situation which is possible only under laboratory conditions). Although this is clearly an approximate approach it appreciably simplifies the treatment of two-fluid problems.

2.2 The Ghyben-Herzberg solution

The Ghyben-Herzberg relation is the most important analytical model to describe the saltwater intrusion problem. It states that, under hydrostatic conditions, the weight of a unit column of freshwater extending from the water table to the interface is balanced by a unit column of saltwater extending from sea level to the same depth as the point on the interface, as shown in Figure 2.1. This implies a static equilibrium and hydrostatic pressure distribution in the freshwater region with stationary seawater. Mathematically this could be expressed as:

$$\rho_s H g = \rho_f (H + h) g \tag{2.1}$$

from which it is possible to obtain the Ghyben-Herzberg equation:

$$h = \frac{\rho_s - \rho_f}{\rho_f} H \tag{2.2}$$

As shown in Figure 2.2, h is the elevation difference between the phreatic surface and the sea level, while H is the elevation difference between the sea level and the seawater-freshwater interface at a given point. ρ_s and ρ_f are the density of the seawater and freshwater respectively.

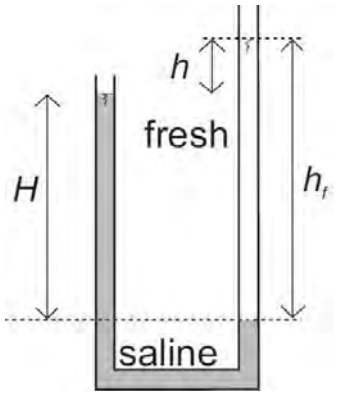

Figure 2.1. Hydrostatic balance between freshwater and saline water (Gualbert H.P., 1959) [28]

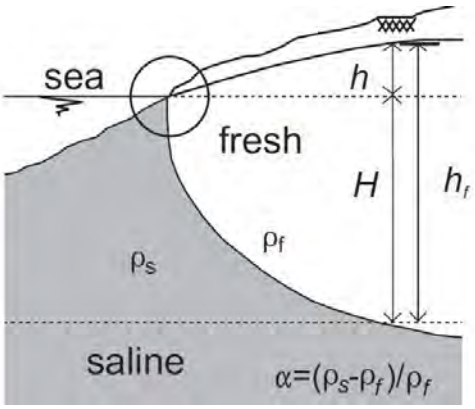

Figure 2.2. Fresh and saline groundwater interaction in an unconfined coastal aquifer (Gualbert H.P., 1959) [28]

For typical seawater conditions, let ρ_s equal to 1.025 g/cm^3 and ρ_f equal to 1 g/cm^3, the equation becomes:

$$H = 40h \tag{2.3}$$

that shows that the change of seawater thickness in the aquifer depends on the change of freshwater thickness. If the water table in a unconfined coastal aquifer is lowered of 1 m, then the saltwater interface will rise 40 m. Where the flow is nearly horizontal, the Ghyben-Herzberg relation gives satisfactory results. Only near the shoreline, where vertical flow components become pronunced, significant errors in the position of the interface occur.
For confined aquifers, the above derivation can also be applied by replacing the water table by the piezometric surface. It is important to note from the Ghyben-Herzberg relation that fresh-salt water equilibrium requires that the water table, or piezometric surface, lies above the sea level and slopes downward toward the sea. Without these conditions, seawater will advance directly inland.

The Ghyben-Herzberg relation has been generalized by Lusczynski (1961) [34] for situations where the underlying saline water is in motion with heads above or below sea level. The result for non-equilibrium conditions has the form:

$$z = \frac{\rho_f}{\rho_s - \rho_f} h_f - \frac{\rho_f}{\rho_s - \rho_f} h_s \tag{2.4}$$

where h_f is the altitude of the water level in a well filled with freshwater of density ρ_f and terminated at depth z, while h_s is the altitude of the water level in a well fixed with saline water of density ρ_s, and also terminated at depth z. When $h_s = 0$, the saline water is in equilibrium with the sea, and equation 2.4 reduces to 2.2.

It is important to point out that the Ghyben-Herzberg solution assumes that sea water remains static and its pressure remains hydrostatic along the vertical. This is true if saltwater does not mix with freshwater, so that the two fluids are separated by a sharp freshwater-seawater interface and flow is in steady-state. The sharp-interface assumption neglects mixing of fresh water and seawater which is one of the the most distinctive features of seawater intrusion and its dynamics. Gingerich and Voss (2002) [24] demonstrated that the Ghyben-Herzberg depth is not a good predictor of the depth of potable water because of its failure to deal effectively with the dynamic response of the mixing zone to changes in pumping or rapid recharge. Seawater is dispersed across the interface and subsequently is returned to the sea by freshwater discharge, thus forming a convection cell (Hilton H. et al., 1964) [31]. The loss of seawater energy associated with this flux causes the interface to recede seaward. Therefore, sharp-interface approximations are conservative and they overestimate saltwater penetration and underestimate sustainable pumping rates.

Pool and Carrera (2011) [39] investigated the error introduced by adopting the sharp-interface approximation as well as the inpact on seawater intrusion. They conclude that an accurate result can be obtained by using an empirically derived correction factor that depends only on the transverse dispersivity α_T and the aquifer thickness b':

$$\epsilon^* = \epsilon\left[1 - \left(\frac{\alpha_T}{b'}\right)^{1/6}\right] \tag{2.5}$$

where $\epsilon = \frac{\rho_s - \rho_f}{\rho_f}$. They demonstrated that good results can be obtained when using sharp interface approximations such as Ghyben-Herberg with ϵ^* instead of ϵ.

2.3 The Glover solution

The Ghyben-Herzberg equation is no longer valid when the interface between fresh and saltwater intercepts the coast line. In this area, in fact, the vertical flux lines are no longer negligeble, as the flow of freshwater does not end on the interface but goes up in a vertical surface, as shown in Figure 2.3.

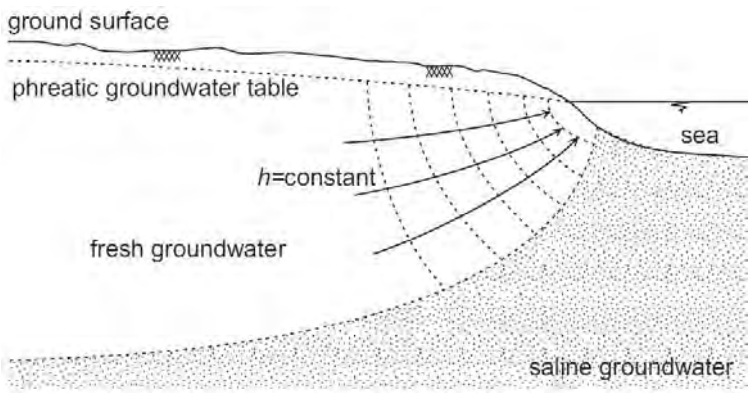

Figure 2.3. Actual aquifer-sea interface at the coast (Gualbert H.P., 2001) [28]

A more exact solution for the shape of the interface was proposed by Glover (1959) [26].

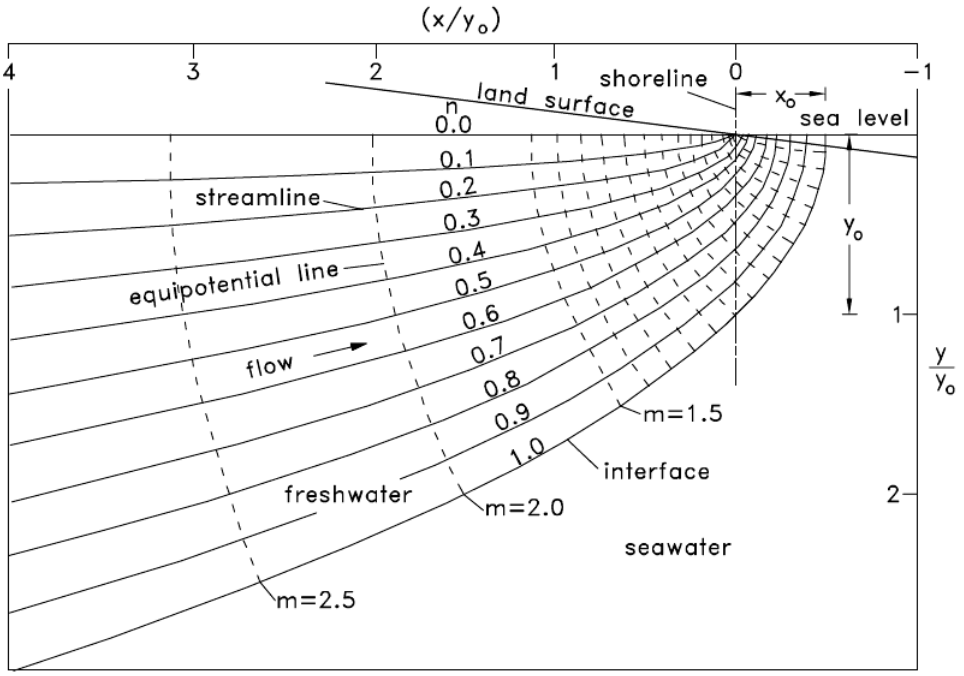

Figure 2.4. Flow pattern near a beach (Darvini G., 2004) [20]

The Glover relationship assumes that freshwater and seawater are at the dynamic equilibrium, which is more physical. It is assumed that the aquifer is homogeneous, confined at the top, and unbounded at the bottom, as shown in Figure 2.5. The saltwater is assumed to be stagnant.

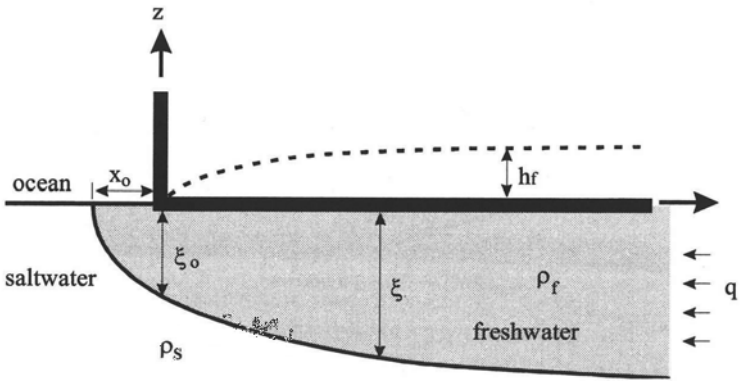

Figure 2.5. The Glover problem (Cheng et al., 1999) [14]

With reference to Figure 2.5 the steady-state freshwater head satisfies the two-dimensional Laplace equation in the vertical plane:

$$\nabla^2 h_f = 0 \tag{2.6}$$

The freshwater head is found as:

$$h_f = \sqrt{\frac{\Delta sq}{K}} \cdot \sqrt{x + \sqrt{x^2 + z^2}} \tag{2.7}$$

where q is the freshwater outflow rate per unit lenght of shoreline, K is the hydraulic conductivity, and Δs is equal to:

$$\Delta s = \frac{\rho_s - \rho_f}{\rho_f} = \frac{\Delta\rho}{\rho_f} \tag{2.8}$$

and represents the difference between seawater and freshwater specific gravity.

The interface depth is given by:

$$\xi(x) = \sqrt{\frac{2qx}{\Delta s K} + \frac{q^2}{\Delta s^2 K^2}} \tag{2.9}$$

The constant second term inside the square root has been added to the Ghyben-Herzberg model to account for the missing seepage face that allows for the vertical components of flow and discharge of the freshwater onto the sea floor.

The size of the outflow face is found from 2.9. The width of the submarine zone through which freshwater discharges into the sea can be obtained for ξ_0 = 0, yelding:

$$x_0 = \frac{q}{2\Delta s K} \tag{2.10}$$

while the depth of the interface beneath the shoreline occurs where x = 0, so that:

$$\xi_0 = \frac{q}{\Delta s K} \tag{2.11}$$

The freshwater head at z = 0 is:

$$h_f = \sqrt{\frac{2\Delta s q x}{K}} \tag{2.12}$$

The geometry reported in Figure 2.5 is unrealistic. In order to make the solution useful, the geometry is usually intepreted to a more practical configuration, as shown in Figure 2.6

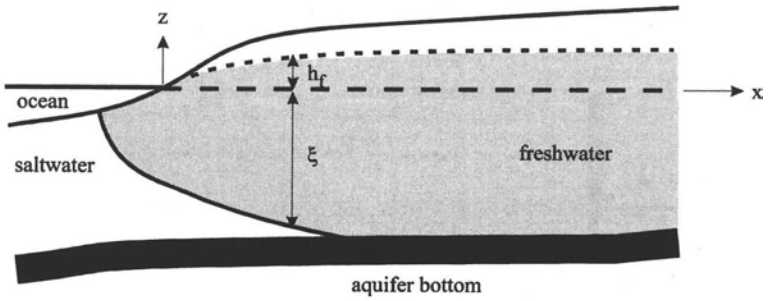

Figure 2.6. Interpretation of the Glover problem (Cheng et al., 1999) [14]

The aquifer is changed from confined at the top to unconfined with a freshwater head given by Equation 2.12. The outflow face terminates at a certain depth under the sea. An impermeable bottom exists that intesects the interface to form a saltwater wedge that terminates at a certain distance inland. These conditions are in violation with the exact mathematical statement that defines the solution. However these discrepancies are expected to be small (Cheng et al., 1999) [14].

According to the Glover model, if the supply of freshwater to the aquifer decreases so that q decreases, than the width of the gap through which freshwater can excape x_0 will also decrease.

2.4 The Dupuit-Ghyben-Herzberg approximation

Although Glover method provides solutions for some relatively simple geometries, for most practical cases this approach is too complicated to be considered as a tool for engineering purposes. A more suitable tool is the Dupuit-Ghyben-Herzberg relation, that follows from the combination of the continuity equation and the Darcy's law with the Ghyben-Herzberg principle and the Dupuit assumptions of horizontal flow.

Considering a phreatic aquifer with uniform accretion N (natural replenishment from prepitation) and assuming that the flow in the aquifer is essentially horizontal and $h(x) = \delta\varphi(x)$, with $\delta = \gamma/(\gamma_s - \gamma_f)$, continuity leads to:

$$q_0 + Nx = -K(h+\varphi)\,\frac{\partial\varphi}{\partial x} = -K(1+\delta)\,\varphi\,\frac{\partial\varphi}{\partial x} \tag{2.13}$$

where q_0 is the infiltration discharge per unit lenght of coastline, φ is the water level above the wedge (measured respect to the coast line), h is the depth of the saltwater-freshwater interface respect to the coast line, K is the hydraulic conductivity of the aquifer.

Integrating from $x = 0$ (assumed the coordinate x starting from the point at which the wedge terminates and directed towards the coast line), $\varphi = \varphi_0$, $h = D$, (where D can be assumed equal to the seawater level) leads to:

$$\varphi_0^2 - \varphi^2 = \frac{2q_0x + Nx^2}{K(1+\delta)} \tag{2.14}$$

For $N = 0$ (no natural replenishment) the solution is:

$$\varphi_0^2 = \frac{2q_0L}{K(1+\delta)} = \frac{D^2}{\delta^2} \tag{2.15}$$

The relation is valid also for a confined aquifer substiting φ with the piezometric head above the toe, and D with the aquifer thickness.

It can be noted that the interface has again a parabolic shape. The interesting outcome, from the practical point of view, is the relationship between q_0 and L. As q_0 increases, L decreases and viceversa. This indicates that the lenght of the seawater intrusion is a decision variable. By controlling q_0 it is possible to control the extent of the seawater intrusion. Equation 2.13 relates φ_0 (piezometric head above the toe) to L (lenght of the salt wedge). By controlling φ_0 (by means of artificial reharge), the water table may be lowered both landward and seaward of the toe, without causing any additional seawater intrusion. Landward of the toe, water levels may fluctuate. If pumpage is taking place seaward of the toe, the interface there will rise and may contaminate wells if their screened portion is not at a sufficient distance above it (Bear, 1972) [6].

2.5 Fetter Oceanic Island solution

Considered a circular oceanic island, supported by a constant surface recharge w, a freshwater lens float on top of saltwater, as shown in Figure 2.7. The solution is provided by Fetter (1972) [21] by taking the Dupuit assumption for freshwater flow, and the Ghyben-Herzberg relation for the interface location. The governing equation for freshwater flow is one-dimensional in the radial direction and the solution of freshwater head is:

$$h_f^2 = \frac{w\Delta s(R^2 - r^2)}{2K(1+\Delta s)} \tag{2.16}$$

where R is the radius of the island, K is the hydraulic conductivity of the aquifer, and Δs is defined in Equation 2.8. The saltwater-freshwater interface depth is then given by the Ghyben-Herzbeg solution:

$$\xi = \frac{\rho_f}{\rho_s - \rho_f} h_f \tag{2.17}$$

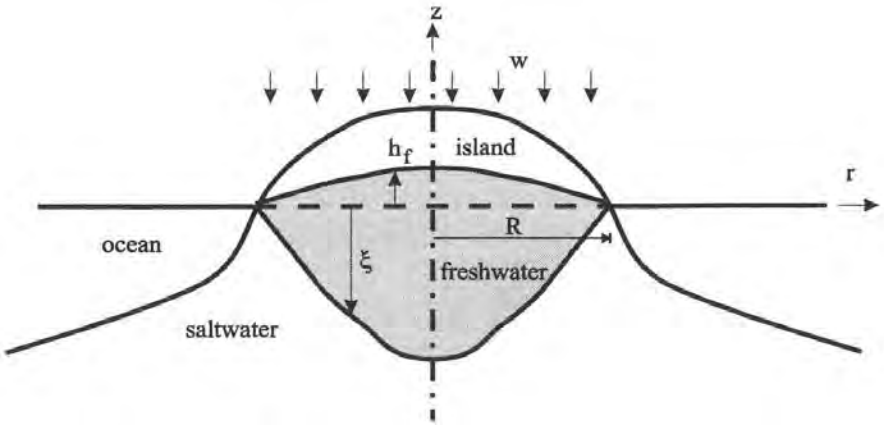

Figure 2.7. Circular island (Cheng et al., 1999) [14]

Chapter 3

Upconing of saline water

When an aquifer contains an underlaying layer of saline water and is pumped by a well penetrating only the upper freshwater portion of the aquifer, a local rise of the interface below the well occurs. This phenomenon is called upconing and it is illustrated in Figure 3.1.

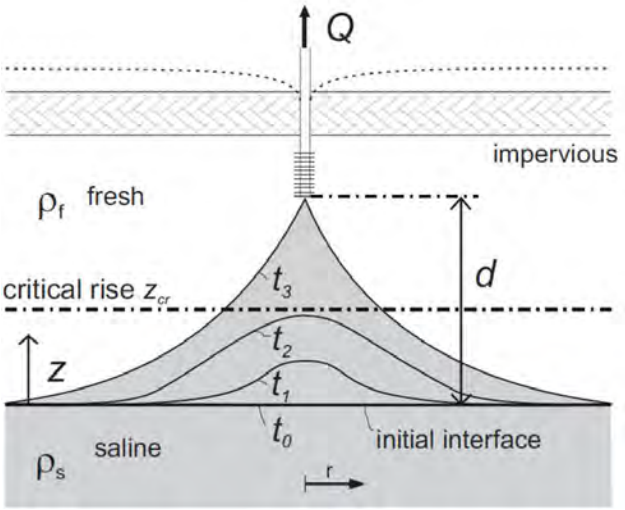

Figure 3.1. Upconing phenomenon (Gualbert H. P., 2001) [28]

The interface is horizontal at the starting time t_0. With continued pumping the interface rises to successively higher levels until eventually it reaches the well. This generally necessitates the well having to be shut down because of the degrading influence of the saline water. When pumping is stopped, the denser saline water tends to settle downward and to return to its former position. From a water supply standpoint it is important to determine the optimum location, depth, spacing, pumping rate, and pumping sequence that will ensure production of the largest quantity of fresh groundwater, while at the same time striving to minimize any underground mixing of the fresh saline water.

3.1 Upconing of an abrupt-interface

Most investigations of upconing assumed an abrupt interface between the two fluids. Although an abrupt interface neglects the physical reality of a transition zone found in groundwater, the assumption has the advantage of semplicity. Furthermore, an interface can be considered as an approximation to the position of the 50 % relative salinity in a transition

zone.

An approximate analytic solution for the upconing directly beneath a well, based on the studies of Bear and Dagan (1968) [19] was reported by Schmorak and Mercado (1969) [43]. The basic assumptions underlying the teoretical development are that the porous medium is homogeneous and non deformable, that the two fluids are incompressible, immiscible and separated by an abrupt-interface and the flow obeys the Darcy Law. Bear and Dagan (1968) [19] used the method of small perturbations (reported by Bear in the book "Dynamics of fluids in porous media") to obtain an approximate solution for the position of the interface, which is a useful tool for obtaining analytical solutions for cases involving small deviations from an initially steady interface (Wagner J. et al., 1982) [50].

For the case of upconing beneath a pumping well partially penetrating a relatively thick confined aquifer, Schmorak and Mercado (1969) [43] reported the Bear and Dagan's solution for the position of the interface, as a function of time and radial distance from the pumping well:

$$X(r,t) = \frac{Q}{2\pi(\Delta\rho/\rho)K_x d} \cdot \left[\frac{1}{(1+R^2)^{0,5}} - \frac{1}{[(1+\tau)^2+R^2]}\right] \tag{3.1}$$

where R ant τ are dimensionless distance and time parameters defined by:

$$R = \frac{r}{d} \cdot \sqrt{\frac{K_z}{K_x}} \tag{3.2}$$

and:

$$\tau = \frac{(\Delta\rho/\rho) \cdot K_z}{2\Theta d} \cdot t \tag{3.3}$$

in which d [L] is the distance from the bottom of the well to the initial interface elevation; K_x and K_z [L/t] are the horizontal and vertical hydraulic conducibilities respectively; Q [L^3/t] is the well pumping rate; r [L] is the radial distance from well axis; t [t] is the time elapsed since start of pumping; X is the rise of the interface above its initial position; $\Delta\rho/\rho$ is the dimensionless density difference between the two fluids; Θ is the porosity of the aquifer.

The application of the method of small perturbations restricts changes in the interface elevation to relatively small values. In terms of the physical problem this restriction requires d to be much smaller than the freshwater and saltwater thickness.

Although the governing differential equations have been formulated for a confined aquifer, the results can be applied to unconfined systems if the drawdown is negligible compared to the saturated thickness of the freshwater zone (Wagner J. et al., 1982) [50].

Equation 3.1, representing the linear relation between the rise of the interface and the pumping rate, is limited to a certain critical rise X_{cr}.This limitation arises from linear approximation of the boundary conditions. As the interface approaches this critical rise, the rate of rise increases. Above the critical rise the interface reaches the pumping well with a sudden jump. Muskat (1946) [36] defines the zone of accelerated rise for $X/d > 0.48$ and the critical rise within the limits of $X/d \simeq 0.60$ to 0.75. Schmorak and Mercado (1969) [43] recommend application of the linear approximation for $X/d \leq 0.5$.

From Equation 3.1 it is possible to obtain the maximum permissible pumping rate which will ensure salt-free water.
For $r = 0$ and $t \to \infty$:

$$X(0,\infty) = \frac{Q}{2\pi(\Delta\rho/\rho)K_x d} \tag{3.4}$$

and:

$$Q_{max} = 2\Theta d \, \frac{\Delta\rho}{\rho} \, K_x \, X_{cr} \tag{3.5}$$

For a decaying mound an imaginary recharge well is superimposed at time t = t* corresponding to the end of the pumping period, and for t > t *:

$$X(r,t) = \frac{Q}{2\pi(\Delta\rho/\rho)K_x d} \cdot \left[\frac{1}{[(1+\tau_1)^2 + R^2]^{0,5}} - \frac{1}{[(1+\tau)^2 + R^2]^{0,5}}\right] \tag{3.6}$$

where:

$$\tau_1 = \frac{(\Delta\rho/\rho) \cdot K_z}{2\Theta d} \cdot (t - t^*) \tag{3.7}$$

In the real-world situations, a transition zone, with a finite thickness of brackish water, occurs above the body of undiluted saline water. The water in the upper edge of the zone is essentially freshwater and moves accordingly. Upward movement of the almost-freshwater occurs readily along with the adjoining freshwater. Consequentely, even with a relatively low pumping rate, no limiting critical rise exists above which saline water will not rise. It follows that with any rate of continuous pumping, some saline water must sooner or later reach a well. Equation 3.4 supports the previous statement. In a transition zone the salinity changes gradually; hence, $\Delta\rho$ in an incremental width at the top of the zone approaches zero. As a result z must tend towards infinity, indicating that there can be no finite limit to z. Similarly in equation 3.5, as $\Delta\rho$ approaches to zero, also must Q_{max} approaches zero (Todd, 1976) [45].

Also Werner et al. (2009) [51] demonstrate this fact. They conducted four saltwater upconing experiments under controlled conditions in a laboratory sand tank. Experiments were designed to evaluate upconing under different mixed convection ratios, obtained by changing the freshwater-saltwater density difference and the rate of groundwater extraction. Relative to real-world situations, the experiments represented a bore constructed in a high-K homogeneous aquifer and positioned near the freshwater-saltwater interface, with relatively short pumping duration. Saltwater resulted in intercepting the well in all cases.

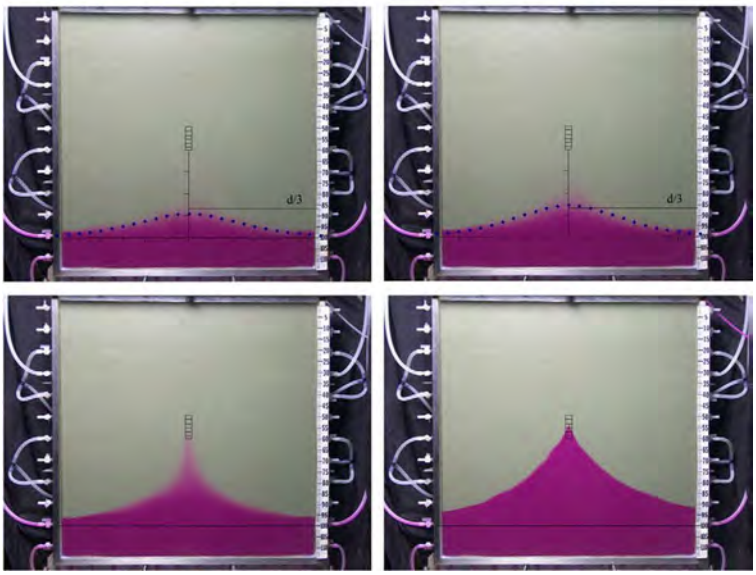

Figure 3.2. Plume upconing from Werner et al. (2009) [51] experiments

Part II

Design of the experimental model

Chapter 4

Design of the sand-box facility

In this Chapter the calculations to verify if the sand-box facility was suitable to the experiment are reported. Moreover the hydraulic conductivity and porosity of the glass beads, and the decrease of salt concentration in time due to dilution are estimated.

The sand-box device was built to study variable density currents, in both free surface and pressurized hydraulic conditions. It is 5 m long (the lenght is intended to be the part of the channel where sand can be placed), 30 cm wide, 60 cm high and can be tilted up to 3 %. The channel is provided with two indipendent tanks, to allow the introduction of fluids with different characteristics. The bigger tank has a capacity of 2 m^3 and is suitable to simulate the "sea" in the experiment. The sand-box facility is made of plexiglass.

Figure 4.1. Sand-box facility used for the experiment [58]

Figure 4.2 reports the original plant and the frontal view of the device.

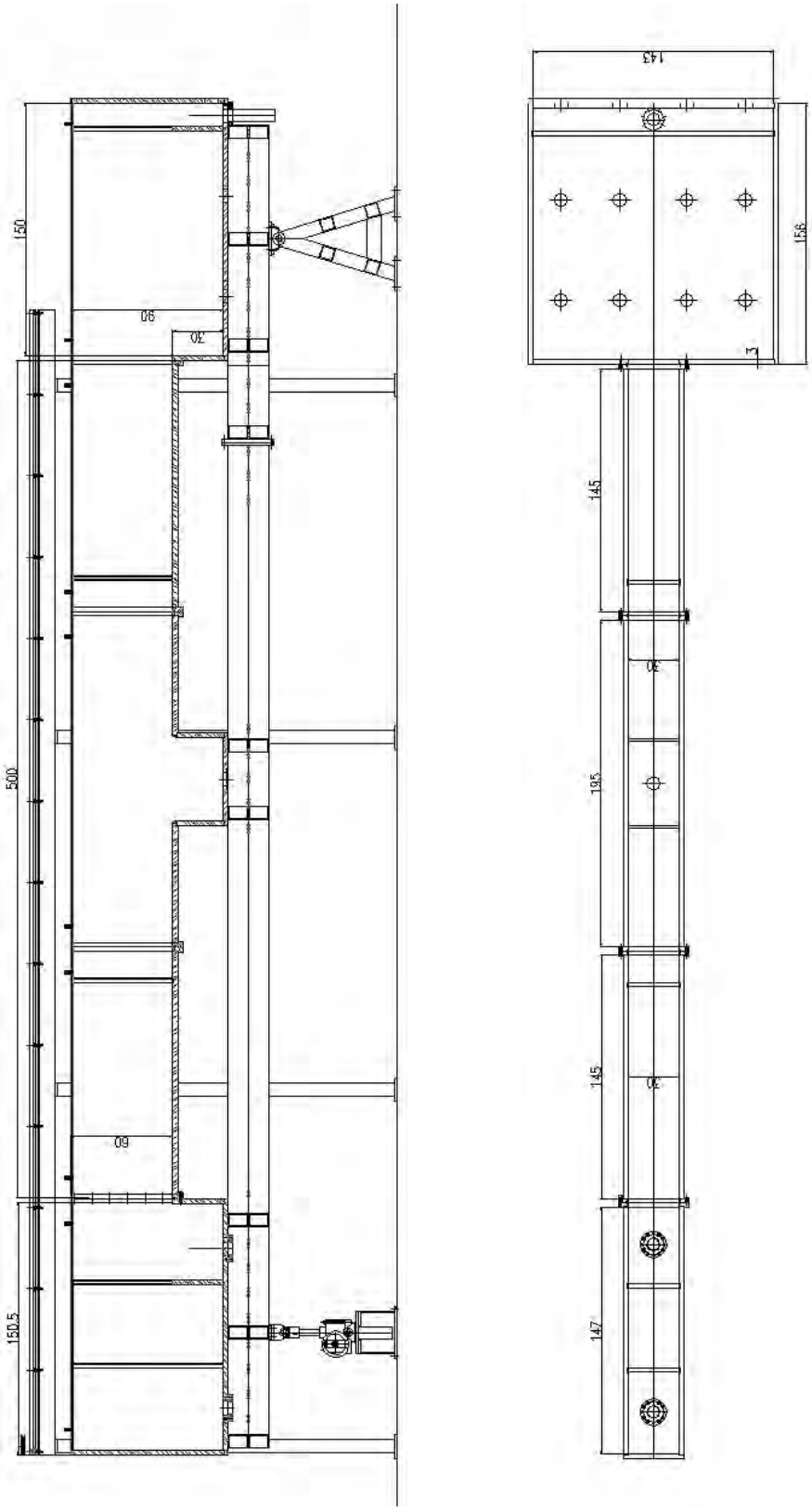

(a) (b)

Figure 4.2. Frontal view (a) and plant (b) of the sand-box facility. Not scaled graphical table

4.1 Implementation of the Ghyben-Herzberg model

The Ghyben-Herzberg model (Ghyben, 1888 [25]; Herzberg, 1901 [30]) was implemented to verify the hydraulic conductivities and infiltration discharges that allow to contain saltwater intrusion within a certain range of lenght, compatible with the dimensions of the sand-box facility. For this purpose the Ghyben-Herzberg equation is rearranged in the following form:

$$\frac{z}{\sqrt{x}} = \sqrt{\frac{2\rho q}{\Delta\rho\, K}} \tag{4.1}$$

Let ρ_s = 1.025 g/cm^3 and ρ_f = 1 g/cm^3 the ratio $2\rho\,/\Delta\rho$ becomes equal to 80.

Consequently it is possible to obtain the values of the ratio z $/\sqrt{x}$ as a function of the freshwater flow per unit lenght q and the hydraulic conductivity K, as reported in Table 4.1.

Table 4.1. Values of the ratio z $/\sqrt{x}$ as a function of q and K

	Freshwater flow per unit lenght q [m^{2}s^{-1}]								
K [ms^{-1}]	$1\cdot10^{-7}$	$2\cdot10^{-7}$	$3\cdot10^{-7}$	$4\cdot10^{-7}$	$5\cdot10^{-7}$	$6\cdot10^{-7}$	$7\cdot10^{-7}$	$8\cdot10^{-7}$	$9\cdot10^{-7}$
10^{-7}	8.94	12.65	15.49	17.89	20.00	21.91	23.66	25.30	26.83
10^{-6}	2.83	4.00	4.90	5.66	6.32	6.93	7.48	8.00	8.48
10^{-5}	0.89	1.26	1.55	1.79	2.00	2.19	2.37	2.53	2.68
10^{-4}	0.28	0.4	0.49	0.56	0.63	0.69	0.75	0.80	0.85
10^{-3}	0.09	0.13	0.15	0.18	0.20	0.22	0.24	0.25	0.27

Fixed the maximum depth of the interface z equal to 40 cm (that is a reasonable value considering that the height of the sand-box facility is 60 cm), x was obtained.

Results are reported in Table 4.2.

Table 4.2. Lenght x of the salt wedge [m] assumed z equal to 40 cm

	Freshwater flow per unit lenght q [m^{2}s^{-1}]								
K [ms^{-1}]	$1\cdot10^{-7}$	$2\cdot10^{-7}$	$3\cdot10^{-7}$	$4\cdot10^{-7}$	$5\cdot10^{-7}$	$6\cdot10^{-7}$	$7\cdot10^{-7}$	$8\cdot10^{-7}$	$9\cdot10^{-7}$
10^{-7}	0.0020	0.0010	0.00067	0.00050	0.00040	0.00033	0.00028	0.00025	0.00022
10^{-6}	0.020	0.010	0.0067	0.0050	0.0040	0.0033	0.0028	0.0025	0.0022
10^{-5}	0.20	0.10	0.067	0.050	0.040	0.033	0.028	0.025	0.022
10^{-4}	2.00	1.00	0.67	0.50	0.40	0.33	0.28	0.25	0.22
10^{-3}	20.00	10.00	6.67	5.00	4.00	3.33	2.86	2.50	2.22

It is important to point out that, for the same value of the hydraulic conductivity K, the value of x halves if the value of q doubles.

Table 4.2 highlights also that, if the value of K increases by one order of magnitude, for a constant value of the infiltration discharge the x value multiplies 10 times too. Assumed for the porous medium an hydraulic conductivity equal to 10^{-3} m/s (that is allowable for a sand), the x values compatible with the sand-box facility dimensions correspond to very low infiltration flows. This implies that is impossible to study the saltwater intrusion simply by controlling the flows but it is necessary to control the hydraulic heads upstram and downstream the device through the use of spillways. It was decided for the experiment to fix the upstream hyraulic load equal to 42 cm, while the downstream hydraulic load equal to 40 cm, in order to obtain a value of the infiltration discharge compatible with the dimensions of the sand-box ($1.64 \cdot 10^{-6}$ m^2/s, for a $K = 1 \cdot 10^{-3}$ m/s).

4.2 Glass beads characteristics

Silica beads, with a nominal size range equal to 400-800 μm, producted by Potter Industries Inc., were used to simulate the porous medium. According to Goswami and Clement (2007) [27], sorption tests indicated that the food dye would not sorb or react with glass beads.

Figure 4.3 reports an electron microscope image of the glass beads that shows that their shape is not perfectly spherical.

(a) (b)

Figure 4.3. Microscope image of the glass beads

The chemical composition of the beads, according with the maker, is:

- $SiO_2 < 20$ %;
- Na_2O <15 %;
- Cao < 10 %;
- MgO < 5 %.

Glass beads look clear and odorless, the density of the solid grains is equal to 2.5 g/cm^3, the PH of the material, classified by the maker as stable, is 11-12, and the melting point is

around 730 °C.

Figure 4.4 reports the atomic composition of the beads that are mainly composed of silica (glass).

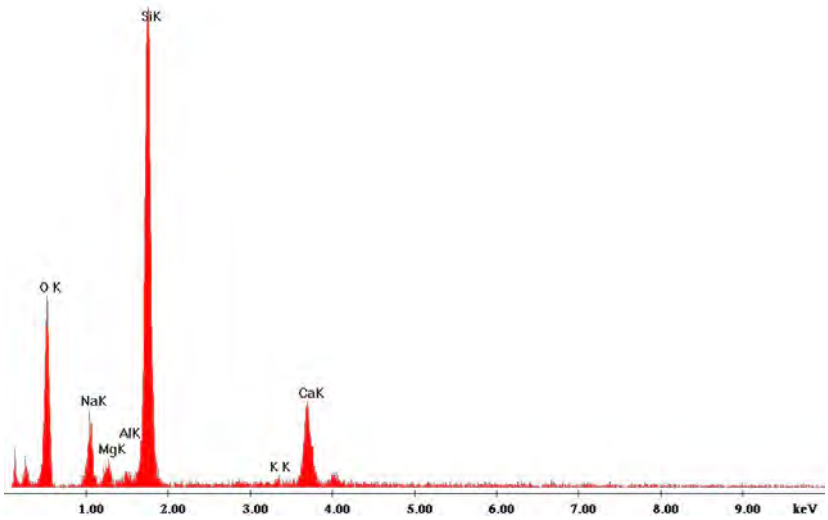

Figure 4.4. Chemical composition of the beads

4.3 Granulometric curve of glass beads

The granulometric curve of a soil is an experimental diagram obtained from the passage of a sampling material through a series of sieves characterized by a different mesh size. The result of the analysis is made clearly visible through the creation of graphics in normal or logarithmic scale. In these graphs the ordinate reports the percentage of material finer than the sieve mesh (which passes through the mesh), while the abscissa reports the minimum width of the sieve mesh. From the analysis of the granulometric curve it is possible to derive the type of soil and the degree of assortment of grains.

The granulometric curve found for glass beads, from which it is possible to characterize the material as a sand, is attached at the end of the thesis. According to the graph the sand has a d_{50} equal to 0.6 mm and a uniform coefficient U (= d_{60}/d_{10}) equal to 1.5.

4.4 Porosity values and quantity of sand necessary to the experiment

The total porosity of a porous material is the ratio between the pore volume and the total volume of a representative sample of the medium. Assuming that the soil system is composed of three phases- solid, liquid (water), and gas (air)- where V_s is the volume of the solid phase, V_l is the volume of the liquid phase, V_g is the volume of the gaseous phase, $V_p = V_l + V_g$ is the volume of the pores, and $V_t = V_s + V_l + V_g$ is the total volume of the sample, then the total porosity of the soil sample, p_t, is defined as follows:

$$p_t = \frac{V_p}{V_t} = \frac{V_l + V_g}{V_s + V_l + V_g} \tag{4.2}$$

Porosity of loose and compacted glass beads was calculated experimentally according to Equation 4.3:

$$D = \frac{D - D'}{D} \cdot 100 \tag{4.3}$$

where D' is the bulk density of the specimen (= weight of the specimen/volume of the specimen), while D is the real density of the material (density of the solid grain = 2500 kg/m^3).

For glass beads, porosity of loose sand resulted equal to 37.91 %, while porosity of compacted sand to 36.74 %. Consequently the quantity of glass beads Q necessary to fill up the sand-box device to 45 cm was calculated:

$$Q = 0.45\ m \cdot 0.3\ m \cdot 5\ m \cdot 2500\ \frac{kg}{m^3} \cdot (1 - 0.36) = 1080\ kg \tag{4.4}$$

in which the porosity was set equal to 36 % considering that the sand would be compacted.

4.5 Conductivity tests

The hydraulic conductivity is often the greatest source of uncertainty in predictive transport models of solute transport in groundwater. Hazen (1982) [29] proposed the following relationship between the saturated hydraulic conductivity and the soil particle diameter:

$$K_s = c \cdot (d_{10})^2 \tag{4.5}$$

where K_s is expressed in cm/s, c is a constant that varies from 1 to 150 [1/(cm · s)], and d_{10} is the soil particle diameter [cm] such that 10 % of all soil particles are finer by weight.

Hazen relationship is applicable to loose granular soils with d_{10} ranging from 0.1 mm to 3 mm and with uniformity coefficient < 5.

Table 4.3 reports some range of values for the c coefficient.

Table 4.3. Values of the c coefficient [56]

Type of soil	**Values of the Hazen coefficient [(cm · s)$^{-1}$]**
very fine sand	40-80
clean-medium sand	80-120
coarse sand-poor sorting	80-120
clean-coarse sand	120-150

According to Equation 4.5, assuming for the c cofficient a value equal to 120 (cm · s)$^{-1}$ and a d_{10} equal to 0.43 mm, that are values compatible with the glass beads, the expected hydraulic conductivity would be equal to 2.2 · 10^{-3} m/s.

The constant-head permeability test is the laboratory testing method used to verify the hydraulic conductivity of the glass beads. The use of this instrument suits the case of soils with high permeability values, such as granular materials. The test was performed at the

laboratory of Geotechnical Engineering of the Padua University.

In this type of laboratory device (reported in Figure 4.5) the water supply at the inlet is adjusted in such a way that the head difference between the inlet and the outlet remains constant during the test period. After a constant flow rate is established, water is collected in a graduated flask for a known duration.

The total volume of water collected may be expressed as:

$$Q = Avt = A\,(Ki)\,t \tag{4.6}$$

where Q is the volume of water collected, A is the area of cross section of the soil specimen and t is the duration of water collection.

Given that:

$$i = \frac{\Delta h}{L} \tag{4.7}$$

where L is the lenght of the specimen and Δh is the hydraulic head difference, Equation 4.7 can be substituted into Equation 4.6 to yield:

$$Q = A\left(K\frac{\Delta h}{L}\right)t \tag{4.8}$$

or

$$K = \frac{QL}{A\Delta h\,t} \tag{4.9}$$

(a) (b) (c)

Figure 4.5. Constant-head permeability device

The permeameter used for the tests had the characteristics reported in Table 4.4

Table 4.4. Characteristics of the permeameter device used for the first test

Area of the cross section A	44.18 cm^2
Distance between the piezometers of the apparatus L	10 cm
Hydraulic head difference Δh	9.6 cm
Tare of the water collector	827 g

Five tests were performed without compacting the sand and hydraulic conductivity was determined using Equation 4.9.

Results are reported in Table 4.5.

Table 4.5. Results of the tests for loose sand

Test	Gross weight [g]	Net weight Q [g]	Time t [s]	Conductivity K [cm/s]
1	1789.5	962.1	92	0.247
2	1779.3	951.9	90	0.249
3	1509.7	682.3	65	0.247
4	1520.2	692.8	65	0.251
5	1561.3	733.9	70	0.247

The final value was calculated as the arithmetic average of the results of each test. To be consistent with the units the value of Q is reported in grams and it is calculated as the difference between the gross weight of the specimen minus its tare.

The final value for the hydraulic conductivity in the case of loose sand is $K = 2.48 \cdot 10^{-1}$ cm/s = $2.48 \cdot 10^{-3}$ m/s.

Other five tests were conducted to calculate the hydraulic conducibility for the compacted sand. The new parameters are reported in Table 4.6.

Table 4.6. Characteristics of the permeameter device used for the second test

Area of the cross section A	44.18 cm^2
Distance between the piezometers of the apparatus L	10 cm
Hydraulic head difference Δh	8.7 cm (15.8 cm for the last test)
Tare of the water collector	2668.7 g

Results of these tests are reported in Table 4.7.

Table 4.7. Results of the tests for compacted sand

Test	Gross weight [g]	Net weight Q [g]	Time t [s]	Conductivity K [cm/s]
1	1229.2	425.4	70	0.158
2	1194.3	390.5	65	0.156
3	1160.7	356.9	60	0.155
4	1154.8	351	60	0.152
5	1726.6	922.8	90	0.147

The final value for the hydraulic conductivity (calculated as the arithmetic average of the results of each test) in the case of compacted sand is $K = 1.54 \cdot 10^{-1}$ cm/s = $1.54 \cdot 10^{-3}$ m/s. It should be noted that the values found for hydraulic conductivity do not differ so much from the value predicted using the Hazen relation.

4.6 Dilution of saltwater in time

The dilution of concentration in time due to the infiltration discharge can be generally studied through the mass balance equation that can be expressed as:

$$Q_i C_i - Q_e Ce \pm generation = V_r \cdot \frac{\Delta C_T}{\Delta t} \tag{4.10}$$

where:

- Q_i = volumetric flow rate of inflow water;
- Q_e = volumetric flow rate of outfow water;
- C = concentration of salt in the tank;
- V_r = volume in the tank (ractor);
- C_i = concentration of entering NaCl;
- C_e = concentration of exiting NaCl;
- C_T = concentration of NaCl in the tank;
- Δt = change in time.
- $\pm$ generation refers to generation of products and consumption of reactants as a result of chemical reaction. If there is no chemical reaction then these terms are zero.

With the assumption of steady state $Q_i = Q_e = Q$; considering that $C_i = 0$, and taking the limit as Δt approaches zero, Equation 4.10 becomes:

$$-QC_e = V_r \frac{dC}{dt} \tag{4.11}$$

Upon integration from t = 0 to a final time and from the concentration at time zero to the concentration at a final time:

$$\int_0^t dt = \frac{V_r}{-Q} \int_{C_0}^{C_t} \frac{dC}{C} dC \tag{4.12}$$

The result of Equation 4.12 is:

$$t = \frac{V_r}{-Q} \cdot (lnC_t - lnC_o) \tag{4.13}$$

Solving for C_t:

$$C_t = C_0 \cdot e^{-tQ/V_r} \tag{4.14}$$

Equation 4.14 is useful in order to estimate the time necessary to have a significant decrease in salt concentration in the saltwater tank.

Assuming the volumetric flow Q [1] equal to the infiltration discharge:

$$Q = K \cdot i \cdot A = 1.54 \cdot 10^{-3} \cdot \frac{0.02}{5} \cdot 0.41 \cdot 0.3 \cdot 1000 = 7.5 \cdot 10^{-4}\ l/s \tag{4.15}$$

the volume of the reactor V_r equal to the volume of the saltwater tank of the sand-box facility device (=1600 l if the hydraulic head in the tank is 40 cm) and the salt concentration equal to 35 g/l, the decrease of concentration in time can be calculated.

Table 4.8. Concentration dilution in time

C_0 [g/l]	t [h]	V_r [l]	Q [l/s]	C_t [g/l]	$\Delta C/C_0$ [%]
35	0.5	1600	0.00075	34.970	0.084
35	1	1600	0.00075	34.941	0.169
35	1.5	1600	0.00075	34.911	0.253
35	2	1600	0.00075	34.882	0.337
35	2.5	1600	0.00075	34.853	0.421
35	3	1600	0.00075	34.823	0.505
35	3.5	1600	0.00075	34.794	0.589
35	4	1600	0.00075	34.764	0.673
35	4.5	1600	0.00075	34.735	0.756
35	5	1600	0.00075	34.706	0.840
35	5.5	1600	0.00075	34.677	0.924
35	6	1600	0.00075	34.647	1.007

Table 4.8 reports the concentration decrease every 30 minutes. The result points out that

[1] the volumetric flow Q is calculated considering the hydraulic conductivity in the compacted case

a decrease of concentration equal to 1% occurs after 6 hours. This implies that salt has to be added every 6 hours in the tank in order to maintain constant the density during the experiment.

4.7 Design of the laboratory facility

It was decided, for the experiment, to set the levels upstream and downstream equal to 42 cm and 40 cm respectively. In this way, according to the Ghyben-Herzberg theory, the salt-water intrusion would be limited within the fist 2.5 m, assuming that at about half of the sand-box device the hydraulic head would be approximately 41 cm. Considering that the Ghyben-Herzberg model provides an overestimated solution, this choice for levels would be cautionary. The hydraulic heads will be maintained through the use of adjustable spillways. In the the upward tank freshwater will be recirculated with a pump having an adequate prevalence. It was decided to use a submersible pump of the type Syncra 5.0, reported in Figure 4.6. The freshwater tank must contain a volume of 50 l at least to avoid the overheating of the pump.

(a) (b)

Figure 4.6. Pump Syncra 5.0

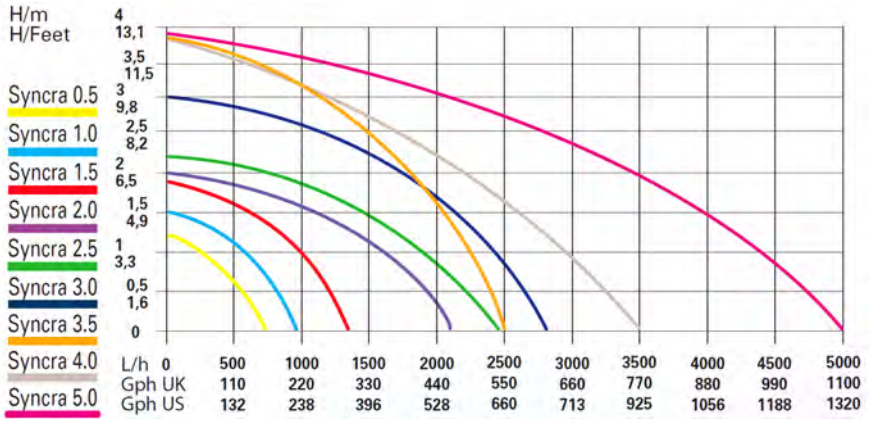

Figure 4.7. Charactheristics of the pump Syncra 5.0 provided by the maker

The device, according with the maker, has a maximum prevalence equal to 3.8 m and can pump up to 5000 l/h (Figure 4.7).

The flow coming out from the pump can be adjusted through the use of a bypass. In this way it is possible to quickly fill the tank closing the bypass pipe, and, reached the decided level (42 cm), to decrease the flow in order to have a negligeble hydraulic head above the spillway.

The spillway in the saltwater tank will discharge the infiltration flow, estimated to be around $7.5 \cdot 10^{-4}$ l/s, considering that the material will be compacted in the sand-box facility, and assuming as following the hydraulic conductivity of the compacted sand. This implies that, in one hour, the expected quantity of water coming out from the device would be 2.7 l. If the hydraulic conductivity calculated for loose sand is considered, the water spilled in one hour would be 4.4 l. Consequentely it was decided to place under the spillway a tank with a capacity equal to 4 l, that will be weighed every hour with a precision balance (that can weigh up to 4 kg). In this way the correct hydraulic conductivity will be calculated.

Moreover, the saltwater tank needs to be mixed to avoid the formation of a stratification between saltwater and intruding freshwater. This will done through the use of another pump, placed inside the tank, that will create a turbolence, avoiding stratification.

The density in the saltwater tank will be constantly monitored and salt will be added when necessary (supposedly every 6 h according to Table 4.8) in order to work in constant-density conditions.

Saltwater will be prepared in a separated tank and pumped into the sand-box with the pump New Jet 3000 (H_{max} = 2.9 m, Q_{max} = 3000 l/h) in order to improve mixing.

At the end of the experiment glass beads will be washed by filtration of freshwater. This will be done by empting the downward tank and discharging saltwater.

The graphical table of the dimensioned sand-box device is reported in Figure 4.10. The scaled graphical table is attached at the end of the thesis.

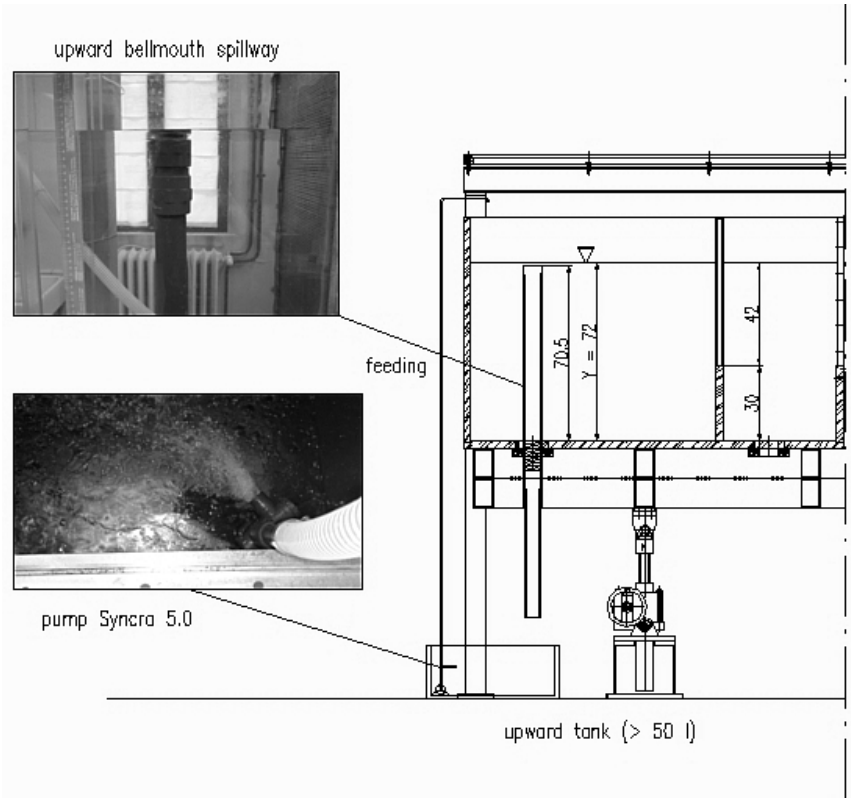

Figure 4.8. Upstream freshwater tank. Frontal view. Not-scaled graphical table

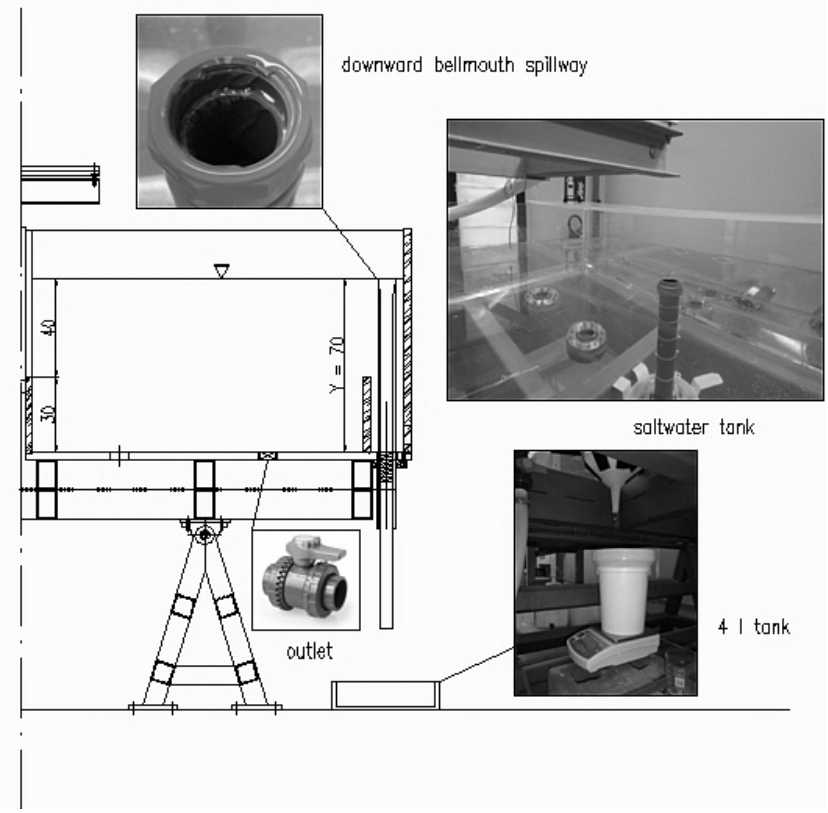

Figure 4.9. Downstream freshwater tank. Frontal view. Not-scaled graphical table

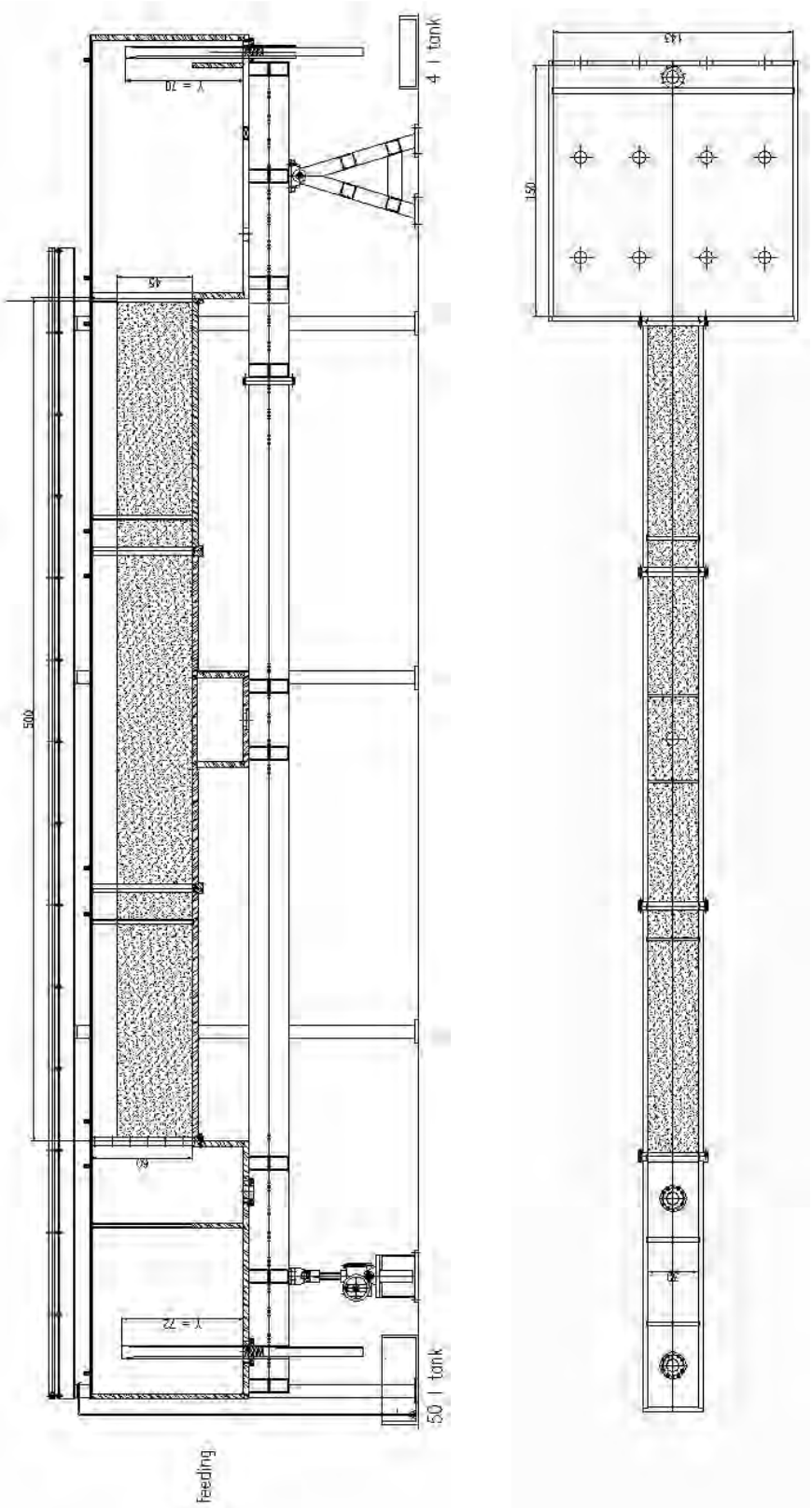

(a) (b)

Figure 4.10. Graphical table of the dimensioned sand-box device. Frontal view (a) and plant (b)

Chapter 5

Preliminary experiments

Some preliminary experiments were developed in order to verify the expected behaviour of the fluids in the sand box facility, to be sure that the chosen dye was a good tracer for saltwater, and to check any other possible problem.

5.1 Experiments to check the best dye to visualize the salt wedge

The first tests were realized in a small tank and had the aim to find what type of tracer was suitable to visualize the saltwater intrusion. A layer of glass beads was positioned in the middle of the tank. The beads were retained by a metallic grid shaped as a box, as shown in Figure 5.1.

Figure 5.1. Tank used to verify some type of dyes

Saltwater was prepared by dissolving 70 g of pure NaCl in 2 liters of water (salt concentration in seawater is equal to 35 g per liter). In the first case methylene blue was used to mark saltwater, while rhodamine to color freshwater, as shown in Figures 5.2(a) and 5.2(b).

The result is reported Figure 5.2. After some minutes saltwater crossed the sand forming a sort of wedge. A stratification was created due to the difference in the fluid densities.

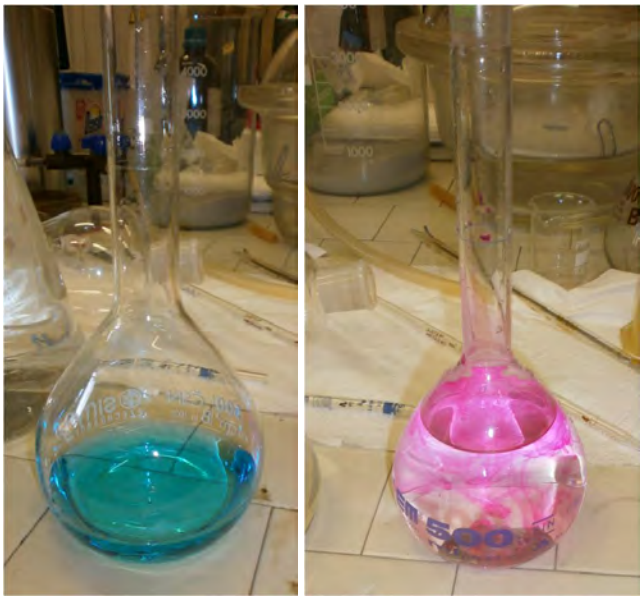

(a) (b)

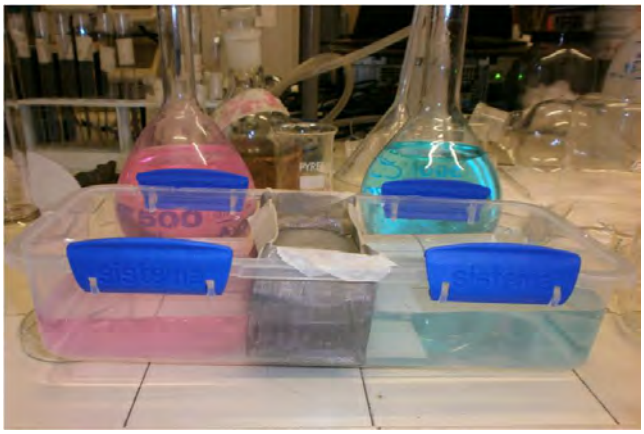

(c)

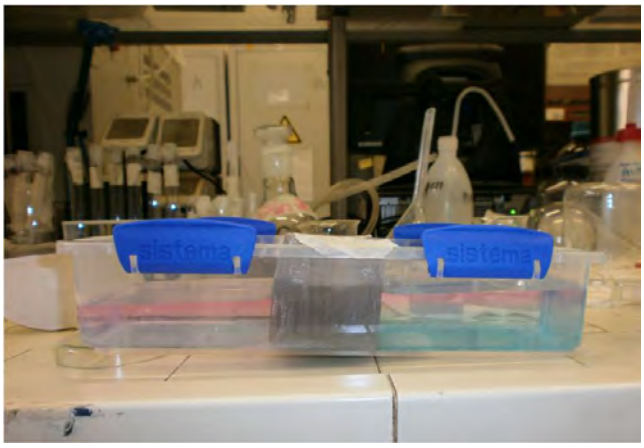

(d)

Figure 5.2. Salt wedge resulting in laboratory. Rhodamina (pink) was used to mark freshwater, while methylene blue to trace saltwater

The second experiment was realized using two types of food dyes (Fiorio Colori S.p.a.) as tracers: yellow was used to mark saltwater, and blue to mark freshwater. This was done to verify the possibility to visualize the saltwater-freshwater interface with an intermediate colour.

The result was satisfactory and the interface between the fluids became green. This option is interesting because it allows to get a visual estimation of the interface thickness. From Figures 5.3 and 5.4 it is possibile to see how the stratification goes on, until the 2 fluids becomes mixed (this happened about 2 days after the experiment).

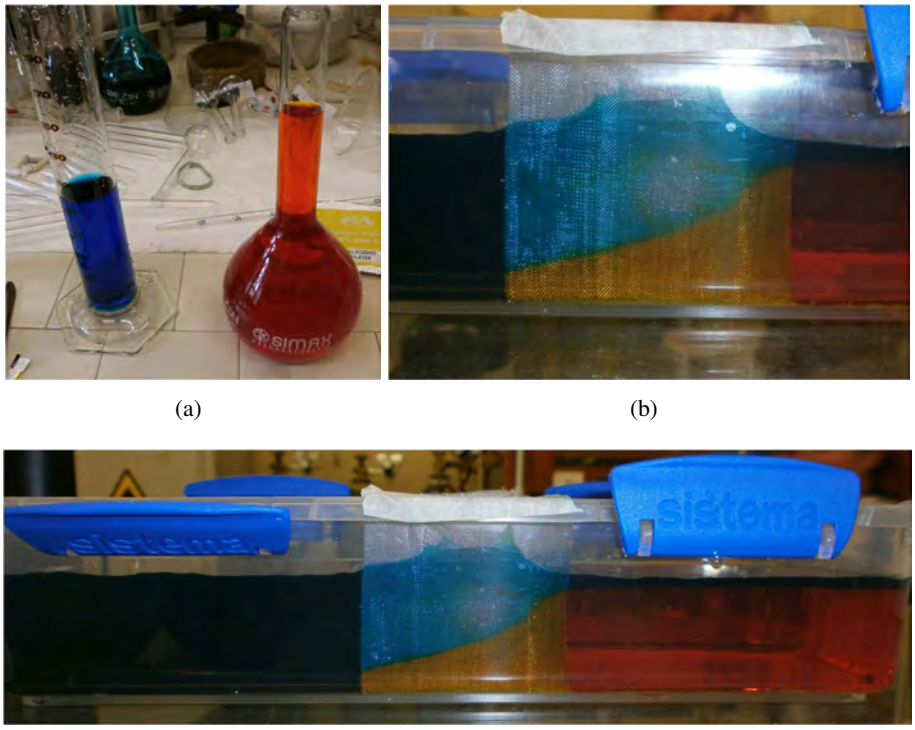

(a) (b)

(c)

Figure 5.3. Salt wedge resulting in laboratory. Blue food colour was used to mark freshwater, while red food colour to trace saltwater

(a) (b)

Figure 5.4. Stratification of saltwater and freshwater after 15 minutes (a) and after 2 days (b)

A third experiment was finally realized using a coloured salt to visualize seawater. This test aimed to avoid the problem of the different diffusion of dye and salt. Saltwater was prepared mixing 8.755 grams of copper sulphate in 250 ml of water in order to obtain the desired concentration of 35 g per liter typical of seawater. The density was calculed and resulted equal to 1021.5 kg/m^3. Also in this case the result was successfull but the obtained color was too light to be a good saltwater tracer; moreover copper sulphate showed the tendency to flocculate.

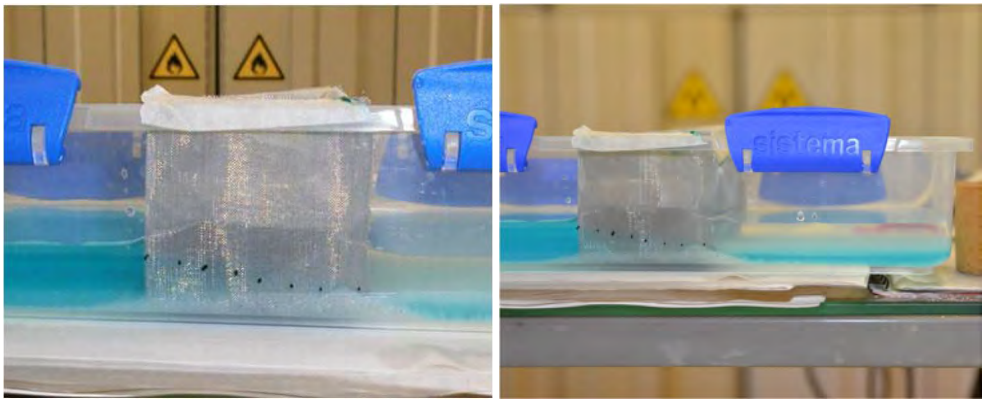

(a) (b)

Figure 5.5. Salt wedge obtained using copper sulphate

From the results of these experiments it was decided not to use rhodamine and copper sulphate in order to avoid problems with the disposal of both these substances and flocculation for the second one.

The use of two colours is very interesting in order to render the wedge interface but it is too complex to manage in a big system involving thousands liters of water. So it was decided to use only one colour to mark saltwater, the red food dye.

5.2 Column tests

Two tests in a chromatographic column were realized. They had the aim to verify if food dye is a good tracer for seawater and diffuses in the same way of salt.

5.2.1 Two colours column test

The first test was done using two tracers for water: blue food dye to mark freshwater and yellow food dye to mark saltwater. Blue dye was diluted 50 times respect to the suggestion, provided by the maker, of mixing 8 grams of it in 0.5 liters of water. This was done to decrease the colour intensity. Yellow saltwater was instead diluted 10 times with clear freshwater for the same reason. It is important to emphasize that this procedure implies that salinity of saltwater also decreased of 10 times respect to the salinity of the original mixture.

The chromatographic column used for this test is reported in Figure 5.6. It is 50 cm high and has a diameter equal to 4 cm. The column was filled with 400 g of glass beads, that reached an height equal to 24.5 cm. Then it was saturated with 200 cc of clear freshwater, as shown in Figure 5.6(b).

During the saturation process the sand was compacted by hand beating the column with a suitable hammer (Figure 5.6(c)).

(a) (b) (c)

Figure 5.6. Chromatographic column used for the tests (a); saturation of the column (b); compaction of the column (c)

Conductivity was measured with the conductivity meter Multiline P4 (Figure 5.7). The device was calibrated by immersion of the measuring cell into the standard control solution 0.01 mol/l KCl. Multiline P4 automatically considers the temperature dependence on the control standard solution.

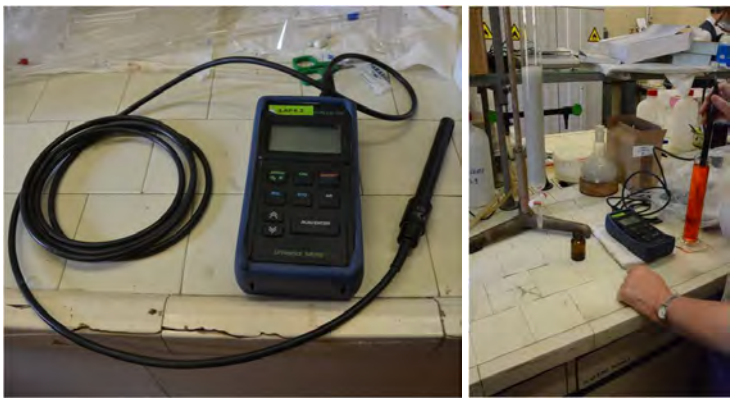

(a) (b)

Figure 5.7. Conductivity meter Multile P4

Two samples of freshwater and coloured saltwater were collected. Their conductivities were equal to 465 μS/cm and 6.83 mS/cm respectively. Conductivity of the initial saltwater mixture was equal to 60 mS/cm. This is because, as already said, coloured saltwater was diluted

10 time with freshwater to decrease blue colour.

After this procedure, 200 cc of yellow coloured saltwater were poured into the column and sampling began. A total number of 26 samples were collected. The first visible yellow sample was number 3.

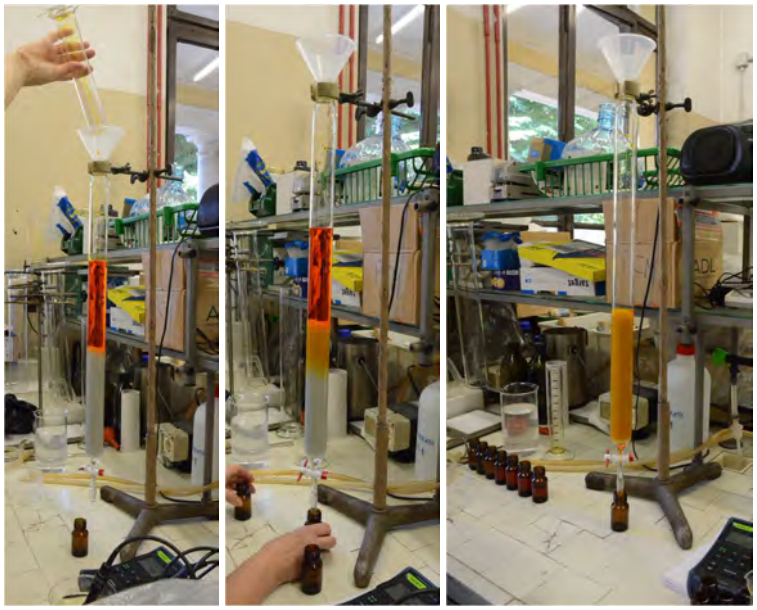

(a) (b) (c)

Figure 5.8. Yellow saltwater was poured into the chromatografic column

After sample number 8 blue freshwater was poured into the column.

(a) (b)

Figure 5.9. Blue freshwater was poured into the chromatographic column

When blue freshwater reached the bottom of the colum saltwater had to be half diluted. After sample number 14, clean freshwater was poured and the column was washed.

(a) (b) (c)

Figure 5.10. Clean freshwater was poured into the chromatographic column

The first 22 samples consisted in 30 ml of water, the last ones of 50 ml. Also 26 samples of 3 cc were collected to measure the absorbance values with the spectrophotometer. Samples from 4 to 19 were further diluted 10 times again in order to avoid problems with the measure range of the spectrophotometer Lambda 25-PerkinElmer (absorbances higher than 3 are in fact not longer reliable).

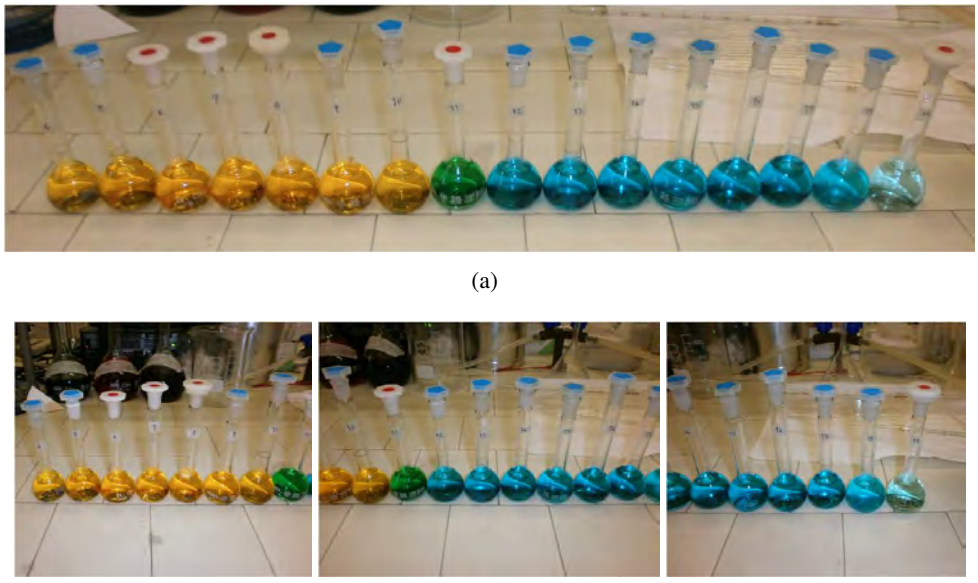

(a)

(b) (c) (d)

Figure 5.11. Samples 4-19 diluted for the absorbance measures. Sample number 4 is the first in the left

The first graph plots conducibilities for all the samples (two measures have been taken to be sure that values were correct).

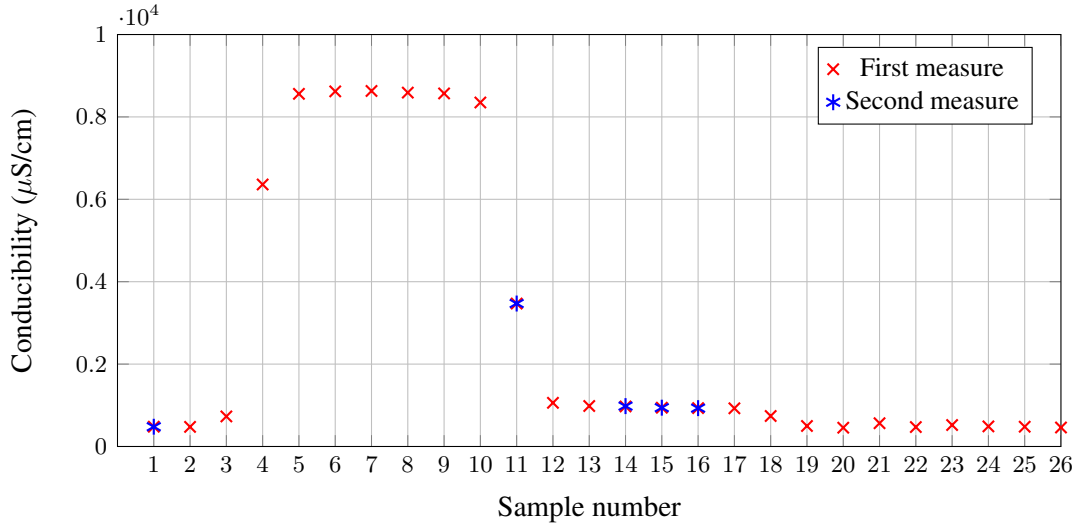

Figure 5.12. Conducibility of samples

The second one reports absorbances of non-diluted samples. Absorbances for samples 4-19 are not reported in this graph because these values need to be multiply 10 times to be directly correlated with the others.

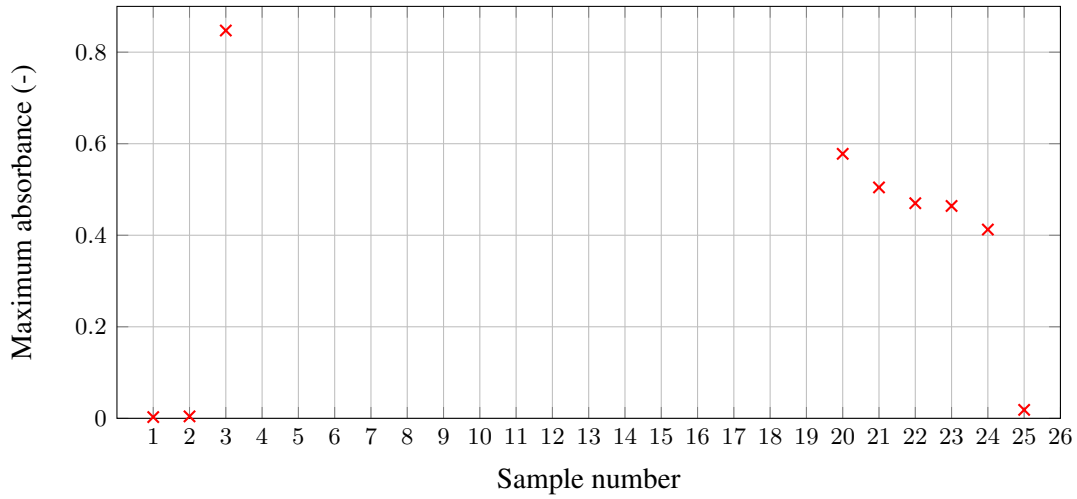

Figure 5.13. Absorbances of non-diluted samples

Absorbance is a quantitative measure expressed as a logarithmic ratio between the radiation falling upon a material and the radiation transmitted through a material:

$$A_\lambda = -log_{10}\left(\frac{I_1}{I_0}\right) \tag{5.1}$$

where A_λ is the absorbance at a certain wavelength of light λ, I_1 is the intensity of the radiation that has passed through the material (transmitted radiation), and I_0 is the intensity of the radiation before it passes through the material (incident radiation).

Figure 5.14 represents the tail of the previous graphs (samples from 20 to 26).

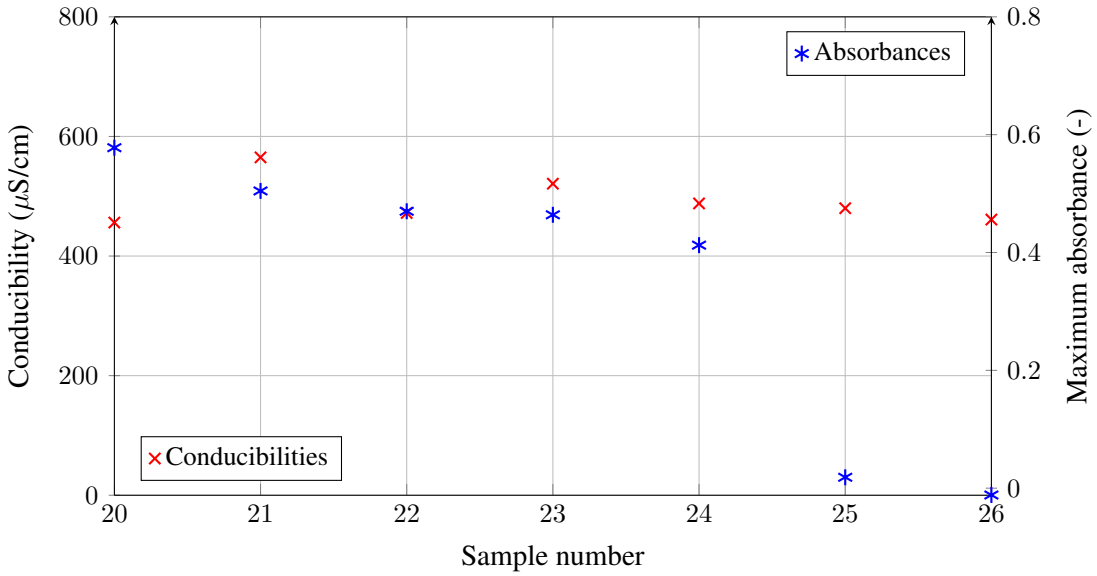

Figure 5.14. Conducibilities versus absorbances for samples 20-26

It is interesting to point out that, in this phase, absorbance has not got the same trend of conducibility. This is because the last two samples are the white ones (uncoulored freshwater). Conducibility is nearly constant in this phase because all samples consist of freshwater.

Conducibilities and absorbances for samples 4-19 are then reported. These measures are not directly correlated because samples for the absorbance measures have been diluted 10 times again. The important point is however that the trend of absorbances and conducibilities is the same.

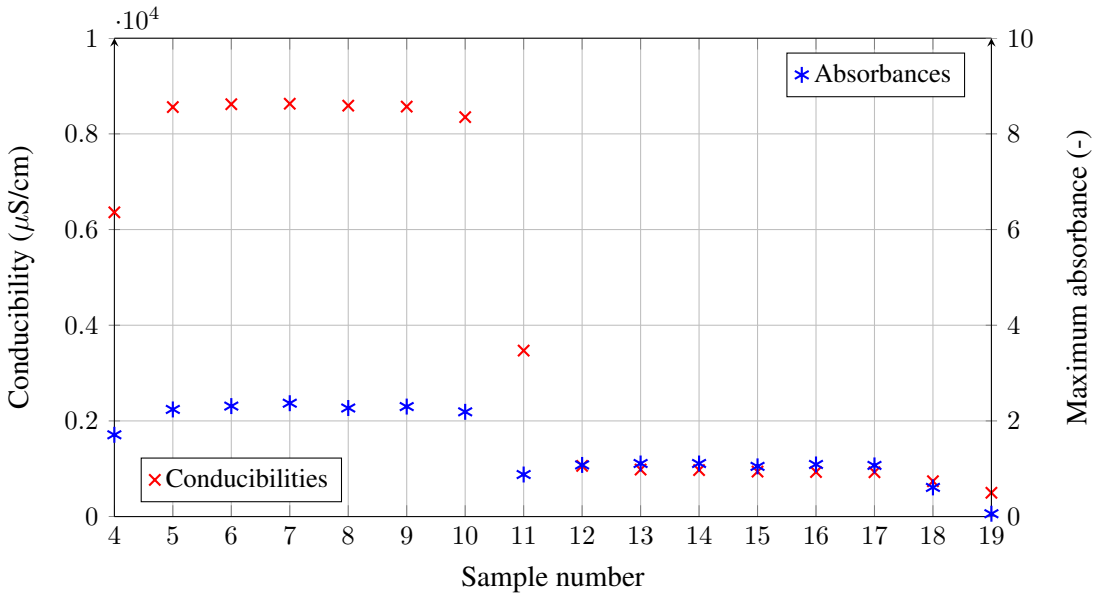

Figure 5.15. Conducibilities versus absorbances for samples 4-19

Then, absorbances of diluted samples have been multiplied 10 times to visualize the full graph. It is evident that absorbance has the same trend of conducibility and so food dye can be used as a tracer to visualize salt concentration of the experiments.

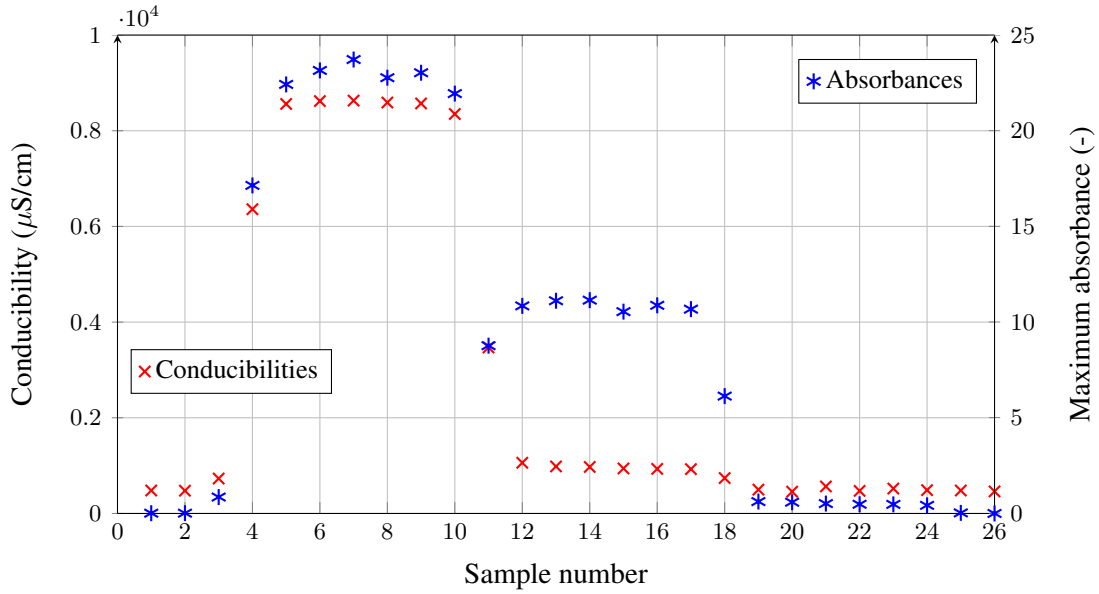

Figure 5.16. Conducibilities versus absorbances for all samples. Two colours column test case

In Figure 5.17 absorbances versus the various wavelenght for samples 4-19 (diluted ones) are reported. It is interesting to point out that yellow samples have a maximum for a wavelenght of around 425 nm, while the blue ones have a peak at around 650 nm. Sample 11 (green dashed line in the graph) is the green one and it is characterized by two peaks of absorbance as the result of two primary colors (blue and yellow).

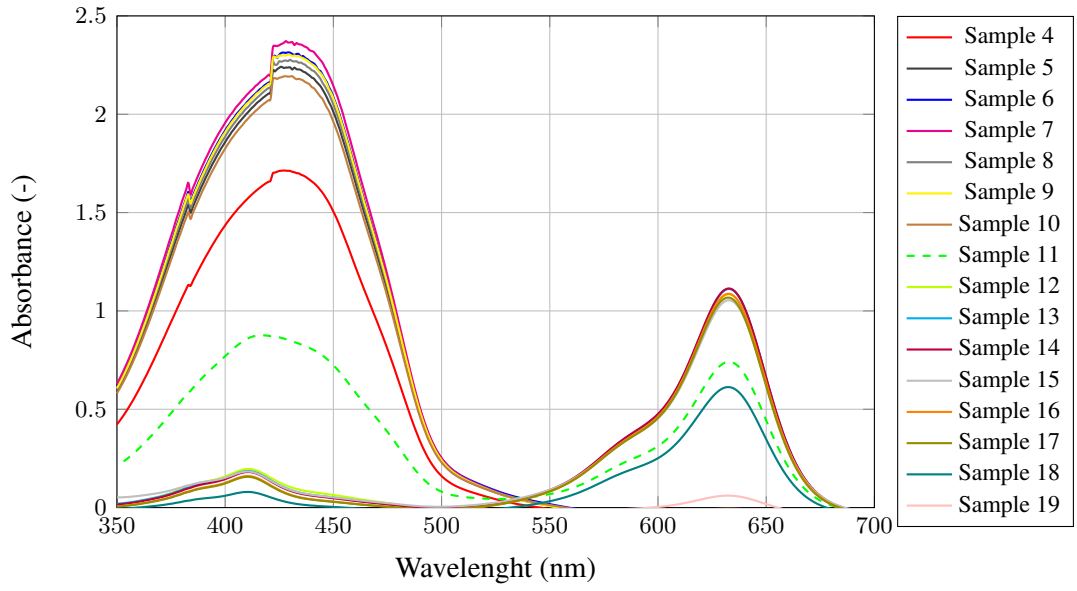

Figure 5.17. Absorbances versus wavelenght for samples 4-19

5.2.2 One colour column test

The second test was realized using only yellow food dye to mark saltwater. In this case yellow saltwater was diluted 20 times (respect to the suggestion of the maker of mixing 8 g of dye in 0.5 liters of water) with uncoloured saltwater. In this way conducibility remained the same of the original mixture. Also in this case the column was filled with 400 g of glass beads that were compacted beating the device by hand. The column was then saturated with 200 cc of uncoulored saltwater. After the saturation, yellow saltwater was poured and sampling began. A total number of 39 samples were collected. The first visible yellow sample was number 5, sample 6 was light orange, sample 7 was orange.

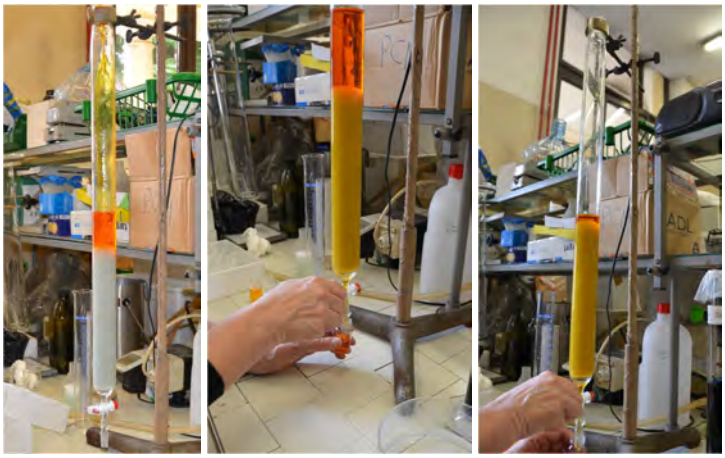

(a) (b) (c)

Figure 5.18. Yellow saltwater was puored into the saturated chromatographic column

After sample 13, 200 ml of clear freshwater were poured into the column.

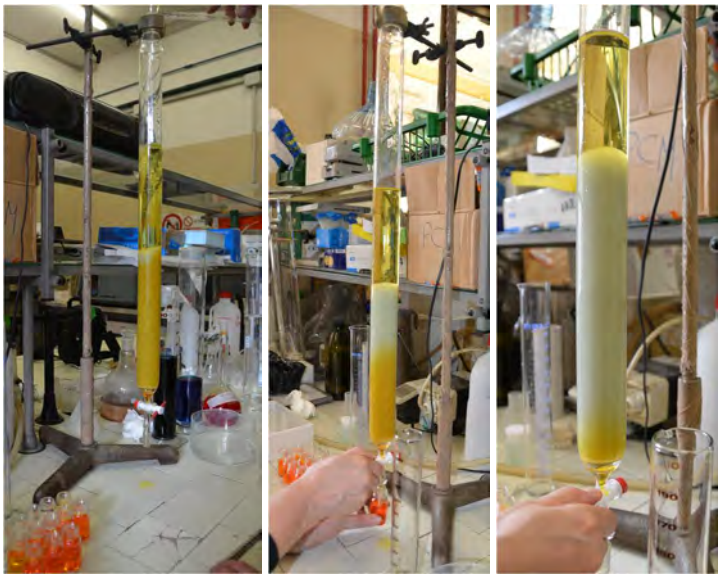

(a) (b) (c)

Figure 5.19. Clean freshwater was puored into the saturated chromatographic column

From sample 19 the colour began to decrease, so also conducibility had to decrease. 100 cc of clean freswater was poured in the column after samples 25 and 30. After sample 34, freshwater was poured into the column again.

Absorbances were measured for samples 4-34. Because colour resulted again too intense to fall within the measure range of the spectrophotometer, samples 6-20 were diluted again by dissolving 2 ml of them in 23 ml of deionized water (so they were diluted 1 to 12.5).

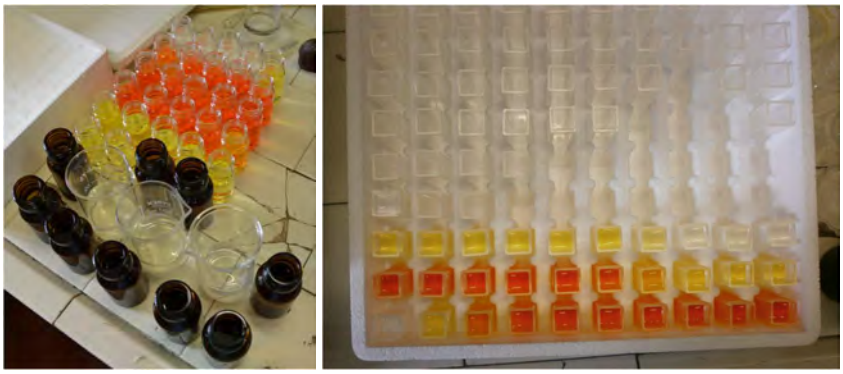

(a) (b)

(c)

(d)

Figure 5.20. Samples collected for the test (a-b) and spectrophotometer used for absorbance measures (c-d)

The results of this test are reported in Figures 5.21, 5.22 and fig:grafico7.

Figure 5.21 represents conducibilities for every sample.

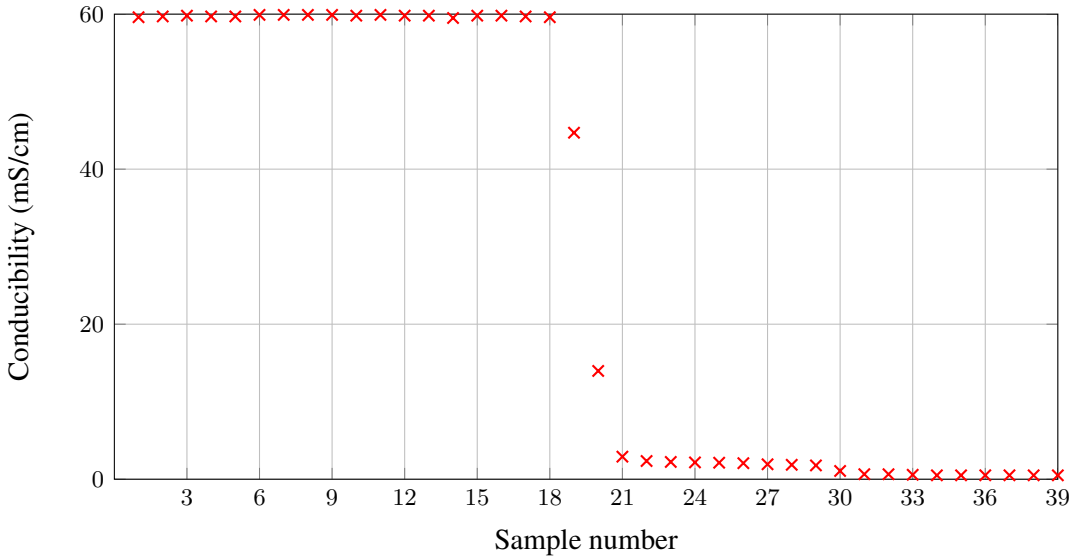

Figure 5.21. Conducibility of samples 1-39

Figure 5.22 plots conducibilities versus the cumulated volume (volume added from one sampling to another) for samples 1-34 (for last samples volumes were not taken).

The step pointed out in the plot (that corresponds to sample 30) is probably due to an experimental error.

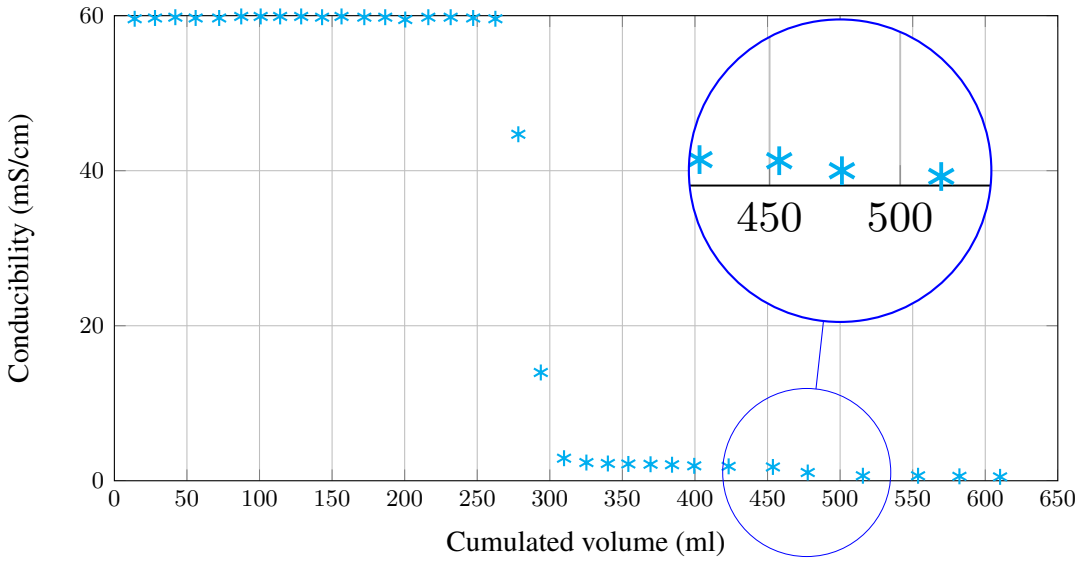

Figure 5.22. Conducibilities versus cumulated volume for samples 1-34

Figure 5.23 represents a comparison between conducibilities and absorbances at the transition between saltwater and freshwater (samples 15-25). As in the previous experiment the trend is very symilar for salt and colour, except for sample 18. This point is reasonably an error due to a improper dilution of the sample. Absorbance is in fact a measure extremely sensitive to dilution.

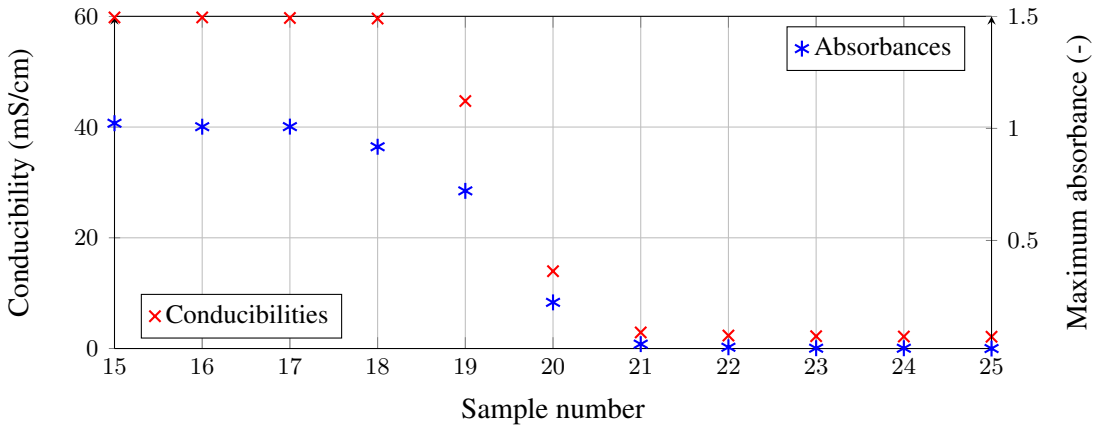

Figure 5.23. Conducibilities versus absorbances for samples 15-25. One colour column test case

The conclusion reached from the column tests was that this type of food dye is a good tracer for saltwater.

5.3 Calibration lines for saltwater

Another matter that was pointed out for the best outcome of the experiment was the necessity to withdraw from the sand-box facility a very small volume of water to measure the salt concentrations in some points of the wedge. The reason for this is to avoid a too large perturbation of the system (upconing). This implies the necessity to dilute the original samples of water in order to have a significant volume available for the conducibility measures. So the calibration line for saltwater was constructed to verify that conducibility is proportional to dilution and that these quantities are characterized by a linear relationship. This was done by preparing a series of cuvettes which contained the same volume of saltwater. Then these samples were diluted with deionized water in different proportions.

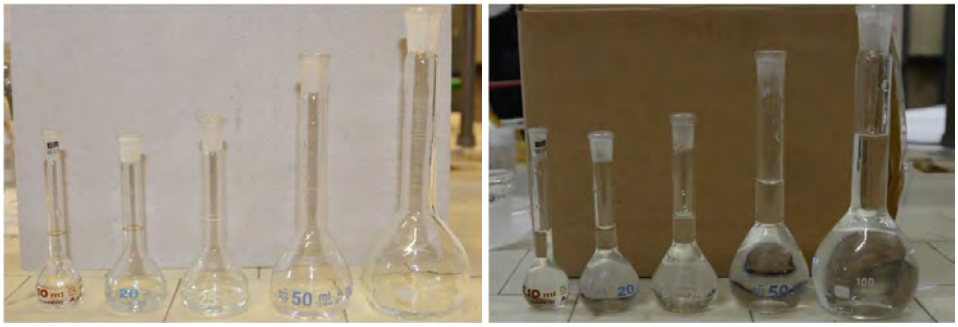

(a) (b)

Figure 5.24. Samples diluted with deionized water to obtain the calibration line

Plotting the dilution rate versus conducibility the result is a straight line intercepting the origin of axis. Four experiments were done in order to obtain a good calibration line. Results are strongly dependent by a precise dilution, as well as the reliability of the conductivity meter.

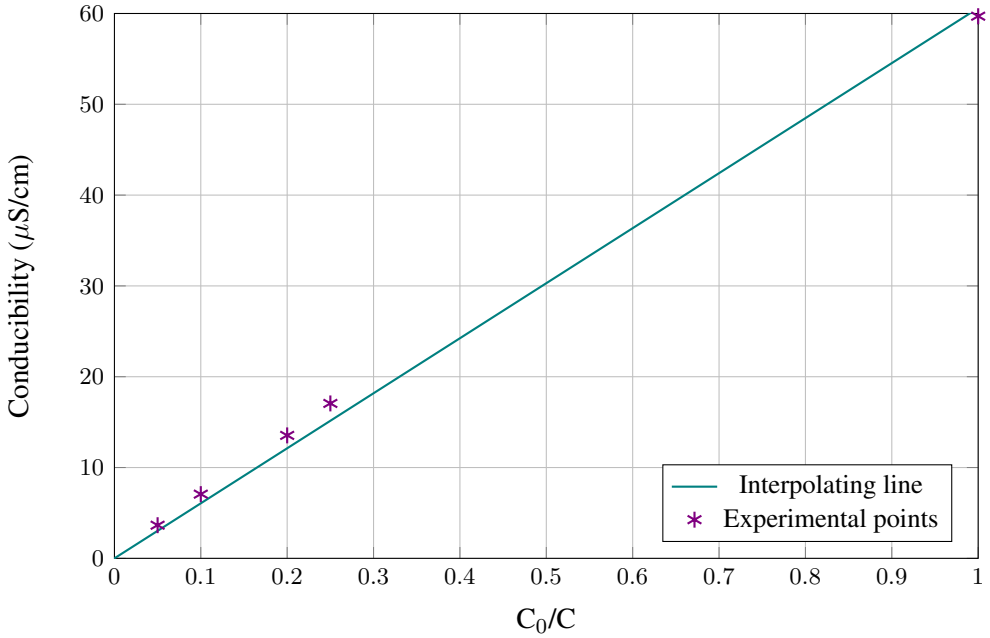

Figure 5.25. First data set. Equation of the interpolating line: y = 60.594 · x. R^2 = 0.9962

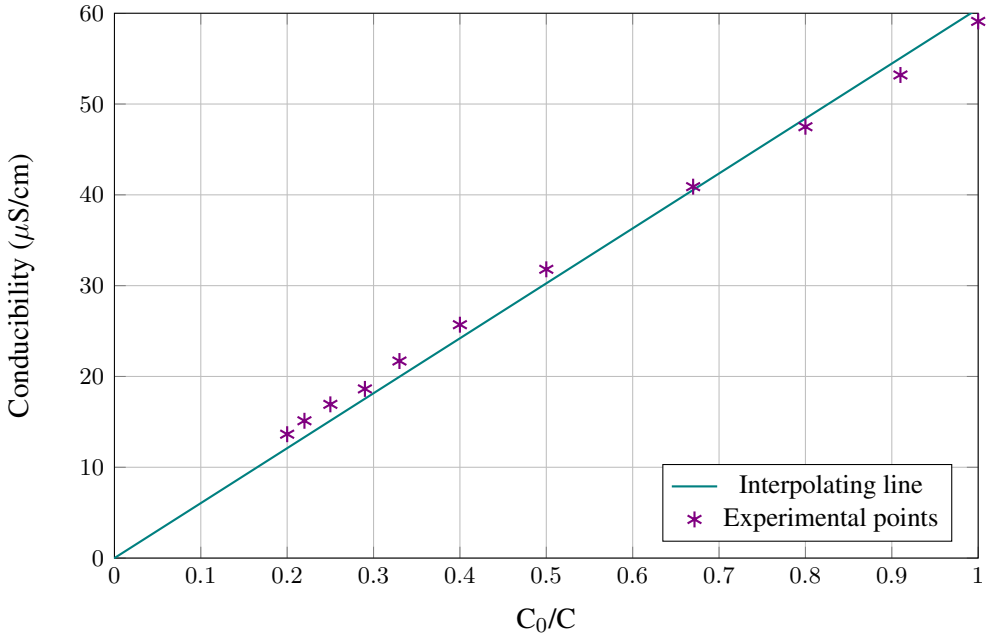

Figure 5.26. Second data set. Equation of the interpolating line: y = 60.506 · x. R^2 = 0.9912

The second calibration line is a bit higher than the expected teoretical one. This happened because samples were left for two days in laboratory until the measures were taken, and

probably evaporation caused an increase in concentration.

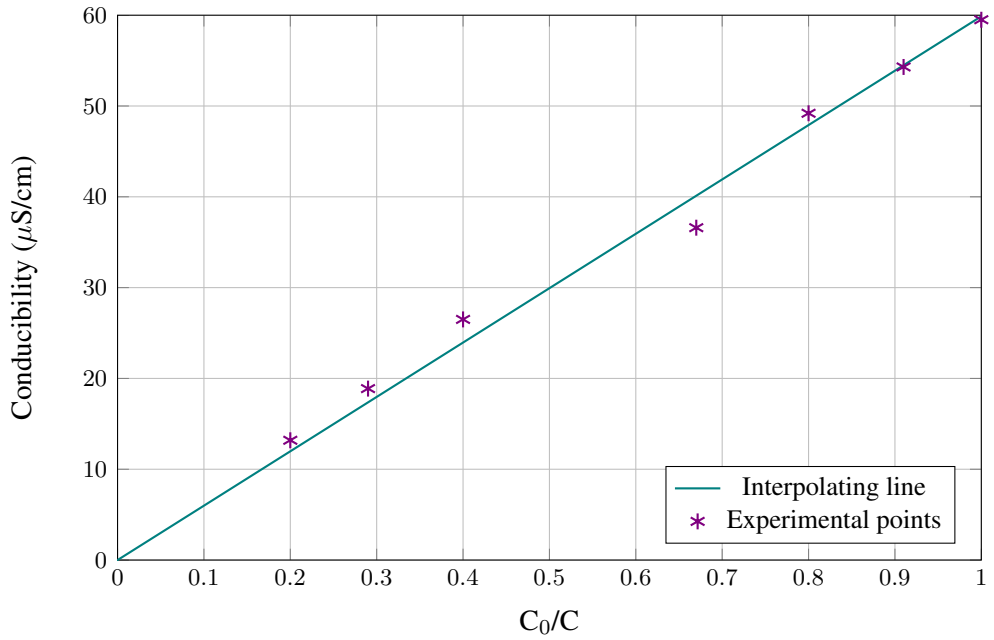

Figure 5.27. Third data set. Equation of the interpolating line: y = 59.876 · x. R^2 = 0.9877

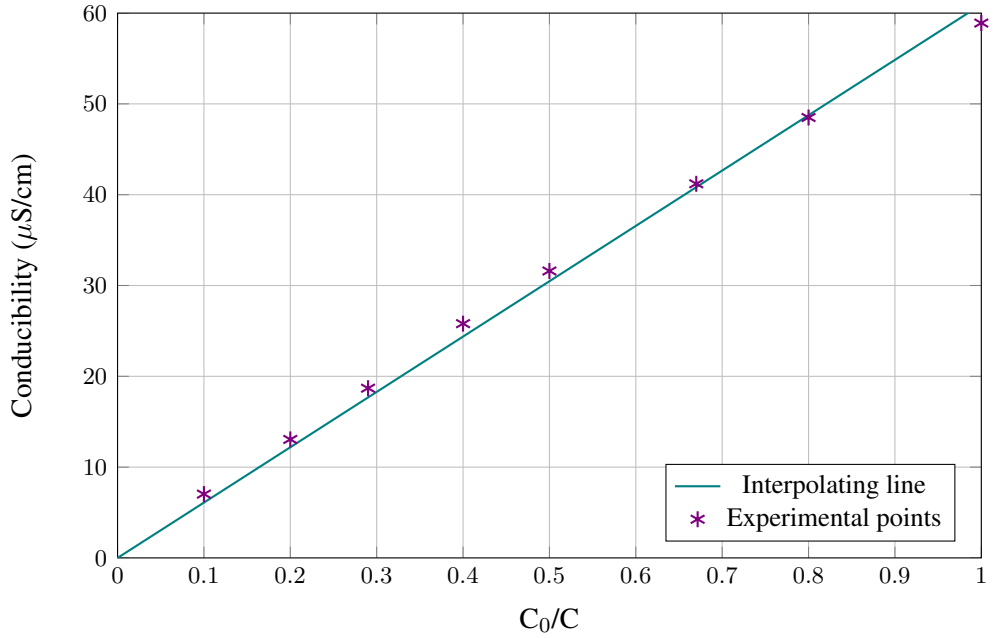

Figure 5.28. Fourth data set. Equation of the interpolating line: y = 60.939 · x. R^2 = 0.9946

The fourth calibration line is the better one; however all the cases present a deviation from the expected value that, in some case, reaches 1-2 mS/cm. This error is mainly due to a not perfect dilution that is very difficult to obtain, and surely has to be taken into account in the experimental model.

5.4 Glass beads washing test

A test was done to verify that the glass beads could be washed without any problem. A smaller sand-box was used for this test, that was characterized by an height equal to 13 cm, a whidt equal to 8 cm and a lenght that could be varied because of the device modular structure. The sand-box was filled with 12 cm of sand to reach a lenght equal to 1.3 m in order to be 3.75 times smaller than the bigger device. 21.84 kg of glass beads were used for the test, that were compated beating the sand layer every 5 cm (Figure 5.30). Beads were retained from a wire mesh dense enough to avoid the passage of the sand, supported by a small frame (Figure 5.30(c)). In the right side of the device, referred to as "downward", a small sluice gate was collocated in order to regulate the infiltration of saltwater.

Figure 5.29. Small sand-box device used for the glass beads washing test

(a) (b)

(c)

Figure 5.30. Compaction of glass beads (a-b) and wire mesh used to support the sand (c)

The sand was then saturated by filtering freshwater from the left side of the sand-box facility, referred to as "upward", as shown in Figure 5.31.

Figure 5.31. Saturation of the sand

After saturation the sand reduced its thickness, also of 0.5-1 cm in some part of the device. This was probably due to a non uniform compaction.

Saltwater was prepared by adding normal salt to freshwater. A concentration of 40.5 g of salt per liter was reached. 8 grams of red food dye were then added in 15 liters of water (Figure 5.32(b)).

(a) (b)

Figure 5.32. Saltwater used for the preliminary test

Since the densimeter was not calibrated (it measured for freshwater a density less than 1000 kg/m^3), a calibration line was built comparing the density measurements obtained from the densimeter and those obtained from a graduated column. This allowed to have consistent density measurements.

Table 5.1 reports the density measures taken with the densimeter and with the graduated column (= net weight of the column divided by its volume), obtained by dissolving different quantities of salt in 325 l of water.

Table 5.1. Density of saltwater for different quantities of dissolved salt

kg of salt	Density from the densimeter [kg/m^3]	Density from the graduated column [kg/m^3]
17,5	1028	1025.5
25	1040	1036.35
38	1061	1058.58
50	1079	1078.79
75	Out of range	1115.71

The calibration line for the densimeter is reported in figure 5.33.

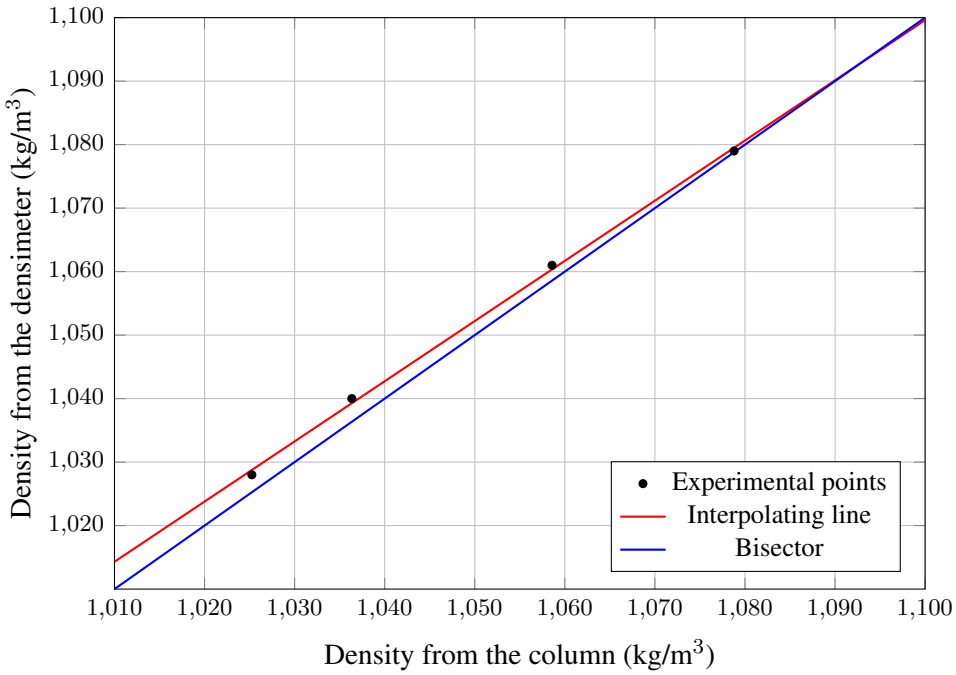

Figure 5.33. Calibration line of the densimeter. Equation of the interpolating line: y = 0.9478 · x + 57.025

From the calibration line it is possible to see that the measurements of the densimeter and the graduated column overlap themselves for high values of density, but are different for low values.

The first test in the small sand-box device was done maintaining a freshwater level upward equal to 10 cm, while the level of saltwater downward was maintained equal to 7.5 cm (i = 0.0187).

The Darcy velocity can be calculated as:

$$v = k \cdot i = 1.54 \cdot 10^{-3} \cdot \frac{0.025}{1.33} = 2{,}89 \cdot 10^{-5} \, \frac{m}{s} \tag{5.2}$$

The infiltration discharge per unit width is:

$$q = v \cdot h = 2.89 \cdot 10^{-5} \cdot 0.0875 = 2.53 \cdot 10^{-6} \frac{m^2}{s} \tag{5.3}$$

Rearranging the Dupuit-Ghyben-Herzberg relationship (reported in Section 2.4) it is possible to obtain an estimation of the salt wedge intrusion:

$$L = \frac{\varphi_0^2 \cdot K \cdot (1 + \delta)}{2q_o} \tag{5.4}$$

According to the calibration line reported in Figure 5.33 the real density of saltwater was equal to 1021.3 kg/m^3 (the density measured from the densimeter was equal to 1024-1025 kg/m^3, as it is possible to see from Figure 5.32. Assuming, as consequence, the Ghyben-Herzberg ratio δ equal to 47, the hydraulic conductivity K equal to $1.54 \cdot 10^{-3}$ m/s, q_0 equal to the discharge calculated with Equation 5.3, and the term φ_0^2 equal to:

$$\varphi_0^2 = \frac{D^2}{\delta^2} = \frac{0.075^2}{40^2} = 2.55 \cdot 10^{-6}\ m^2 \tag{5.5}$$

where D is the water level downward, the lenght of the salt wedge L is 4 cm.

It is interesting to point out how this relationship provides a good estimation of the saltwater intrusion. From the test the lenght of the wedge was equal to around 5 cm after 40 minutes. Taking into account the errors that could have been committed in maintaining levels manually, this result can be considered a good approximation.

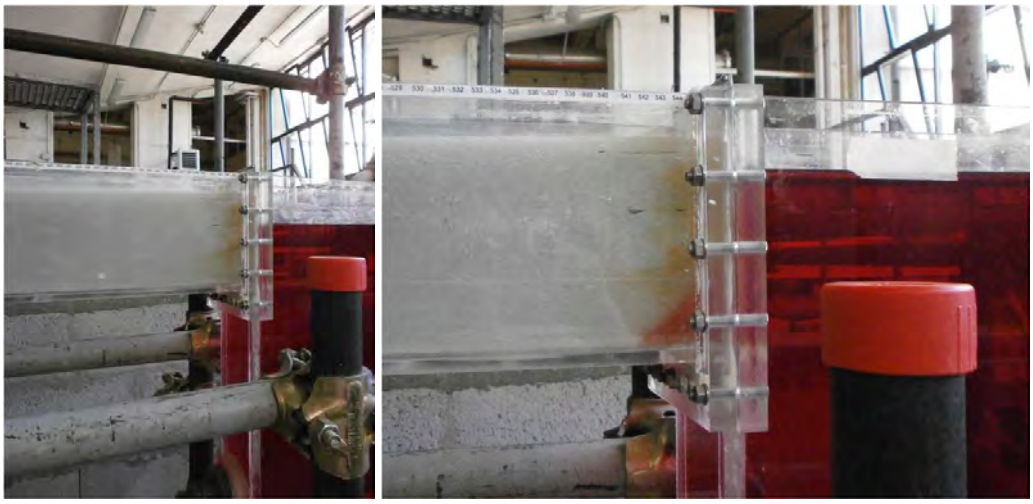

(a) (b)

Figure 5.34. Saltwater intrusion in the first test: upward level equal to 10 cm, downward level equal to 7.5 cm

In the second test the hydraulic gradient was reduced in order to decrease the infiltration discharge and increase the saltwater intrusion. The water level downward was set equal to 9 cm so the new hydraulic gradient was equal to 0.0075.

From Figure 5.35(b) it is possible to see that there was a decrease in saltwater density due to dilution with freshwater. The Figure reports the new density that was equal to around

1021 kg/m^3 from the densimeter. The expected real density is equal to 1017 kg/m^3. This implies that the Ghyben-Herzberg ratio δ becomes equal to 58. Consequently the estimated L becomes equal to 10 cm that is, also in this case, a good approximation of the physical result.

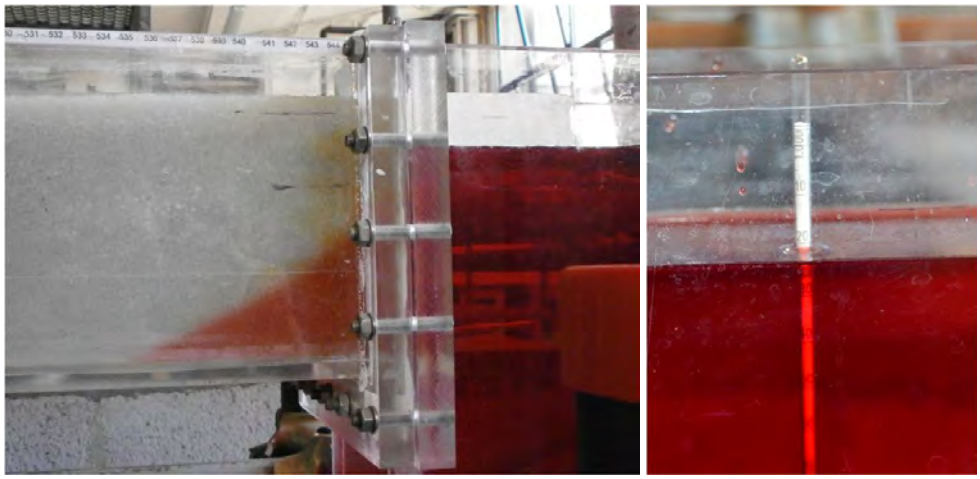

(a) (b)

Figure 5.35. Saltwater intrusion in the second test: upward level equal to 10 cm, downward level equal to 9 cm (a); reduction of saltwater density due to dilution (b)

In the third test the saltwater level was increased as much as possible in order to maximize the salwater intrusion. Then the saltwater tank was emptied and the upward freshwater level was increased in order to verify beads washing. Glass beads were flushed with around 20 l of freshwater. Figure 5.36 reports what happened.

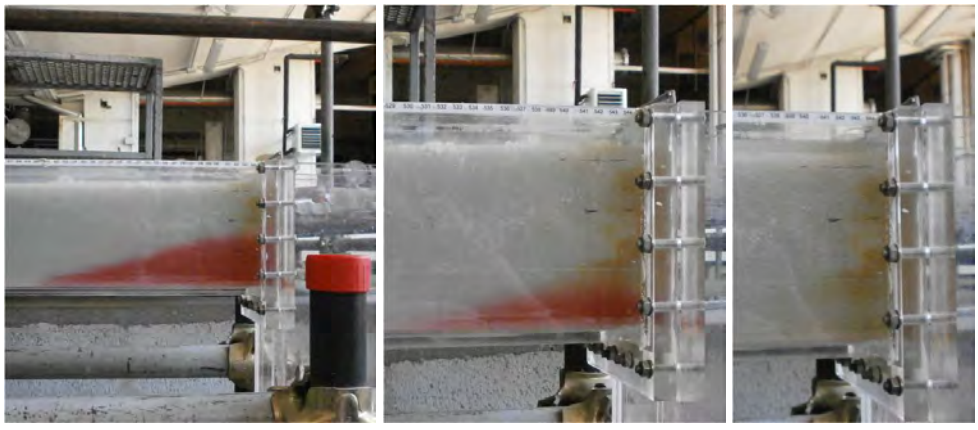

(a) (b) (c)

Figure 5.36. Washing of glass beads

Washing was carried on without particular problems. Some samples were collected to verify that spilled water was effectively clean. Conducibility of the last sample was equal to 453 μS/cm, that is the conducibility of standard freshwater.

From these tests some important matters have been pointed out. The first was the necessity to position and to compact the sand in a uniform way, that is important for the homogeneity of the material. Another point was the requirement to saturate the sand "from below" to avoid air bubbles that can disturb freshwater infiltration and alter hydraulic conductivity. Finally, these tests highlight the need to mark the colour. In fact the transition zone was not so evident.

5.5 Samples taking test

Some tests were done to verify the influence of the sampling volume on saltwater upconing. Obviously a greater sampling of water implies an higher upconing. Figure 5.37 shows the upconing of saltwater when the suck volume was equal to 1 ml (Figure 5.37(a)) and 5 ml (5.37(b)). In the second case the disturb was much more evident.

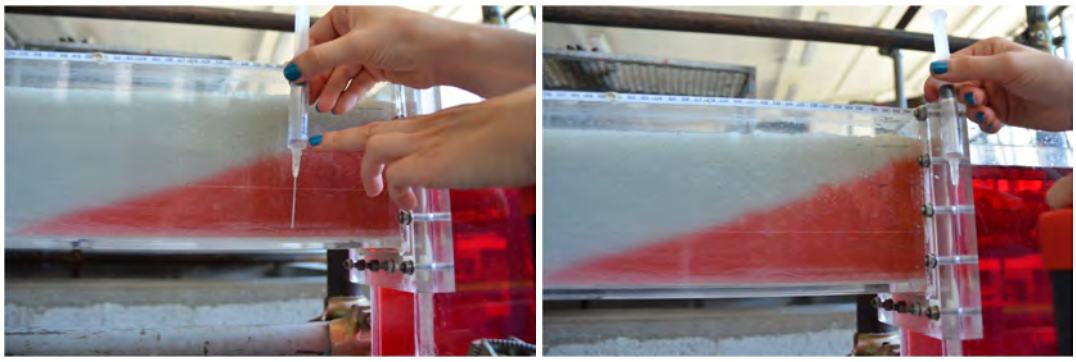

(a) (b)

Figure 5.37. Influence of the sampling volume on saltwater upconing

Finally two types of syringes were tested in order to verify the clogging of needles.

The first test was performed using a microsyringe, composed by a very thin needle. This one did not seem to suck air bubble despite the fact that it broke easily. In this case upconing was very evident probably due to a more concentrated sampling.

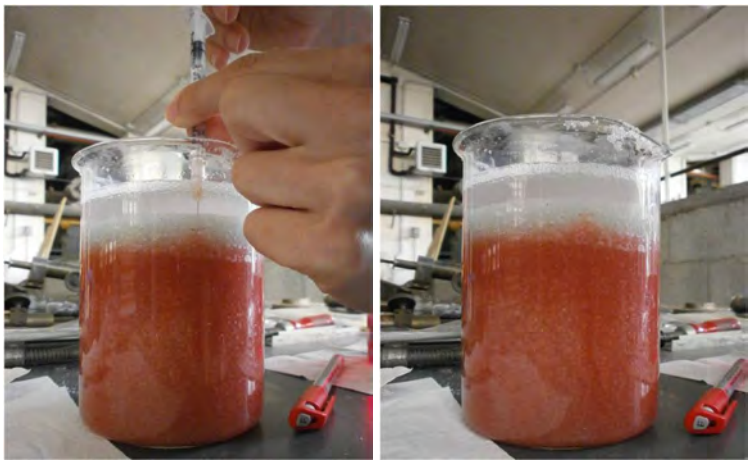

(a) (b)

Figure 5.38. Influence of the needle opening in the upconing of saltwater. Microsyringe used for sampling

The second test was performed using a normal syringe made by a larger needle that seemed to resist sampling more than the first one. Larger openings seemed to have a minor influence in upconing, but this was probably due to the fact that these needles contain more air than the others and sampling was not constant.

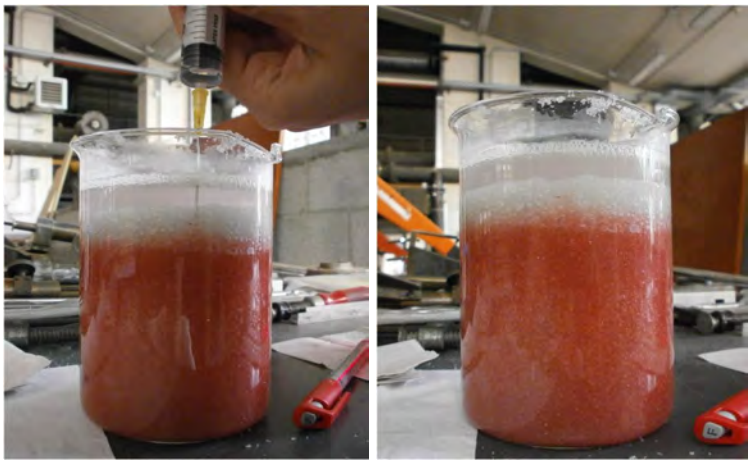

(a) (b)

Figure 5.39. Influence of the needle opening in the upconing of saltwater. Normal syringe used for sampling

Both types of needles had clogging problems. It is it is reasonable to consider that, when dealing with very long needles (40-50 cm) as in our case, very thin devices would probably resist sampling more than larger ones. However both cases presented some kind of problems. For the experiment it was decided to use normal needles for sampling, aware of the fact that they would probably be clogged after use.

Part III

Numerical model

Chapter 6

The SUTRA code

The USGS's SUTRA (acronym for Saturated-Unsaturated Transport) is a computer program that simulates fluid movement and the transport of either energy or dissolved substances in a subsurface environment. The code was written to solve the basic equations presented by Bear (1979) [7] which cover most types of groundwater flow and transport physics known. The code is routinely used for hydrological analysis and for many practical engineering studies. The original version of the code was released by Voss (1984) [47].

SUTRA employs a two- o three- dimensional finite-element and finite-difference method to approximate the governing equations that describe the two interdependent processes that are simulated: the first one is a fluid density-dependent saturated or unsaturated groundwater flow; the second one can be either the transport of solute in the groundwater or the transport of energy in the groundwater and solid matrix of the aquifer. Standard finite-element approximations are employed only for terms in the balance equations which describe fluxes of fluid mass, solute mass and energy. All other non-flux terms are approximated with a finite-element mesh version of the integrated finite-difference methods. The hybrid method is the simplest and most economical approach which preserves the mathematical elegance and geometric flexibility of finite-element simulation while taking advantage of finite-difference efficiency.

SUTRA provides, as the primary calculated results, fluid pressures and either solute concentrations or temperatures, as they vary with time, everywhere in the simulated subsurface system.

Flow simulation may be employed for 2D areal, cross-sectional and 3D modeling of saturated groundwater flow systems, and for cross-sectional and 3D modeling of unsaturated zone flow. Solute-transport simulation may be employed to model natural or man-induced chemical species transport, including processes of solute sorption, production and decay. Energy-transport simulation may be employed to model thermal regimes in aquifers, subsurface heat conduction, aquifer thermal-energy storage systems, geothermal reservoirs, thermal pollution of aquifers, and natural hydrogeologic convection systems.

Mesh construction employs quadrilateral finite elements in 2D cartesian or radial-cylindrical coordinate systems, and hexahedral finite elements in 3D systems. Permeabilities may be anisotropic and may vary in both direction and magnitude throughout the system, as may most other aquifer and fluid properties. Boundary conditions, sources and sinks may be time dependent. An option is available for storing intermediate results and restarting a simulation at the intermediate time. Output options include fluid velocities, fluid mass and solute mass or energy budgets, and time varying observations at points in the system. Both the mathematical basis for SUTRA and and the program structure are highly general, and are modularized to allow for straightforward addition of new methods or processes to the simulation.

SUTRA is compiled with a Fortran-90 code.

6.1 Physical-Matematical basis of SUTRA

The SUTRA model is a numerical solver of two balance equations for variable-density single phase saturated-unsaturated flow and single-species (solute or energy) transport (Bear, 1979) [7].
The general fluid mass balance equation that is usually referred to as the "groundwater flow model" is:

$$\left(S_w \rho S_{op} + \epsilon \rho \frac{\partial S_w}{\partial p}\right)\frac{\partial p}{\partial t} + \left(\epsilon S_w \frac{\partial \rho}{\partial U}\right)\frac{\partial U}{\partial t} - \nabla \cdot \left[\left(\frac{\mathbf{k} k_r \rho}{\mu}\right) \cdot (\nabla p - \rho \mathbf{g})\right] = Q_p \quad (6.1)$$

where S_w is the fractional water saturation, ϵ is the fractional porosity, p is the fluid pressure [kg/(ms^2], t is the time [s], U is either solute mass fraction, C [kg$_{solute}$/kg$_{fluid}$], or temperature T [°C], $\mathbf{k}$ is the permeability tensor [m^2], k_r is the relative permeability for unsaturated flow, μ is the fluid viscosity [kg/(ms)], $\mathbf{g}$ is the gravity vector [m/s^2], and Q_p is a fluid mass source [kg/(m^{3}s)].

ρ is the fluid density [kg/m^3], and it can be expressed as:

$$\rho = \rho_0 + \frac{\partial \rho}{\partial U}(U - U_0) \quad (6.2)$$

where U_0 is the reference solute concentration or temperature, ρ_0 is fluid density at U_0, $\partial\rho/\partial U$ is the density change with respect to U (assumed constant). For mixtures of freshwater and seawater at 20 °C, when U is the mass fraction of total dissolved solids, U_0 is equal to 0, and ρ_0 is equal to 998,2 kg/m^3, then the factor $\partial\rho/\partial U$ is approximately 700 kg/m^3.

S_{op} is the specific pressure storativity [kg/m $\cdot$ s^2]$^{-1}$ defined as the volume of water released from saturated pore storage due to a unit drop in fluid pressure per total solid matrix plus pore volume.

$$S_{op} = (1 - \epsilon)\alpha + \epsilon\beta \quad (6.3)$$

where α is the compressibility of the porous matrix [kg/(m $\cdot$ s^2)]$^{-1}$, and β is the compressibility of the fluid [kg/(m $\cdot$ s^2)]$^{-1}$.

Fluid velocity $\mathbf{v}$ [m/s] is given by a general form of the Darcy Law, which is commonly used to describe flow in porous media:

$$\mathbf{v} = -\frac{\mathbf{k} k_r \rho}{\epsilon S_w \mu} \cdot (\nabla p - \rho \mathbf{g}) \quad (6.4)$$

where v [m/s] is the average fluid velocity, k [m^2 is the solid matrix permeability, k_r [1] is the relative permeability to the fluid flow (assumed to be independent of direction), g [m^2] is the gravitational acceleration.

The solute mass balance and the energy balance are combined in a unified solute-energy balance equation usually referred to as the "transport model":

$$\begin{aligned}[\epsilon S_w \rho c_w + (1-\epsilon)\rho_s c_s]\frac{\partial U}{\partial t} + \epsilon S_w \rho c_w \mathbf{v} \cdot \nabla U - \nabla \cdot \{\rho c_w [\epsilon S_w (\sigma_w \mathbf{I} + \mathbf{D} + (1-\epsilon)\sigma_s \mathbf{I}] \cdot \nabla U\} \\ = Q_p c_w (U^* - U) + \epsilon S_w \rho \gamma_1^{\mathrm{w}} U + (1-\epsilon)\rho_s \gamma_1^{\mathrm{s}} U_s + \epsilon S_w \rho \gamma_0^{\mathrm{w}} + (1-\epsilon)\rho_s \gamma_0^{\mathrm{s}} \quad (6.5)\end{aligned}$$

where c_w is the specific heat capacity of the fluid [J/(kg $\cdot$ °C)], c_s is the specific heat capacity of the solid grains in the porous matrix [J/(kg $\cdot$ °C)], ρ_s is the density of the solid grains in porous matrix [kg/m^3], ρ_w is the diffusivity of energy or solute mass in the fluid, ρ_s is the diffusivity or energy or solute mass in the solid grains, $\mathbf{I}$ is the identity tensor, $\mathbf{D}$ is the dispersion tensor [m^2/s], U* is the temperature or concentration of a fluid source, γ_0^{w} is the first order solute production rate [s^{-1}], γ_1^{s} is the first order sorbate production rate [s^{-1}], γ_0^{w}

is an energy source [J/(kg · s)], or solute source [kg$_{solute}$/(kg$_{fluid}$ · s)], within the fluid (zero order production rate), γ_0^s is an energy source [J/(kg · s)], or solute source [kg$_{solute}$/(kg$_{fluid}$ · s)] within the fluid (zero order production rate).

In the case of seawater intrusion equations 6.1, 6.4, 6.5 are semplified. The fluid mass balance becomes:

$$\rho S_{op}\frac{\partial \rho}{\partial t} + \epsilon \frac{\partial \rho}{\partial U}\frac{\partial U}{\partial t} - \nabla \cdot \left[\frac{\mathbf{k}\rho}{\mu} \cdot (\nabla p - \rho \mathbf{g}\right] = Q_p \tag{6.6}$$

The fluid velocity is given by:

$$\mathbf{v} = -\frac{\mathbf{k}\rho}{\epsilon\mu} \cdot (\nabla p - \rho \mathbf{g}) \tag{6.7}$$

and the solute mass balance is:

$$\epsilon\rho\frac{\partial U}{\partial t} + \epsilon\rho \mathbf{v} \cdot \nabla C - \nabla \cdot [\epsilon\rho(D_m \mathbf{I} + \mathbf{D}) \cdot \nabla U] = Q_p(C^* - C) \tag{6.8}$$

Equations 6.6, 6.7 and 6.8 deal with variable density saturated flows with non-reactive solute transport of total dissolved solids or chloride, and with no internal production of solute.

6.2 Numerical methods

The numerical technique employed by SUTRA to solve the equations reported above is a modified two-dimensional Galerkin finite-element method with bilinear quadrilateral elements.

Solution of the equations in the time domain is accomplished by the implicit finite-difference method. Modifications to the standard Galerkin method that are implemented are the following. All non-flux terms of the equations (for example time derivatives and sources) are assumed to be constant in the region sourrounding each node (cell), in a manner symilar to integrated finite-differences. Parameters associated with the non-flux terms are thus specified nodewise, while parameters associated with flux terms are specified elementwise. This achieves some efficiency in numerical calculations while preserving the accuracy, flexibility, and robustess of the Galerkin finite-element technique (Bear et al., 1999) [49].

A modification to the standard finite-element method that is required for variable-density flow simulation is implemented in SUTRA. This modification provides a velocity calculation within each finite element based on consistent spatial variability of the pressure gradient, Δp, and the term $(\rho \cdot \mathbf{g})$, in Darcy Law. This avoids generation of spurius velocities, which would be caused by local mismatching of the discretized pressure gradient term and density-gravity term. For example, in an hydrostatic system where densities vary spatially, Δp must equal $(\rho \cdot \mathbf{g})$ to yield a zero vertical velocity. However, if Δp and $(\rho \cdot \mathbf{g})$ do not locally cancel because of the discretizations chosen, then erroneous vertical velocities are generated. The spurius velocities make it impossible to simulate a narrow zone transition zone between freshwater and seawater with the standard method, irrespective of how small a dispersivity is specified for the system.

The two governing equations, fluid mass balance and solute mass balance, are solved sequentially on each iteration or time step. Iteration is carried out by the Picard method with linear half-time-step projection of non-linear coefficients on the first iteration of each time step. Iteration of the solution for each time step is optional. Velocities required for solution of the transport equation are the result of the flow equation solution from the previous iteration.

SUTRA is coded in a modular style, making it convenient for sophisticated uses to modify the code or to add new processes. Addition of new terms to the governing equations is a straightforward process usually requiring changes to the code in very few lines.

To create time dependent boundary conditions the user must modify the subroutine BCTIME. In addition, any desired unsaturated functions may be specified by user modification of the subroutine UNSAT.

6.3 SUTRA specifications

6.3.1 Boundary conditions

For SUTRA, when no pressure value, source, or sink is specified along a model boundary, the boundary becomes closed to fluid flow. When either of these is specified, flow may occur across the boundary at that point.

SUTRA requires specifications of pressure rather than hydraulic heads, when the simulation deals with variable fluid density. The most typical specification of pressure along a vertical boundary in a cross sectional model is an hydrostatic pressure. The specified hydrostatic pressure distribution must be matched to the vertical distribution of fluid density expected along the boundary and the fluid density need not to be constant. To calculate the pressure distribution, the incremental pressure increases ($\rho_i g \Delta E_i$, where ρ_i is the mean density of fluid in vertical increment ΔE_i between adjacent nodes) should be simply summed starting at the top of the boundary, and working downward through the nodes along the boundary. Along such a boundary the only requirement is that the vertical pressure gradient is hydrostatic. An higher or lower hydraulic head along the boundary relative to that found inside the modeled area may be applied. This is done by specifying an higher or lower starting pressure as the top pressure of the boundary prior to calculating the hydrostatic distribution. The vertical distribution of the fluid density at such an arbitraty boundary is not always well known. Provost et al. (1998) [40] used a modification to SUTRA user-programmed subroutine BCTIME for time-dependent boundary conditions that implements such a self-consistent condition.

When specifying pressure at a node in SUTRA simulation, the solute concentration of any fluid that may enter the model domain at that location must also be specified. This is quite different from specifying the solute concentration of the fluid within the model itself. The fluid that enters at the specified pressure node first must mix with fluid existing within the model at that point, before the model concentration can be determined. Specifying concentration directly in a model is possible, but is usually not realistic for representing field situations.

Another means of adding solute to a model is used by SUTRA's solute source, which contributes solute mass without water to the system.

Another consideration for cross-sectional simulation of variable density flow concerns numerical precision. When pressures are specified along a boundary they must be given with the complete precision of of values stored in the computer, usually 15 significant digits of computer double precision (Bear, 1999) [48]. In fact, when fluid velocities are calculated by SUTRA, very small spatial differences in pressure may give rise to fluid flow at any depth.

6.3.2 Initial conditions

Because the pressure distribution in a variable-density fluid depends on the density distribution, the initial pressures for a simulation may not be specified indipendently of the initial concentration. The initial pressure field must be consistent with the boundary conditions affecting the pressures.

Creation of a series of consistent pressures requires a preliminary run of the SUTRA code. This preliminary run is a steady-state pressure solution using the desired flow-field

boundary conditions, the desired initial concentration field, and arbitrary (for example blank) initial pressure. The resulting steady-state pressures calculated by SUTRA are consistent with the initial concentrations and boundary conditions. The arbitrary pressures in the initial conditions input file should then be replaced with the new consistent pressures.

A further complication occurs when the initial concentration distribution for the time period to be simulated is not well known. If concentrations (and fluid densities) are known at only a few points within the region to be modeled and are assigned assumed initial values in-between, then false flows will be calculated by SUTRA. One practical solution is to run a simulation starting at some simple initial conditions. It should be run in a transport mode until such time when the simulation result is similar to that observed in the field. This simulation result may then be used as initial conditions for the desired transient analysis. Another solution is to assume that the known conditions of initial concentration are approximately in steady state. This also requires a second preliminary run to establish the steady-state conditions. This run may be started with any concentration distribution, but starting with a guess that is closer to the correct steady-state solution will result in faster convergence and shorter real simulation times. The SUTRA simulation should be transient and should use the set of boundary conditions applicable at the time at which the concentration field is desired. The simulation is continued until the concentration distribution no longer changes. Most often this is the longest and most difficult simulation of an entire modeling analysis, as it begins with poor initial conditions for pressure and concentrations. Subsequent transient analysis use this result as an initial condition. These are quiete often easier to carry out and suffer less from any numerical instability. This approach, though appealing and simpler than the one suggested above, beacuse it allows the assumption than the system is at steady state, suffers from the same ambiguity as before. It therefore also requires sensitivity runs to determine the impact of the underlying assumed model structure on the aspect of the system being studied by the simulations.

6.3.3 Spatial discretization

For most constant-density transport simulations with SUTRA, in order to avoid general oscillations in the concentration distribution, finite element size must be limited. The limit is at most four times the longitudinal dispersivity (where size is measured along the direction of fluid flow). This is the mesh Peclet number criterion presented by Voss (1984) [47] where the mesh Peclet number is defined as:

$$Pe_m \simeq \frac{\Delta_L}{\alpha_L} \tag{6.9}$$

In the case of variable-density simulations, this requirement may often be relaxed. Oscillation occurs only in regions where there is a significant concentration gradient along the flow direction. Many seawater intrusion situations exhibit very low concentration gradients along the the flow direction, due to the fact that variable-density flow phisycs causes freshwater to flow parallel to, rather than towards, the inland margin of intruding seawater. Thus, in many cross-sectional models where flow tends to be parallel both to the land surface and the intruding seawater wedge, the lateral element size may safely violate the mesh Peclet number criterion by ten times or more.

To carefully reproduce narrow transition zones, vertical discretization often need to be finer than lateral discretization. An adequate rule of thumb is that $\Delta_{L,T} < 10\ \alpha_T$ where $\Delta_{L,T}$ is the local element dimension transverse to the flow direction.

Narrow transition zones generally occur when transverse dispersion is the major mixing process, or in some coastal systems where low-amplitude tidal pumping generates the zone.

In other types of variable-density systems where longitudinal mixing is more significant, discretization must be adjusted according to the mesh Peclet number criterion.

In cross-sectional variable-density simulation, freshwater flow may converge to a narrow disharge area. In such areas the flow velocity increases significantly near the discharge. This is the most likely area for another type of numerical instability to develop in a SUTRA simulation despite the fact that it was properly discretized for the mesh Peclet number criterion. The instability may tipically appear as a stationary region of negative solute concentration around the discharge area. This situation is most often alleviated by finer spatial discretization (along the flow direction) near the discharge and by finer time discretization. Occasionally the time or space discretization required to remove instability would be impratictically small. The two alternatives are suggested. The first one consists in applying higher values of dispersivity near the discharge. The second one is to ignore instability if it does not disturb the rest of the simulated field, and if the area of interest is sufficiently far away from instability.

For coastal seawater intrusion problem with two water types (freshwater and seawater), when transverse dispersivity and molecular diffusivity are set both to zero, the exact steady-state solution contains a perfectly sharp interface between freshwater and seawater. For the type of finite-elements used in SUTRA, a perfectly sharp interface is not possible to represent in the mesh, and for this problem, a more gradual transition will be the result. Such a simulation will give an indication of the minimum width of the transition zone that the mesh can represent. If this minimum width is much smaller than the minimum width required for the analysis, than the discretization across the zone is fine enough. If the minimum zone has about the same width as the required zone, then the simulation is not reproducing the variable-density flow and transport physics sufficiently well; rather, the transition zone that appears is caused by poor discretization. In this case, further mesh refinement is required in the direction across the transition zone, usually vertically.

6.3.4 Iteration and time discretization

Iteration refers to re-solving each time step a number of times in order to resolve physical or chemical non-linearities. It does not refer to iterations that may be required to solve the matrix equations for the SUTRA unkowns when using an iterative matrix solver.

The non-linearity in variable-density flow is primarly systematic (dependent on the coupling of the flow field with the fluid density distribution) rather than parametric (as in unsaturated flow where parameter values themselves are highly dependent on the state of the system). The parametric non linearity is generally mild as density is nearly a linear function of concentration. In variable-density systems with energy transport the parametric non-linearity is greater due to the exponential dependence of fluid viscosity on temperature, but it is still only a minor non-linearity.

There is not a-priori rule that determines when to use iterative solution for a variable-density flow problem. The practical approach is to try a simulation twice: with and without iteration. If iteration provides a different result, then iteration must be used for similar simulations. The same philosophy applies to selection of time-step size. A simulation should be tried with a reduced step size. If the result is different, then an even smaller time step should be tested and used.

Convergence of the iterative process in SUTRA is considered to have occurred when the absolute change in all pressures and concentrations between subsequent iterations drops below user-selected values.

6.3.5 Proper use of the physical units in SUTRA

In order to evaluate the output of the SUTRA code in an appropriate way it is indispensable to use the proper physical units for the various physical parameters in the input. As a general rule all the variables should be used with the same physical based units. The most suitable unit system is the MKS (meters, kilograms, seconds system). Given this system the following units should be used for the density, the viscosity, the permeability and the hydraulic pressure, which are all inputed into the program: density ρ = 1000 kg/m^3; viscosity μ = 0,001 kg/(m $\cdot$ s); permeability k in m^2; pressure head p_{bc} in kg/(m $\cdot$ s^2). Other important parameters to be imputed into the programs are the flow source and the solute flow source in kg/s. If these values are specified in such a way, then the concentration has to be given in kg_{solute}/kg_{flow}, which is the ratio of the relative mass fraction of the solute to the mass of the flow.

6.3.6 Model setup

- **Model domain**
  The spatial cross-sectional domain of the SUTRA model should be selected to include the areas of interest for seawater intrusion, and is ideally extended to natural hydrogeological boundary such as practically impermeable units, groundwater divides, or surface water bodies. Often is not possible to end the model domain at natural boundaries. Many coastal models have a seaward vertical boundary located at an arbitrary point offshore.

- **Thickness**
  When using SUTRA for seawater intrusion in 2D cross section, the model thickness refers to the direction perperficular to the plane of the vertical section. The arbitrary assignmenent of some or all pumping in an aquifer to an arbitrary thick cross section is the main ambiguity that exists in 2D modeling of a 3D system. An approach may be to make the model thickness equal to the entire width of the aquifer system. Then it is natural to include all sources in the aquifer, such as vertical recharge and pumping within the section. This will give an aquifer-width-averaged simulation that will likely underestimate the amount of seawater intrusion occurring near any specific well at a given pumping rate. In contrast, taking all pumping from a unit-thickness section would likely overestimate the intrusion. A practical 2D approach must be based on trying a range of source values assigned to the section considered and observing the resulting range of simulation responses.

- **Permeability**
  Variable-density flow field are sensitive to permeability distribution. Regions of constant permeability differing by as little as about ten times in permeability will likely host separately circulating flow cells. Thus, initial parameterization of permeability in a new model should consist of, at most, two or three regions of uniform permeability.

- **Dispersivity**
  The dispersion of the solute in a porous media is due to mechanical dispersion and molecular diffusion. Mechanical dispersion is due to the inhomogeneities of the porous media. The void inhomogeneites in the porous media cause fluctuation of the mainstream flow velocity in longitudinal and lateral directions which results in a spreading of the concentration front. Molecular dispersion is a consequence of the concentration differences at the molecular level of the solute. According to Fick's Law any concentration gradient will induce a mass transport in the direction of the gradient.

Briefly:

$$D = D_m + D^* \tag{6.10}$$

with D_m the coefficient of mechanical dispersion which is given by:

$$D_m = \alpha_L \cdot v \tag{6.11}$$

where α_L is the dispersivity and v is the groundwaterflow velocity.
D^* is the coefficient of molecular diffusion which is of the order of 10^{-9} m^2/s.
α_L is very much scale-dependent and might vary from o(0,01 m) in the laboratory to o(100 m) in the field (Koch et al., 1990) [33]. In a porous media the effect of the mechanical dispersion is generally some orders of magnitude more important than the effect of the molecular diffusion.

SUTRA allows both the longitudinal and transverse dispersivity values to vary depending on the direction of flow. Sometimes dispersivity has an unimportant effect on results (for example when the width of the simulated transition zone is not of concern). Then it may be simply be set to a value that guarantees spatially-stable concentration solutions.

Flow direction-dependent dispersivity is indeed a useful generalization in some cases. For example it may be expected that flow parallel to layering in a layered medium and flow perpendicular to the layering do not necessarily have the same longitudinal dispersivity.

- **Porosity**
  An appropriate value for porosity is not always easy to select for transport modeling in eterogeneous aquifers. Grain size analysis and other laboratory measurements give a value of the total porosity, whereas the transport equations employs the porosity associated with the fluid that moves (effective porosity). These two values can be quite different in heterogeous media. Flow may occur within only a few percent of the total pore volume, while most of the water volume exists in pores within low-permeability regions located between the flowing channels. For relatively fast flow through such a medium, the existance of the static water may be neglected and porosity may be set to the value of the effective porosity. If not available from a large-scale tracer test, this porosity value must be determined in an ad-hoc manner or by trial and error. In contrast, for very slow-flow through such a system, the flow in permeable channels is not much faster than through the low-permeability regions, and solute concentrations may equilibrate between flowing channels and relatively-immobile zones through solute diffusion. In this case, an appropriate value of effective porosity tends to be higher, approaching the value of total porosity.

  In some variable-density systems, there is a wide range of fluid velocity with the lowest values usually found in deep dense fluids. In such a case, and when the medium is heterogeneus, there is no one value of effective porosity that is appropriate everywhere, although the average permeability, total porosity and structure may be constant throughout. In the fast-flowing portion of the system, the nearly immobile water does not partecipate to the transport. In the slow-flowing portion, the immobile water may act as source or sink of solutes with transport through the immobile water by slow flow or diffusion. Thus, to some extent, the appropriate value of effective porosity depends on fluid velocity which itself may be time-dependent. SUTRA is not based on dual-porosity type of formulation. It allows only time constant porosity to be specified.

Chapter 7

Numerical model details

The numerical description of the experimental setup involves a rectangular domain of 500 by 45 cm, as shown in Figure 7.1. The numerical model intended to reproduce the dimensions of the sand-box facility. The mesh consists of 22500 elements each of the size equal to 1 cm. The thickness of the model was set equal to 0.3 m (remind that the thickenss in SUTRA refers to the direction perpendicular to the plane of the vertical direction).

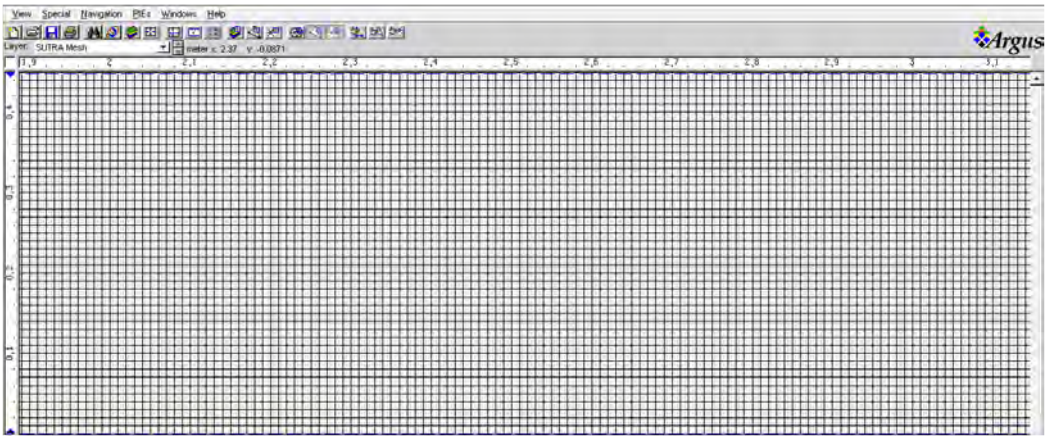

Figure 7.1. Mesh of the numerical model

The parameters used to implement the model derived both from the preliminary laboratory tests (for permeability and porosity), and from literature when preliminary laboratory investigations were not possible (for example in the case of dispersivities). This implies that the results reported in the following Sections are not perfect predictors of the physical results, but the numerical model was useful in order to have a qualitative estimation of the physical reality.

The main parameters assumed in the model are reported:

- maximum permeability = minimum permeability k = 1.57 $\cdot$ 10^{-10} [m^2]. It derives from the hydraulic conductivity calculated in laboratory for compacted sand K = 1.54 $\cdot$ 10^{-3} [m/s] according to the relation $k = (K \cdot \mu)/(\rho \cdot g)$;
- porosity ϵ = 0.367. The porosity is set equal to the mean values found for compacted beads in laboratory.
- density of the saltwater ρ_{sea} = 1025 [kg/m^3]; in this case an average value was assumed.

- concentration of salts in seawater C_{sea} = 0.0357 [kg (dissolved solids)/kg (seawater)]. 35 [kg/m^3] is the value for concentration theoretically necessary to obtain the previous reported saltwater density;
- variation of seawater density respect to concentration $\frac{\partial \rho}{\partial C}$= 700 [kg(seawater)]^2/[kg(dissolved solids) $\cdot$ m^3]
- density of freshwater ρ_0 = 1000 [kg/m^3], assumed as the density of fluid at the base concentration (0 in the model);
- density of the solid grains ρ_s = 2500 [kg/m^3];
- gravity acceleration g = - 9.81 [m/s^2];
- molecular diffusion D_m = 1.477 $\cdot$ 10^{-9} [m^2/s];
- longitudinal dispersivity coefficient α_L = 0.0075 [m]; this topic is developed in section 7.2.
- tranversal dispersivity coefficient α_T = 0.00075 [m]; the value of the tranversal dispersivity was always assumed one order of magniture lower than the longitudinal dispersivity;

Initial conditions were obtained through a preliminary simulation in order to have consistent steady pressures. It was assumed that, at the beginning, the sand-box facility was filled with 42 cm of freshwater.

Boundary conditions were forced setting the hydrostatic pressures and the concentrations at freshwater and saltwater sides. Pressure of seawater was calculated as ($\rho \cdot g \cdot h$) = (1000 + 700 $\cdot$ 0.0357) $\cdot$ 9.81 $\cdot$ (0.40 - Y) [kg/(m $\cdot$ s^2)], where (0.40 - Y) is the depth. No boundary conditions were forced at the top and bottom of the computational domain, and in the nodes above the fixed water levels.

Unsaturated properties associated to a coarse sand were chosen to implement the model. The procedure to obtain the correct saturation-capillary pressure relation is reported in section 7.1.

Transient simulations (Δt = 1 min) were implemented to investigate the advancing of the salt wedge, to predict the effects of pumping, of an infiltration discharge and the effectiveness of a barrage respect to different positions. Two sensitivity analysis for permeability and dispersivities were also performed.

7.1 Saturated-unsaturated properties

"Unsaturated flow" is a term used to describe the flow of water and water vapor through a soil where the void space is partially filled with air. Essentially, this is a case of simultaneous flow of two immiscible fluids, water and air, except that often the assumption is made that air is practically immobile.

The volume of void space that may be fully or partly filled with gas or liquid, is commonly referred to as the pore volume. Porosity ϵ(x,y,[,z],t) [-] is defined as a volume of voids in the soil matrix per total volume of voids plus matrix.

As said in chapter 6, SUTRA employs only one type of porosity, ϵ. In some instance there may be need to distinguish between a porosity for pores which take part in the fluid flow (effective porosity) and pores which contains both stagnant and flowing fluid (total porosity).

In SUTRA the fraction of total volume filled by the fluid is ϵS$_w$ where S_w(x,y,[z],t) is the water saturation (volume of water per volume of voids). When S_w is equal to 1, the void

space is completely filled with fluid and is said to be saturated. When S_w is minor than 1, the void space is only partly flled and is referred to as being unsaturated. When S_w is minor than 1, water adheres to the surface of solid grains by surface tension effects, and the fluid pression is less than the atmospheric. Fluid pressure, p, is measured with respect to background or atmospheric pressure. The negative pressure, p_c(x,y,[z],t) [M/(L · s^2)], is defined as capillary pressure, and exists only for p < 0. Briefly:

$$\begin{cases} p_c = -p & \text{if p} < 0 \\ p_c = 0 & \text{if p} \geq 0 \end{cases}$$

In a saturated porous medium, as fluid pressure drops below zero, air may not directly enter the void space, but may enter suddely when a critical capillary pressure is reached. This pressure p_{cent} [M/(L · s^2)] is the entry pressure (or bubble pressure). Typical values for p_{cent} range from about $1 \cdot 10^3$ kg/(m · s^2) for coarse sand and $5 \cdot 10^3$ kg/(m · s^2) for fine silty sand (Voss and Provost, 2010) [48].

The relation between fluid saturation and capillary pressure in a given medium is typically determined by laboratory experiments and, except for the portion near bubble pressure, tends to have an exponential character.

Different functional relationships exists for different materials. In addition a number of general functions with parameters to be fitted to laboratory data are available. Because of the variety of possible functions, no particular function is setted by SUTRA and any desired function may be specified for simulation of unsaturated flow (Voss and Provost, 2010) [48].

In this study it was decided to implement the Van Genucthen model. According to this model the soil water content as a function of the pressure head is given by:

$$\Theta = \Theta_r + \frac{\Theta_s - \Theta_r}{[1 + (\alpha h)^n]^m} \tag{7.1}$$

In the equation h is the pressure head and it is assumed to be positive (Van Genuchten, 1980) [46].

Θ_s and Θ_r indicate the saturated and residual values of the soil water content, respectively. Θ_s is equal to the porosity n and it is always available as it is easily obtained experimentally. The residual water content is defined as the water content for which the gradient dΘ/dh becomes zero. From a practical point of view it seems sufficient to define Θ_r as the water content at some large negative value of the pressure head, for example at the permanent wilting point (h = − 15 cm) (Van Genuchten, 1980) [46]. Also Θ_r may be measured experimentally, for example, by determining the water content on very dry soil.

α, m and n are the model parameters. According to Mualem model m can be calculated as follow (Van Genuchten, 1980) [46]:

$$m = 1 - \frac{1}{n} \tag{7.2}$$

Equation 7.1 contains four independent parameters (Θ_r, Θ_s, α, and n) that, in this study, have been estimated from soil-water retention data, fitting the curves reported in Salandin (1988) [42] with the experimental ones for four class of soil, respectively coarse sand, fine sand, silt and clay.

The three parameters of the model estimated for coarse sand are $n[-] = 2.8$, $\alpha[1/Pa] = 5.61 \cdot 10^{-4}$, $\Theta_r/\Theta_s[-] = 0$:

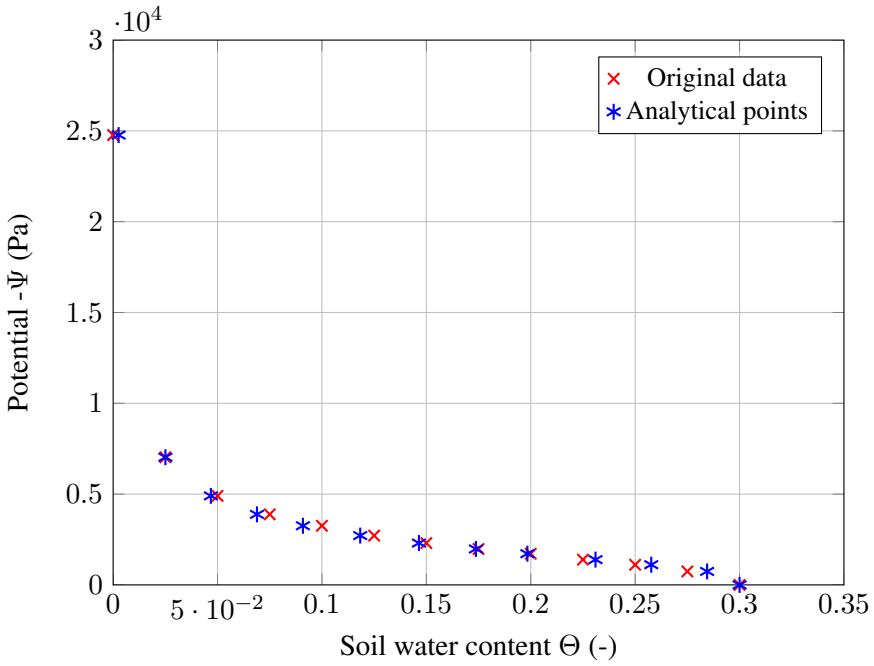

Figure 7.2. Soil-water retention curve for coarse sand

The three parameters of the model estimated for fine sand are $n[-] = 2.95$, $\alpha[1/Pa] = 1.94 \cdot 10^{-4}$ $\Theta_r/\Theta_s[-] = 0.14$:

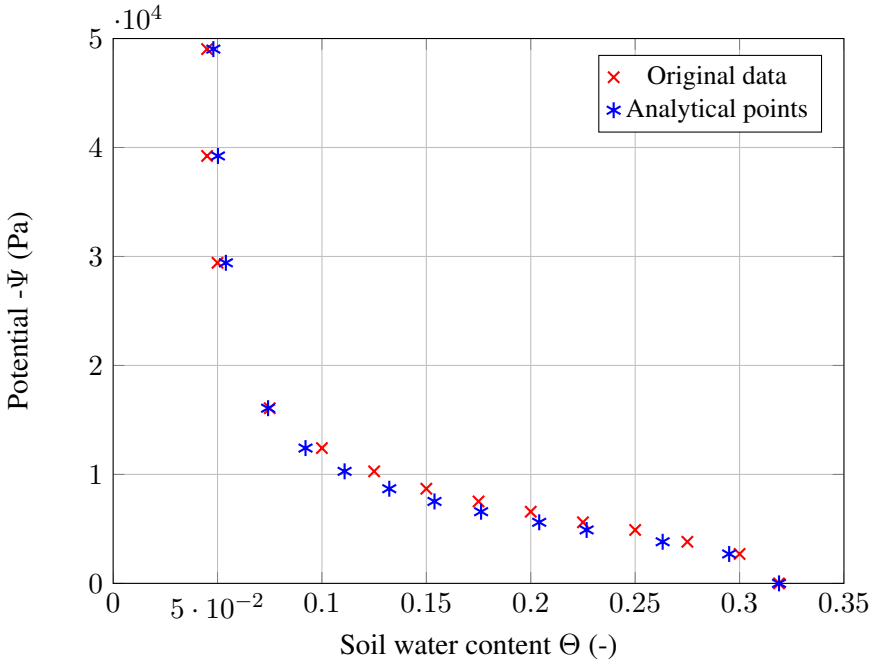

Figure 7.3. Soil-water retention curve for fine sand

The three parameters of the model estimated for silt are $n[-] = 3.2$, $\alpha[1/Pa] = 6.12 \cdot 10^{-5}$, $\Theta_r/\Theta_s[-] = 0.62$:

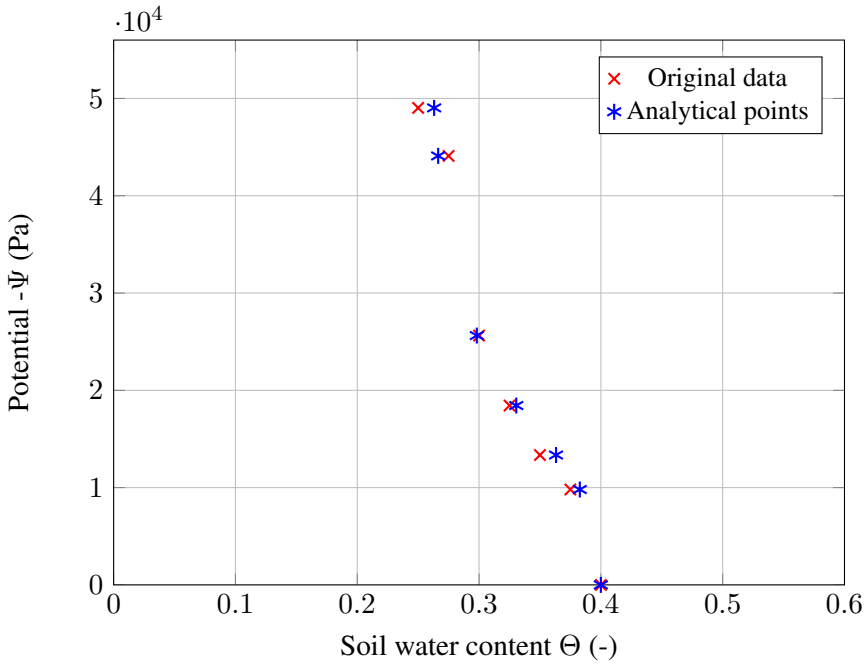

Figure 7.4. Soil-water retention curve for silt

The three parameters of the model estimated for clay are $n[-] = 2.5$, $\alpha[1/Pa] = 2.04 \cdot 10^{-4}$, $\Theta_r/\Theta_s[-] = 0.5$:

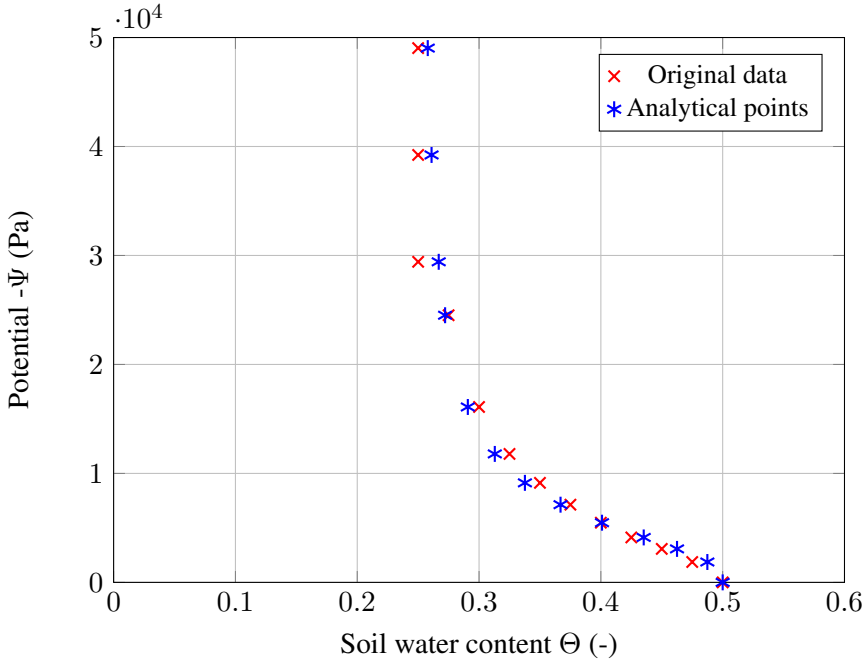

Figure 7.5. Soil-water retention curve for clay

The unsaturated flow function has to be programmed in subroutine UNSAT.
Van Genuchten model is programmed by default in the code. The subroutine is divided into three main sections that correspond to the three functions required by SUTRA. The first one is the saturation, SW in the code, as a function of pressure (given in terms of Θ/Θ_s, and calculated according to Equation 7.1). The second one is the derivative of saturation SW with respect to pressure, DSWDP. The third is the relative permeability, called RELK id the code, as a function of pressure or saturation.

The equation for predicting the relative hydraulic conductivity from knowledge of the soil-water retention curve was derived by Mualem (1976) [37]:

$$k_r = \Theta^{0,5} \cdot \left[\frac{\int_0^{\Theta} \frac{1}{h(x)} dx}{\int_0^1 \frac{1}{h(x)} dx} \right]^2 \tag{7.3}$$

where h is the pressure head and Θ is the dimensionless water content:

$$\Theta = \frac{\Theta - \Theta_r}{\Theta_s - \Theta_r} \tag{7.4}$$

To solve Equation 7.3 an expression relating the dimensionless water content to the pressure head is needed:

$$\Theta = \left[\frac{1}{1 + (\alpha h)^n} \right]^m \tag{7.5}$$

where α, n and m were previously defined.

Closed form equations for $k_r(\Theta)$ can be derived when certain restrictions are imposed upon the values of of m and n in Equation 7.4 (Van Genuchten, 1980) [46]. Solving this equation for $h = h(\Theta)$ and substituting the resulting expression into Equation 7.1, the result is:

$$k_r(\Theta) = \Theta^{0,5} \cdot \left[\frac{f(\Theta)}{f(1)} \right]^2 \tag{7.6}$$

where:

$$f(\Theta) = \int_0^{\Theta} \left[\frac{x^{\frac{1}{m}}}{1 - x^{\frac{1}{m}}} \right]^{\frac{1}{n}} dx \tag{7.7}$$

Substitution of $x = y^n$ into Equation 7.7 leads to:

$$f(\Theta) = m \cdot \int_0^{\Theta^{1/m}} y^{m-1+1/n} (1-y)^{-1/n} dy \tag{7.8}$$

that for the particular case where m = 1 − 1/n becomes:

$$f(\Theta) = 1 - (1 - \Theta^{1/m})^m \tag{7.9}$$

and because $f(1)$ = 1 Equation 7.6 becomes (Van Genuchten, 1980) [46]:

$$k_r(\Theta) = \Theta^{0,5} \cdot [1 - (1 - \Theta^{1/m})^m]^2 \tag{7.10}$$

So, the ultimate results for each section are computed starting from the model parameters required by the code: SWRES (equal to Θ_r/Θ_s), AA (α), and VN (n), obtained fitting the plots reported previously. In this study four regions were created (one for each type of soil). The unsaturated properties associated to a coarse sand were then chosen to implement the numerical model.

7.2 Longitudinal and tranverse dispersivities

Longitudinal and tranverse dispersivities are important parameters in order to predict the toe location and the thickness of the transition zone.

The value of the longitudinal dispersivity chosen for numerical simulations was assumed equal to that reported in the study of Nasab el al. (2009) [38], and it is also in agreement with the values found by Benekos et al. (2006) [8]. The sand used in their experiment had a porosity equal to 0.365 and a very narrow particle distribution (0.8-1.2 mm), very similar to this case. In fact, according to Xu et al. (1997) [52], porosity and uniformity of grain size are the two most important factors affecting dispersivities.

On the other hand, Abarca and Clement (2009) [1] suggest lower values of dispersivities for uniform glass beads having a diameter equal to 1.1 mm and a porosity equal to 0.39; in particular they state that α_L could be varied from 0.0001 m and 0.002 m, while the ratio α_L/α_T could be varied within a range of 2 to 40. These values are similar to those reported in the study of Xu et al. (1997) [52] for sands with the same caracteristics.

Frippiat et al. (2008) [23] instead found for glass beads with a uniform coefficient equal to 1.42, a mean diameter equal to 1.445 mm, and porosity equal to 36.2, values of α_L equal to 30.1-30.4 mm, much higher than the previous ones.

The choice of the dispersivities values in this study is mainly related to numerical instabilities that increase as the values of dispersivities decrease and consequently the grid Peclet number increases.

The chosen discretization (element size equal to 1 cm $\cdot$ 1 cm) respects the rhule suggested by Voss (2010) [48] according to which the local element dimension parallel to the flow direction ΔL_L has to be lower than 4 times the longitudinal dispersivity, but violates the rhule binding the local element dimension transverse to the flow direction, that should be less than 10 times the transverse dispersivity. This implies that some numerical instabilities occurred in the simulations, even though errors were limited at 5 % at most in the concentration values (this means that the code returns concentration values at least 5 % higher than the maximum set).

A better result would be obtained by making the existing discretization finer, but the finer the discretizations are, the more computationally expensive the simulations become.

In order to check for an adequate discretization a simulation was done with a finer mesh (element size equal to 0.5 cm $\cdot$ 0.5 cm) in which no instabilities occurred, and results were compared. Since no telling differences appeared from the point of view of the transport model, then the coarser discretization was used. The final configuration is a reasonable compromise between accuracy of computation, CPU time and memory requirements.

Chapter 8

Numerical model results

8.1 Initial conditions of the model

Freshwater concentration and naturally steady-state pressure were initially set everywhere in the model assuming an hydraulic head equal to 42 cm at the beginning of the experiment. These initial conditions are obtained through a preliminary simulation that calculates consistent steady pressures. The time step was set equal to 1 minute and the simulation was stopped after 60 time steps (one hour).

Figure 8.1 reports the values of pressure associated to every colour.

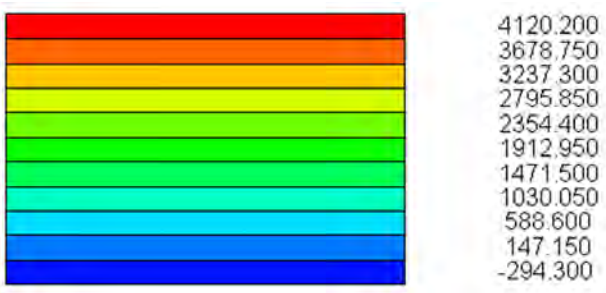

Figure 8.1. Legend for initial steady state pressures. Results are given in Pa [kg/(m · s^2)]

Figure 8.2 reports the result of the code for pressure.

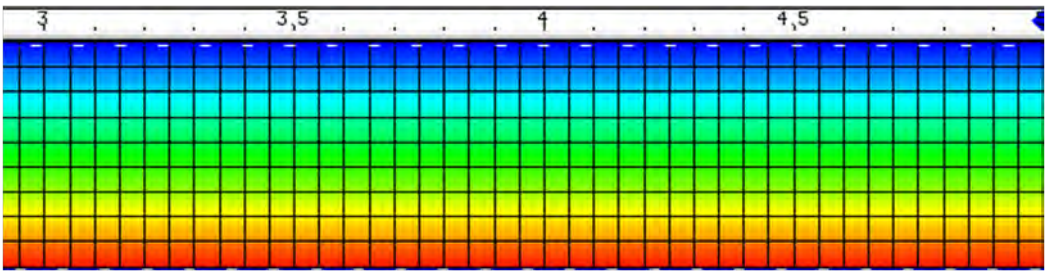

Figure 8.2. Steady state initial pressures

Initial saturation conditions results are normalized respect to the porosity, and are in agreement with the soil-water retention curve of a coarse sand.

Figure 8.3. Legend for saturation values

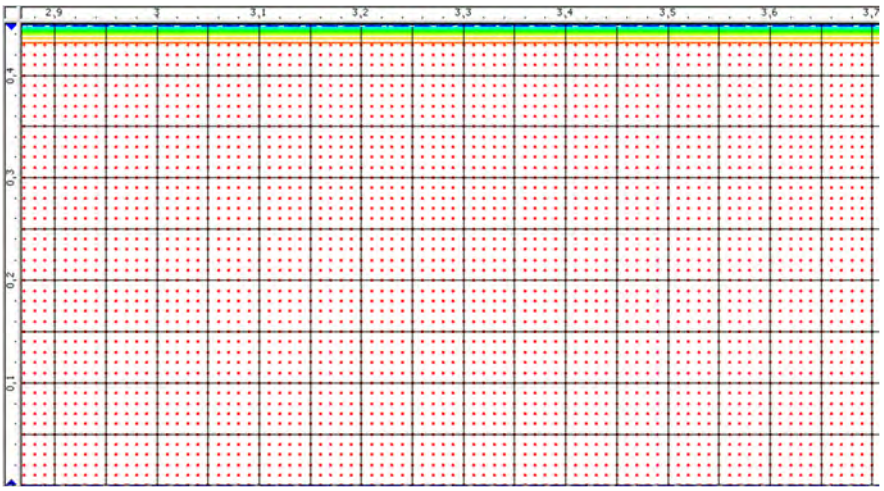

Figure 8.4. Initial saturation conditions

The unsaturated zone is very narrow, and practically the sand can be considerend saturated.

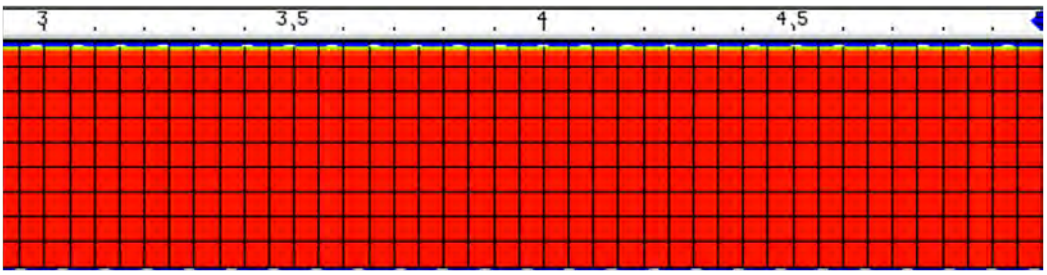

Figure 8.5. Initial saturation condition. Saturated soil

8.2 Salt wedge intrusion

A transient simulation to visualize the advancing of the saltwater wedge in time and the mixing zone was carried on.

The simulation was stopped after 24 h (time step = 1 minute) in order to be sure that the steady-state was reached (the Dupuit-Ghyben-Herzberg equation provides a lenght of the wedge equal to of 1.25 m). According to the model, the intrusion never stops due to dispersion. However it is reasonable to stop the simulation when the advancing of the wedge is not more appreciable in time.

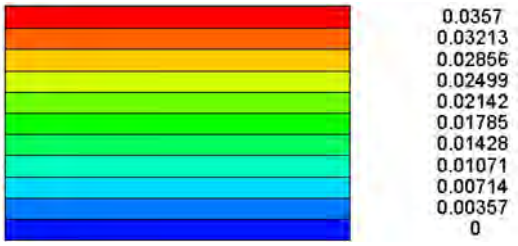

Figure 8.6. Legend for concentration. Results are given as $\mathrm{kg}_{solute}/\mathrm{kg}_{seawater}$

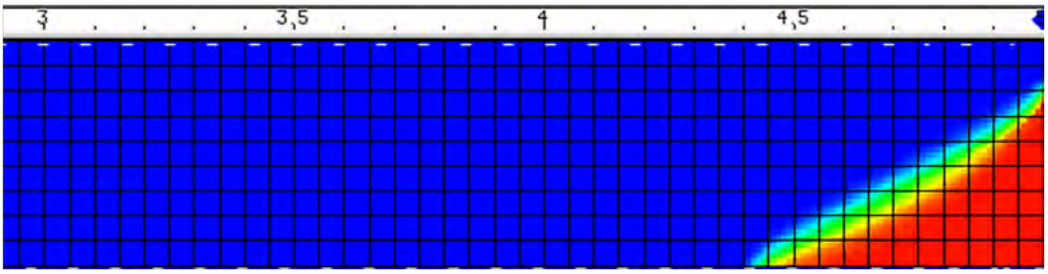

Figure 8.7. Saltwater intrusion after 4 hours

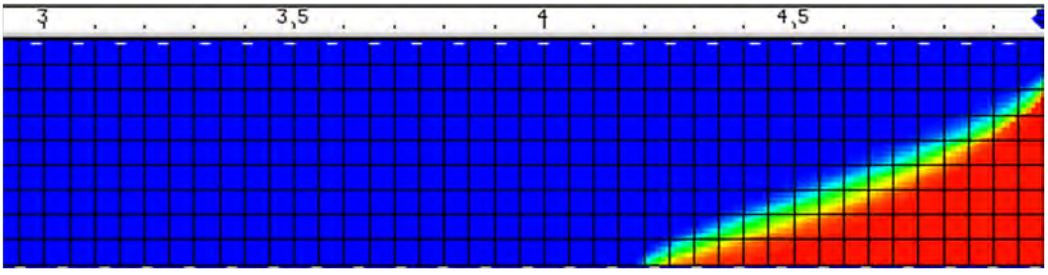

Figure 8.8. Saltwater intrusion after 8 hours

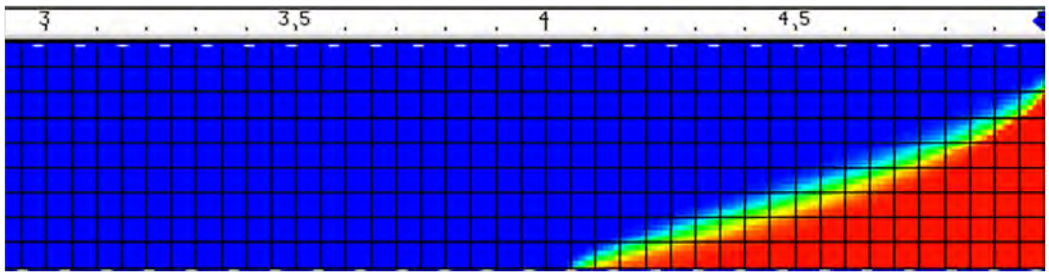

Figure 8.9. Saltwater intrusion after 12 hours

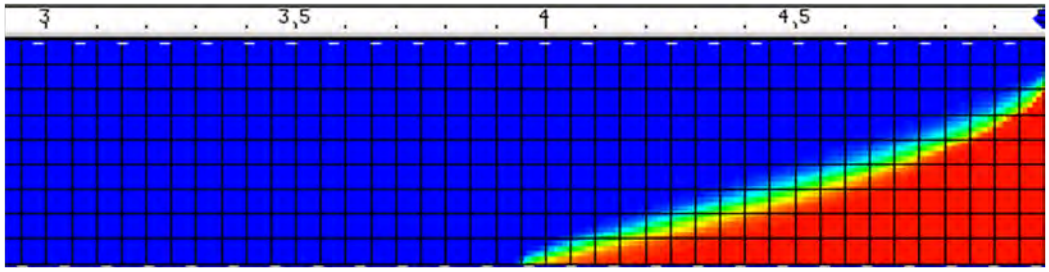

Figure 8.10. Saltwater intrusion after 16 hours

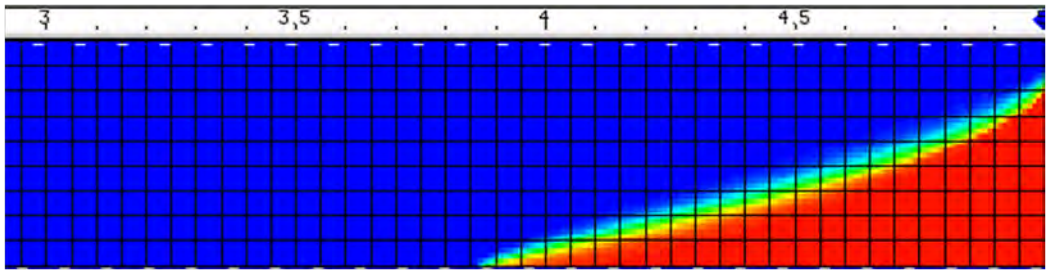

Figure 8.11. Saltwater intrusion after 20 hours

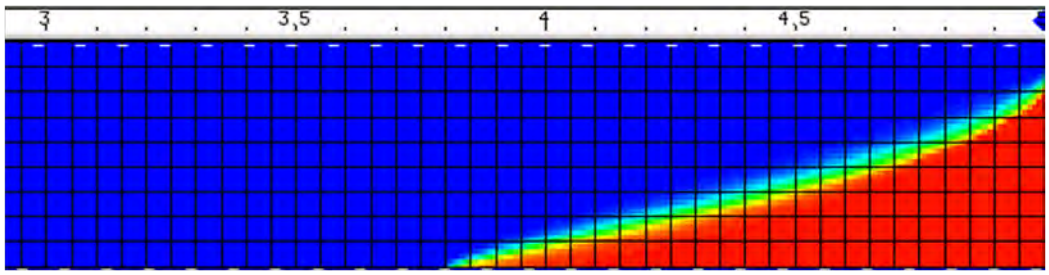

Figure 8.12. Saltwater intrusion after 24 hours

8.3 Transition zone

A simulation was developed to better visualize the transition zone. This was done by decreasing the mesh size vertically and horizontally where the saltwater intrusion is expected (in the last 1.5 m). The new elements of the mesh have a size equal to 0.5 by 0.5 cm in the last 1.5 m, and 1 cm by 0.5 cm (vertically) in the fist 3.5 m. In this way the thickness of the transition zone is much better defined. The numerical instability disappears but, on the other hand, the simulation time increases a lot (1.5 h for a simulation of 24 h).

The result is reported in Figure 8.13

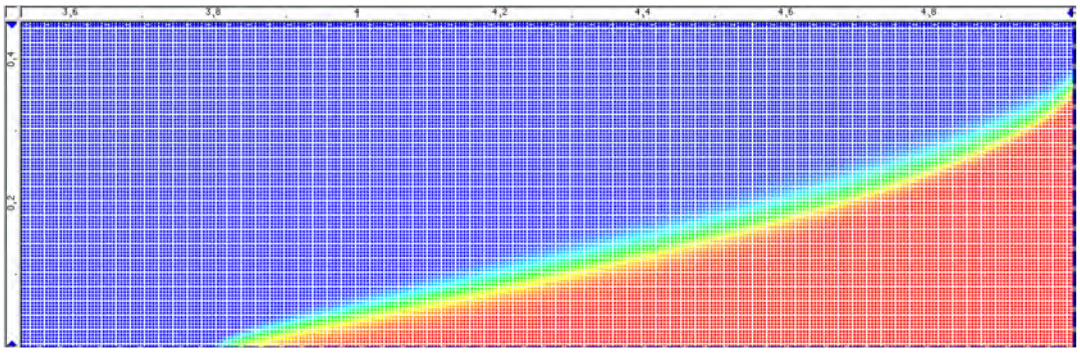

Figure 8.13. Visualization of the transition zone after 24 hours of simulation

8.4 Sensivity analysis for permeability

A sensitivity analysis for permeability was performed varying hydraulic conductivity from $7.7 \cdot 10^{-4}$ to $2.31 \cdot 10^{-3}$ m/s (with increments and reductions of 25 % and 50 % respect the original hydraulic conductivity).

In order to have results comparable with the previous simulations, time was scaled according to the relation:

$$t^* = \frac{tK}{L} \tag{8.1}$$

where t* is the dimensionless time, t is the original simulation time (24 h), K is the hydraulic conductivity and L is the lenght of the saltwater intrusion. According to this equation, when K doubles, the simulation time has to be halved in order to obtain comparable values of L.

It is interesting to point out that, when the hydraulic conductivity increases, the infiltration discharge for a constant gradient is higher too. So, for the same value of the saltwater hydrostatic pressure, a reduced saltwater intrusion for an higher value of K is expected. This is evident in Figure 8.18.

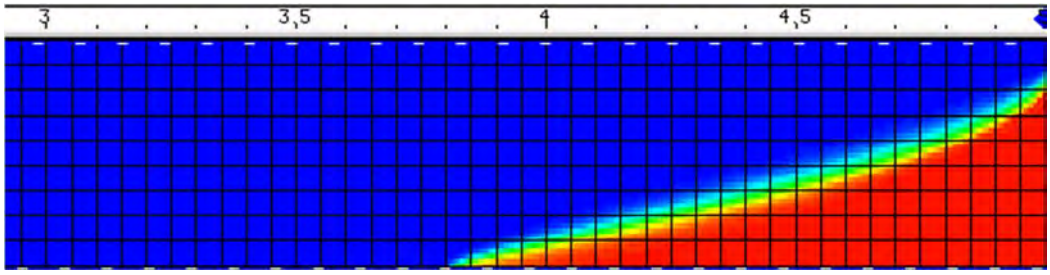

Figure 8.14. Saltwater intrusion after 48 hours for an hydraulic conductivity equal to $7.7 \cdot 10^{-4}$ m/s: -50 % respect to the standard case

Legend for concentration values is reported in Figure 8.6

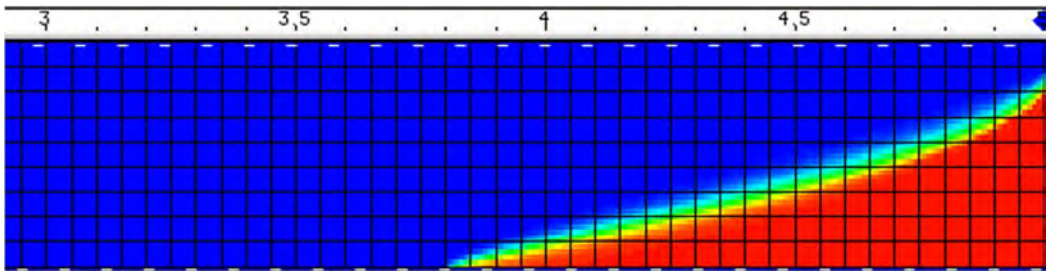

Figure 8.15. Saltwater intrusion after 32 hours for an hydraulic conductivity equal to 1.15 · 10^{-3} m/s: -25 % respect to the standard case

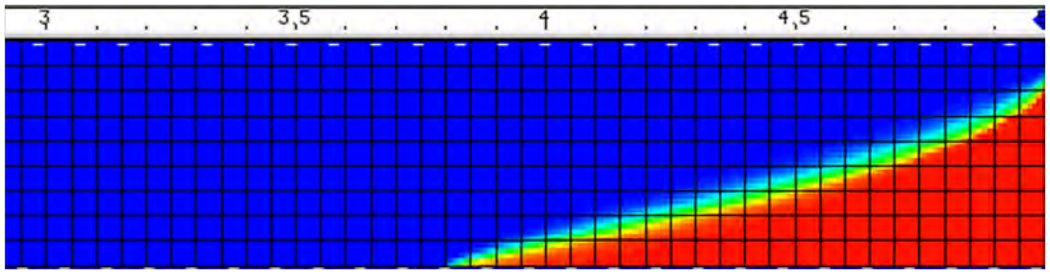

Figure 8.16. Saltwater intrusion after 24 hours for an hydraulic conductivity equal to 1.54 · 10^{-3} m/s: standard case

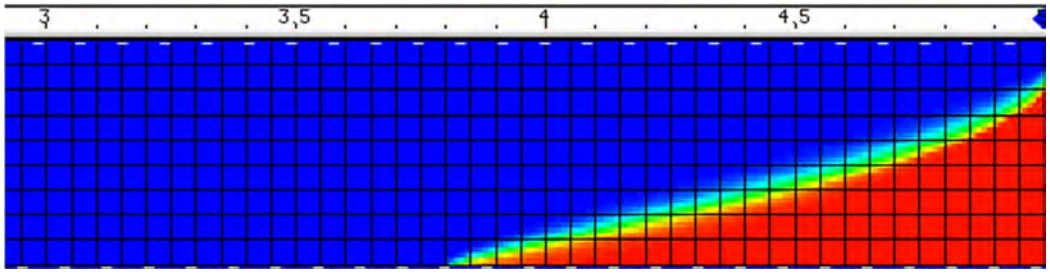

Figure 8.17. Saltwater intrusion after 19.2 hours for an hydraulic conductivity equal to 1.925 · 10^{-3} m/s: +25 % respect to the standard case

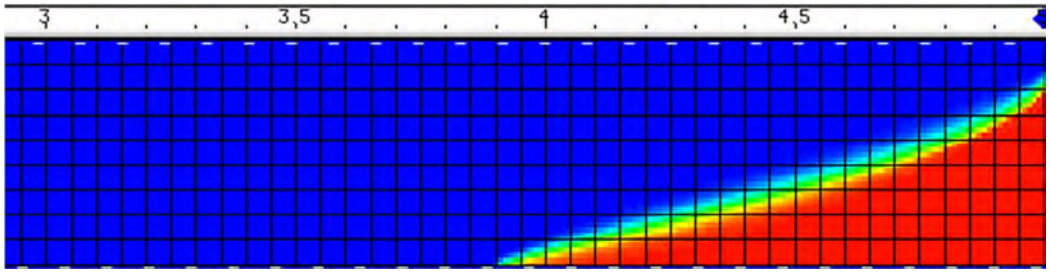

Figure 8.18. Saltwater intrusion after 12 hours for an hydraulic conductivity equal to 2,31 · 10^{-3} m/s: +50 % respect to the standard case

Legend for concentration values is reported in Figure 8.6

8.5 Sensitivity analysis for dispersivities

A sensitivity analysis for the dispersivity coefficients was also performed. Longitudinal dispersivity was halved and doubled respect to the original one (Figure 8.20). Transversal dispersivity was always maintained one order of magnitude lower than the longitudinal one.

The results highlight that higher values of dispersivities imply a reduced saltwater intrusion and a greater thickness of the interface. The opposite happens if the value of the dispersitivity coefficients are lower.

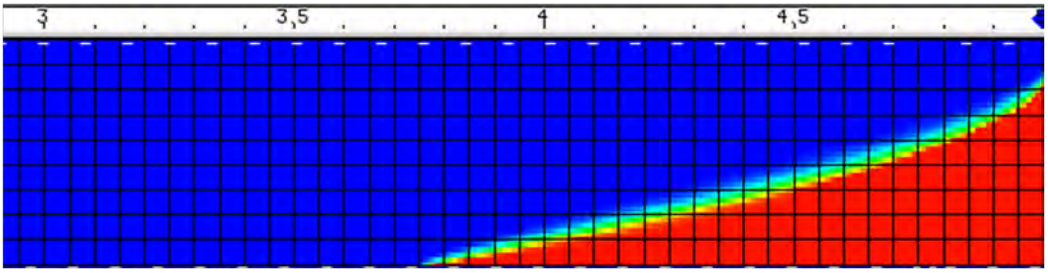

Figure 8.19. Saltwater intrusion after 24 hours. α_L = 0.00375 m, α_T = 0.000375 m: -50 % respect to the standard case

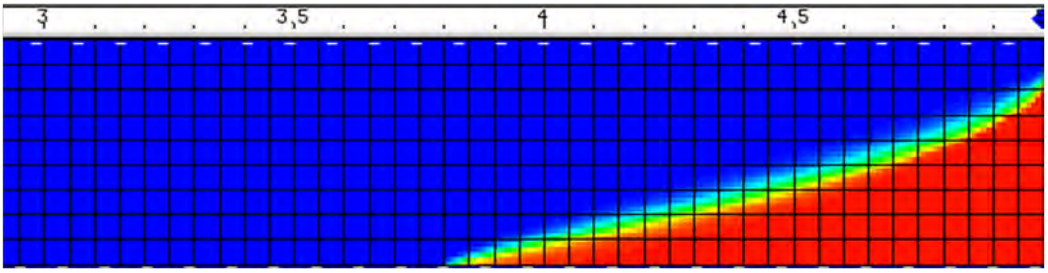

Figure 8.20. Saltwater intrusion after 24 hours. α_L = 0.0075 m, α_T = 0.00075 m: standard case

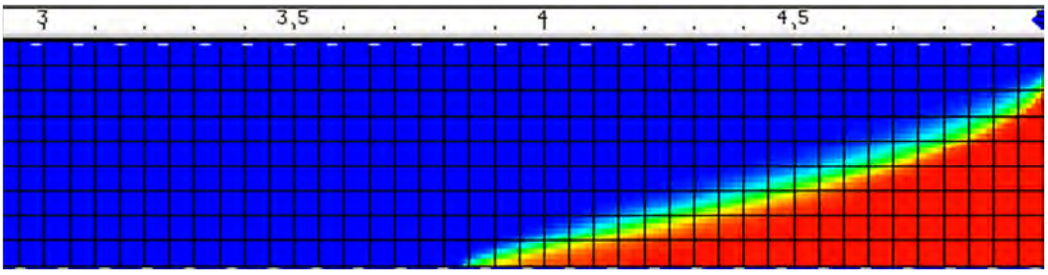

Figure 8.21. Saltwater intrusion after 24 hours. α_L = 0.01125 m, α_T = 0.001125 m: -50 % respect to the standard case

Legend for concentration values is reported in Figure 8.6

8.6 Critical pumping

This simulation wanted to point out the critical pumping rate, at which upconing occurs. According to the numerical results, this happens when the pumping rate becomes higher than 10^{-4} l/s, in particular when the pumping rate is about half of the infiltration discharge (equal to $7.6 \cdot 10^{-4}$ l/s, according to the Dupuit equation).

The effect of pumping is, in every case, an higher saltwater intrusion. This is due to the reduction of the infiltration discharge.

Pumping was always maintained positioned at 1 m from the coast line and 10 cm deep.

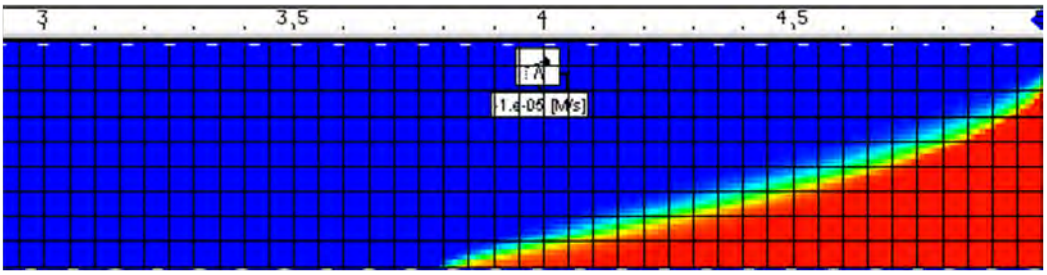

Figure 8.22. Pumping rate = $1 \cdot 10^{-5}$ l/s

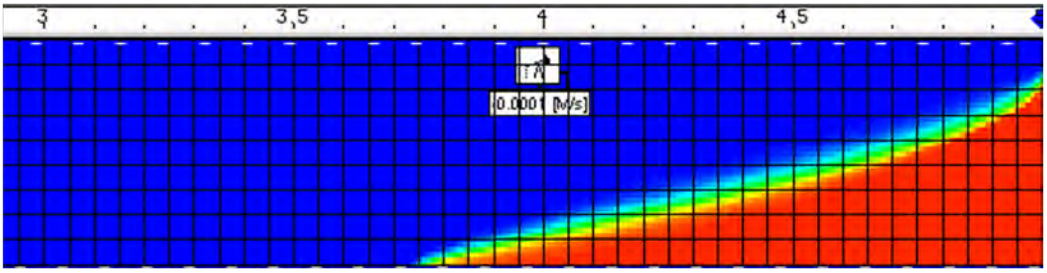

Figure 8.23. Pumping rate = $1 \cdot 10^{-4}$ l/s

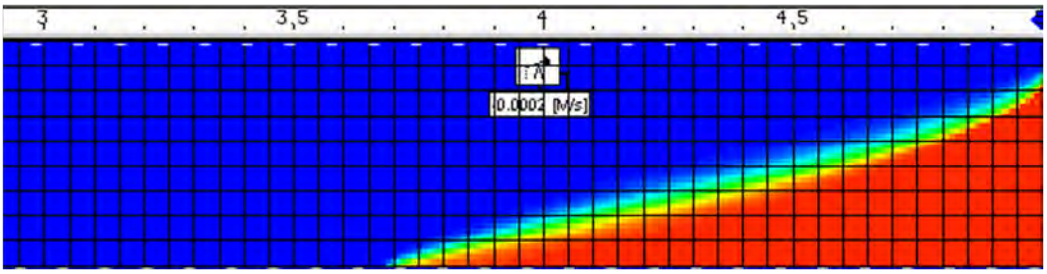

Figure 8.24. Pumping rate = $2 \cdot 10^{-4}$ l/s

Legend for concentration values is reported in Figure 8.6

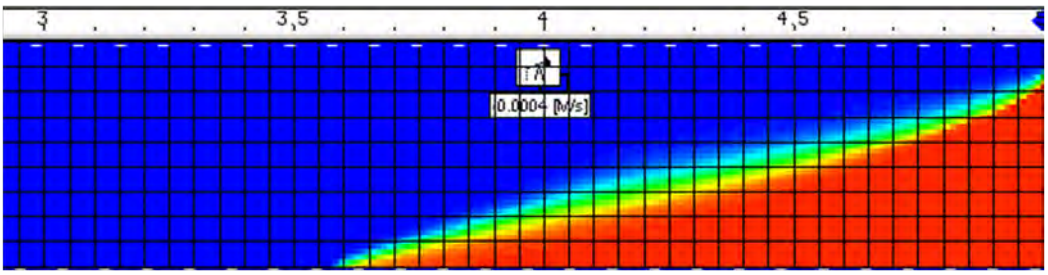

Figure 8.25. Pumping rate = $4 \cdot 10^{-4}$ l/s

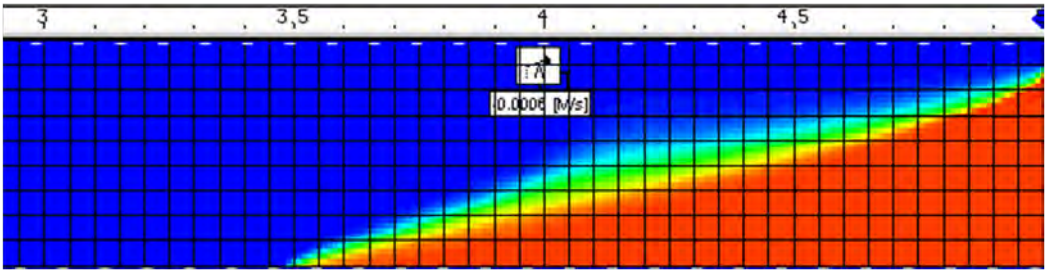

Figure 8.26. Pumping rate = $6 \cdot 10^{-4}$ l/s

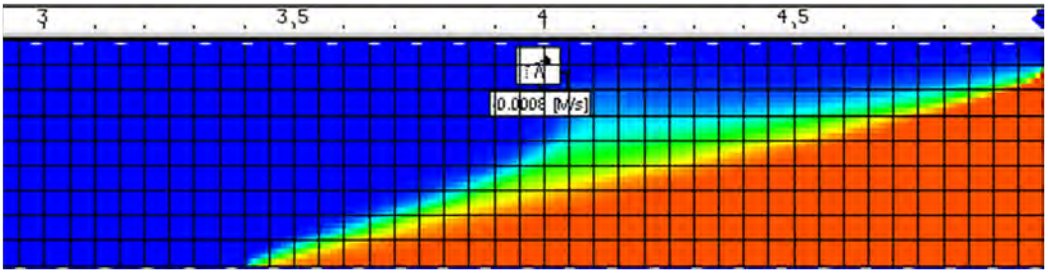

Figure 8.27. Pumping rate = $8 \cdot 10^{-4}$ l/s

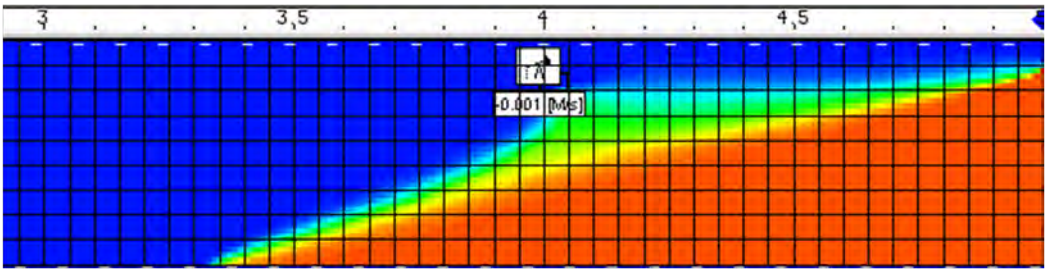

Figure 8.28. Pumping rate = $1 \cdot 10^{-3}$ l/s

Legend for concentration values is reported in Figure 8.6

8.7 Effect of a subsurface barrage

Two sensitivity analysis were developed to verify the best position and lenght of a subsurface barrage, in order to decrease the saltwedge intrusion. Hydraulic conductivity of the barrage was set equal to 10^{-9} m/s and porosity to 0.5. Simulations were stopped after 24 hours (time step = 1 minute).

8.7.1 Effect of a different depth barrage positioned at 0.9 m from the coast line

In this simulations the pumping rate was maintained equal to $8 \cdot 10^{-4}$ l/s (that is a pumping rate at which upconing is evident), collocated at 1 m from the coast line and at a depth of 10 cm. The barrage was positioned immediately after pumping (0.9 m from the coast line) and its depth was varied and set equal to 10, 15 and 20 cm.

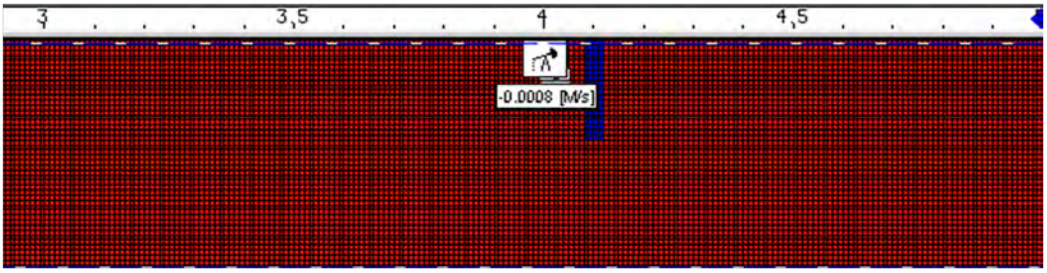

Figure 8.29. Position of the barrage respect to pumping

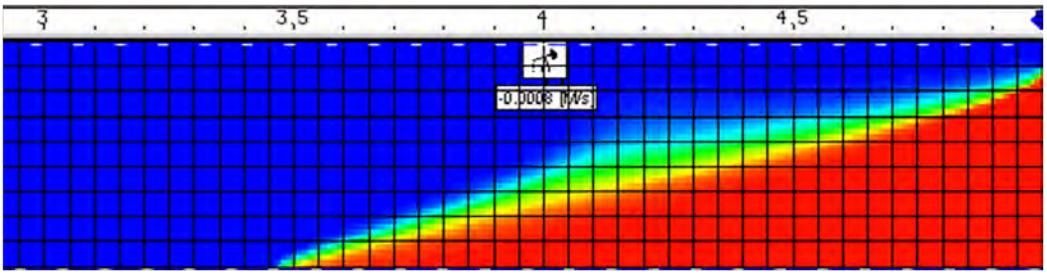

Figure 8.30. Barrage collocated at 0.9 m from the coast line and 10 cm deep

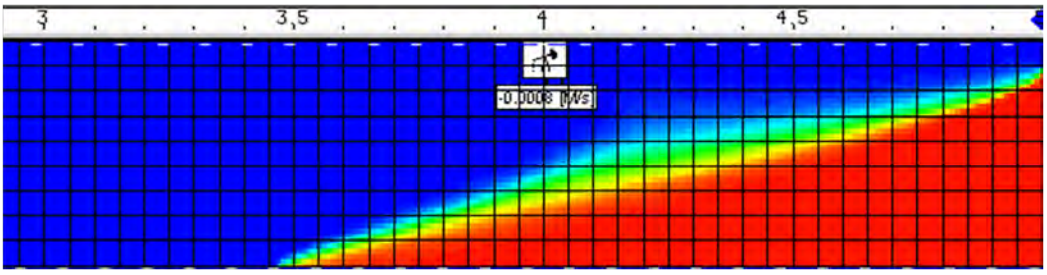

Figure 8.31. Barrage collocated at 0.9 m from the coast line and 15 cm deep

Legend for concentration values is reported in Figure 8.6

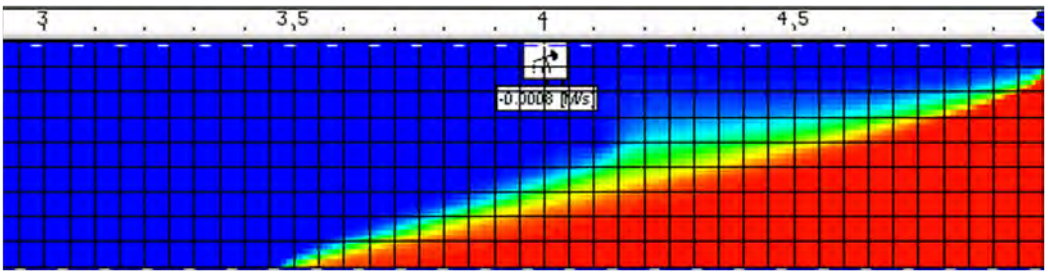

Figure 8.32. Barrage collocated at 0.9 m from the coast line and 20 cm deep

From the results it is evident that a barrage collocated in this position does not influence so much the saltwater wedge intrusion.

8.7.2 Effect of a different depth barrage positioned at the coast line

Also in this simulations the pumping rate was maintained fixed and equal to $8 \cdot 10^{-4}$ l/s. The subsurface barrage was positioned at the coast line and its depth was varied and set equal to 10, 15 and 20 cm. Pumping was collocated at a 1 m from the coast line a at a depth equal to 10 cm.

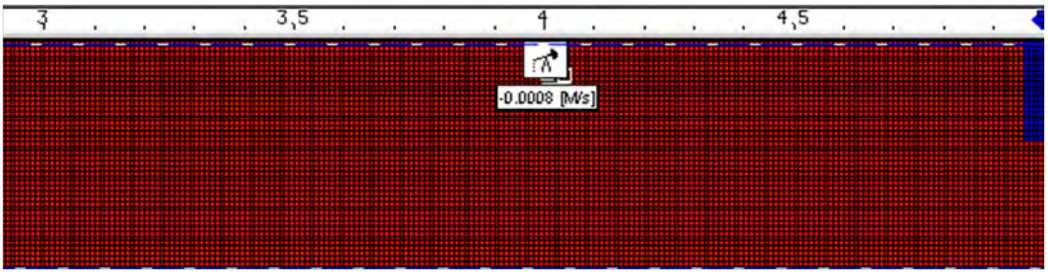

Figure 8.33. Position of the barrage respect to pumping

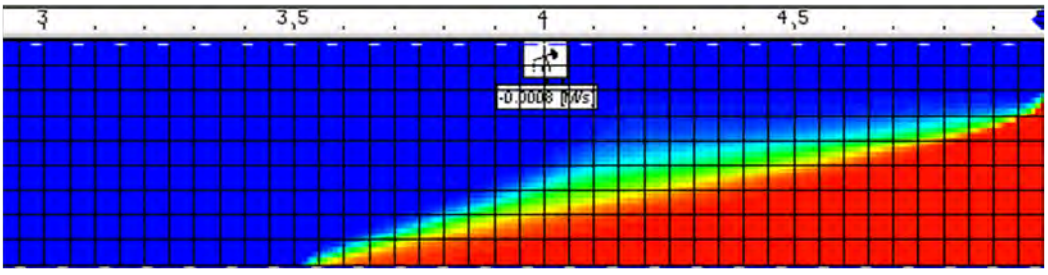

Figure 8.34. Barrage collocated at the coast line and 10 cm deep

Legend for concentration values is reported in Figure 8.6

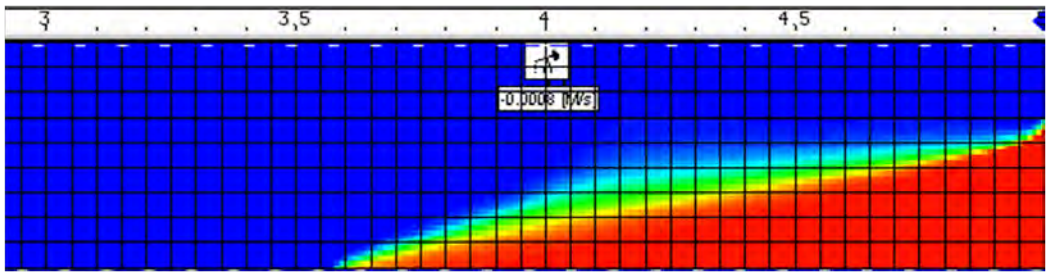

Figure 8.35. Barrage collocated at the coast line and 15 cm deep

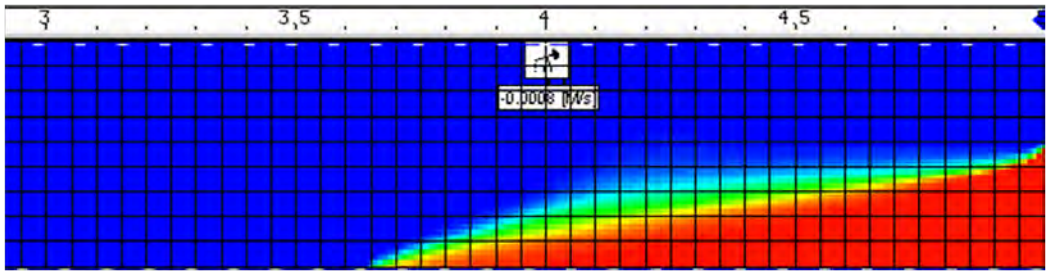

Figure 8.36. Barrage collocated at the coast line and 20 cm deep

In this case the result was a more evident reduction of the saltwater intrusion, that decreases visibly also when the barrage is 10 cm deep.

8.7.3 Comparison between the effects of the subsurface barrage 20 cm deep collocated at 0.9 m from the coast line and at the coast line

These results want to point out the reduction of the saltwater intrusion with a barrage positioned at the coast line.

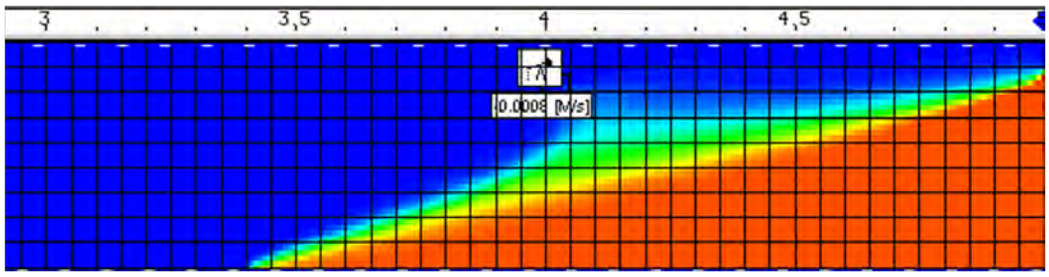

Figure 8.37. Only pumping without a barrage

Legend for concentration values is reported in Figure 8.6

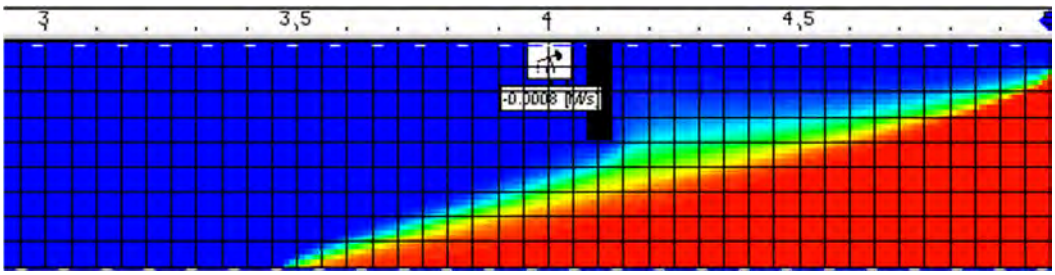

Figure 8.38. Barrage collocated at 0.9 m from the coastline and 20 cm deep

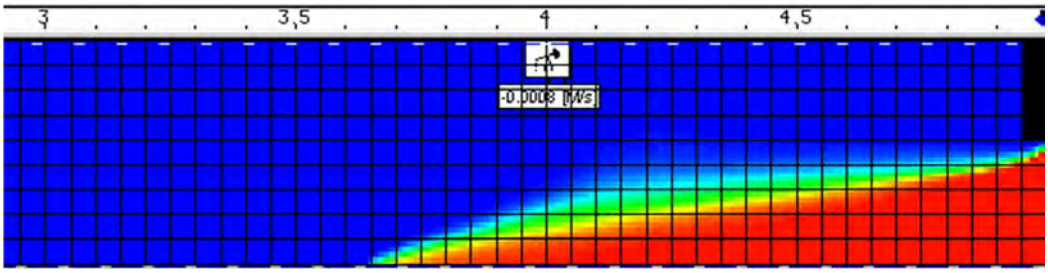

Figure 8.39. Barrage collocated at the coast line and 20 cm deep

Results highlight that the reduction of the intrusion is not significant when the barrage is collocated near pumping, at 0.9 m from the coast line, while becomes evident in the case of a barrage collocated at the coast line.

8.8 Effects of a freshwater recharge by infiltration

This simulation aimed to verify the effect of an infiltration discharge from the top boundary of the model. The imposed discharge was set equal to the infiltration flow coming from the left boundary, calculated starting from the x velocity results.

It is important to point out that in SUTRA "velocity" refers to the average fluid velocity relative to the stationary solid matrix. It is an average velocity in the sense that it represents fluid movement as viewed at the model scale, rather than at the microscopic (pore) scale.

The average fluid velocity is not to be confused with the Darcy velocity, which is a measure of the volumetric flux of fluid and is equal to $\epsilon S_w \mathbf{v}$, where ϵ is porosity, S_w is saturation, and $\mathbf{v}$ is the average fluid velocity.

According to the x velocity results of the model, assuming the porosity equal to 0.367 and saturation equal to 1, the infiltration flow from the left boundary is $1.34 \cdot 10^{-5}$ m/s $\cdot$ 0.367 $\cdot$ 0.3 m $\cdot$ 0.41 m = $6 \cdot 10^{-4}$ l/s. This flow was forced to infiltrate from different positions of the top boundary in the case of upward hydraulic heads equal to 41 cm and 42 cm.

Legend for concentration values is reported in Figure 8.6

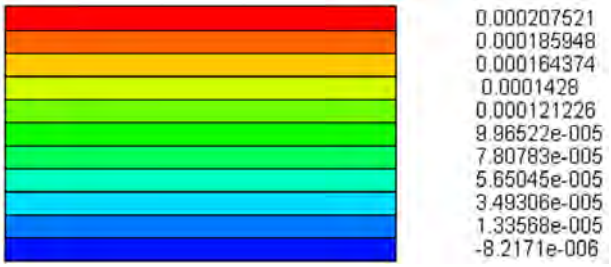

Figure 8.40. Legend for x velocity results. Values are given in m/s

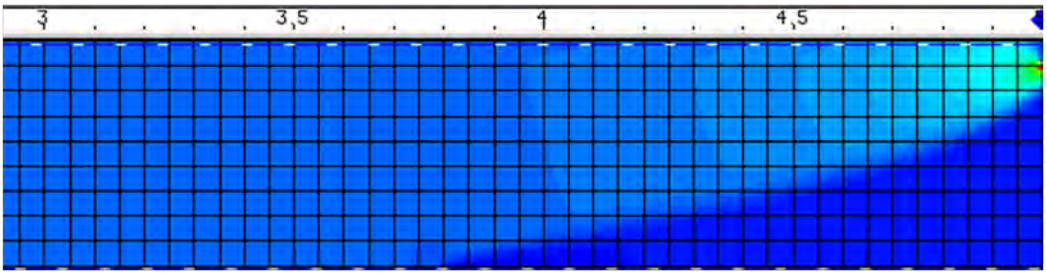

Figure 8.41. X velocity results. Simulation time = 24 h

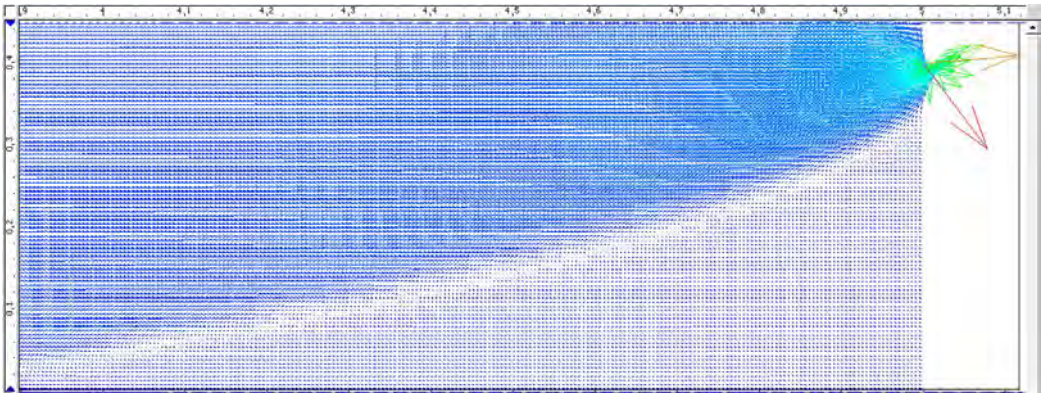

Figure 8.42. Velocity vectors. Simulation time = 24 h

Figure 8.43 reports the seawater intrusion after 20 days of simulation when the hydraulic head upward is reduced and infiltration discharge strongly decreases.

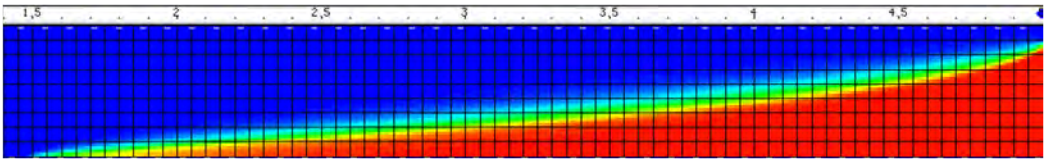

Figure 8.43. Saltwater intrusion after 10 days of simulation when the upward hydraulic head is equal to 41 cm

Legend for concentration values is reported in Figure 8.6

8.8.1 Effect of a freshwater recharge forced to infiltrate through all the top boundary

In these simulations a freshwater recharge equal to $6 \cdot 10^{-4}$ l/s was forced to infiltrate through all the top boundary. The results showed that there is not a significant reduction of the seawater intrusion.

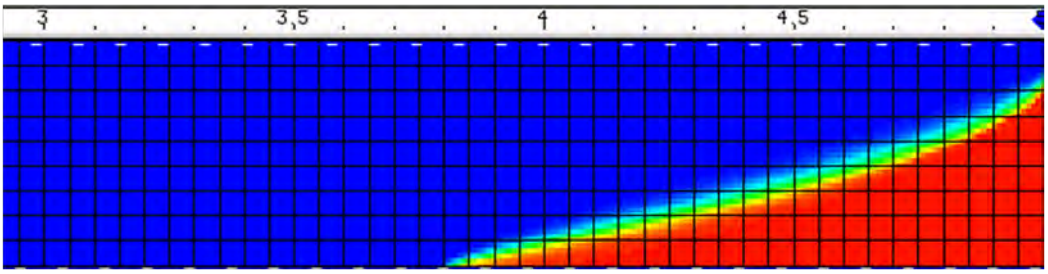

Figure 8.44. Standard simulation. Upward level = 42 cm; no freshwater recharge

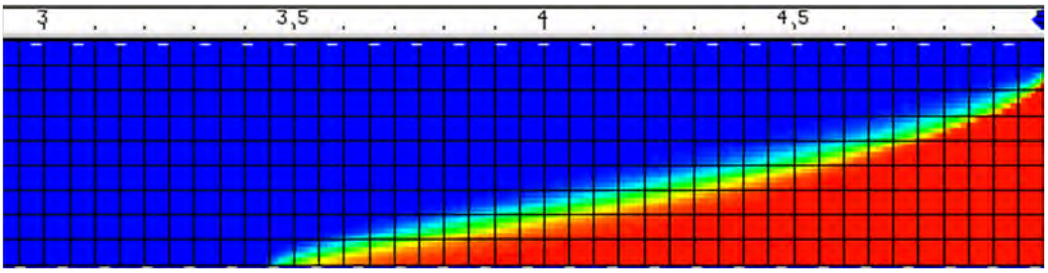

Figure 8.45. Upward level = 41 cm; freshwater recharge forced to infiltrate through the full lenght of the top boundary

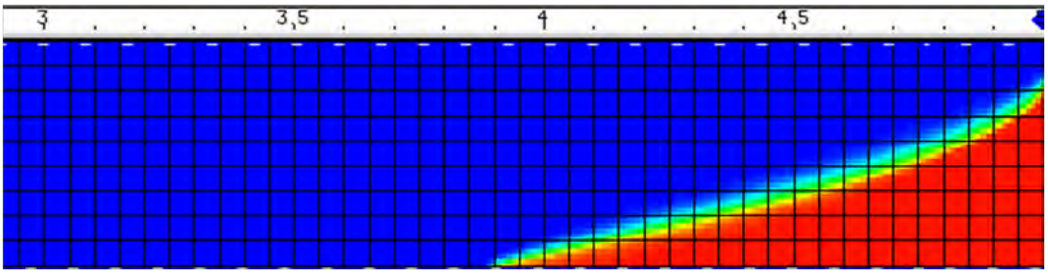

Figure 8.46. Upward level = 42 cm; freshwater recharge forced to infiltrate through the full lenght of the top boundary

Legend for concentration values is reported in Figure 8.6

8.8.2 Effect of a freshwater recharge forced to infiltrate through the first 2.5 m of the top boundary

In these simulations a freshwater recharge equal to $6 \cdot 10^{-4}$ l/s was forced to infiltrate in the first 2.5 m of the top boundary. Also in this case there is not a significant improvement in pushing back the salt wedge.

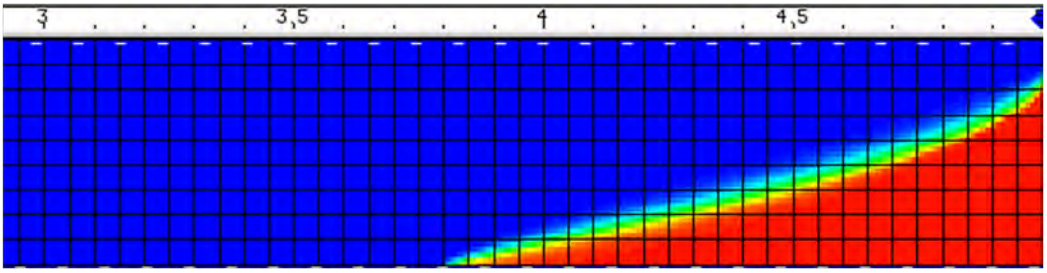

Figure 8.47. Standard simulation. Upward level = 42 cm; no freshwater recharge

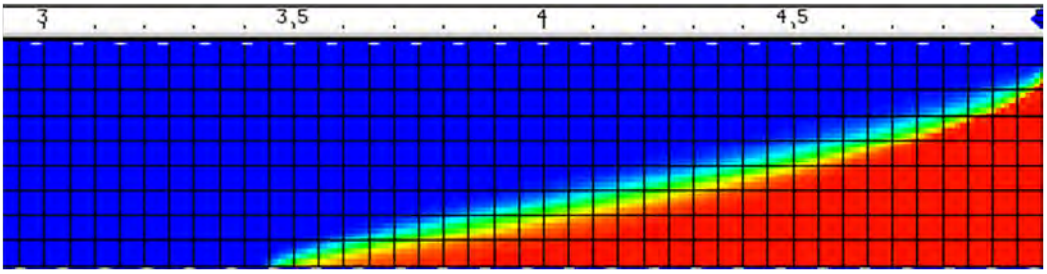

Figure 8.48. Upward level = 41 cm; freshwater recharge forced to infiltrate through the first 2.5 m of the top boundary

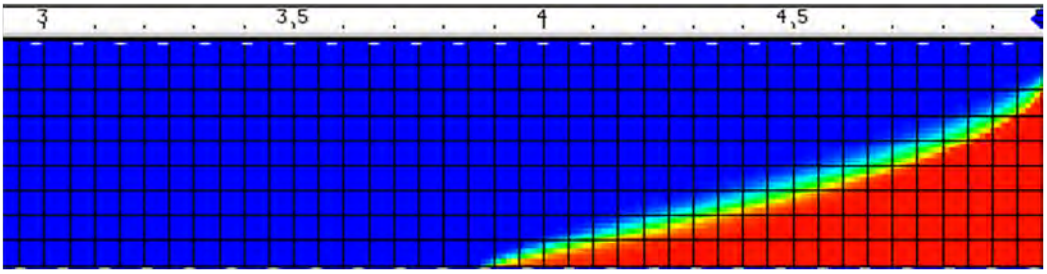

Figure 8.49. Upward level = 42 cm; freshwater recharge forced to infiltrate through the first 2.5 m of the top boundary

Legend for concentration values is reported in Figure 8.6

8.8.3 Effect of a freshwater recharge forced to infiltrate through the last 2.5 m of the top boundary

In these simulations a freshwater recharge equal to $6 \cdot 10^{-4}$ l/s was forced to infiltrate in the last 2.5 m of the top boundary.

This configuration implies an improvement in pushing back the salt wedge respect to the previous cases. The best result occurs when the upward hydraulic head is set equal to 42 cm and the freshwater recharge is forced through the last 2.5 m of the top boundary.

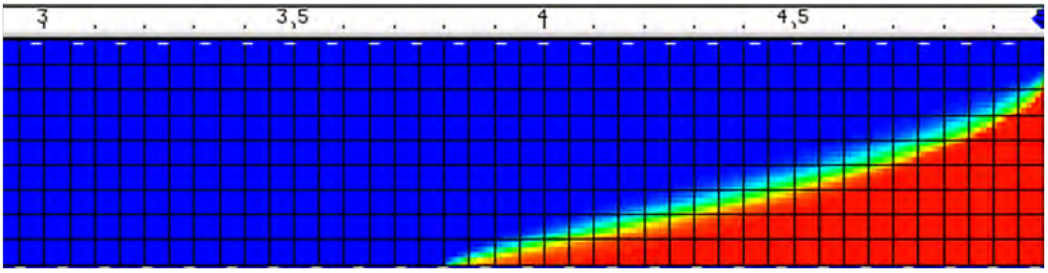

Figure 8.50. Standard simulation. Upward level = 42 cm; no freshwater recharge

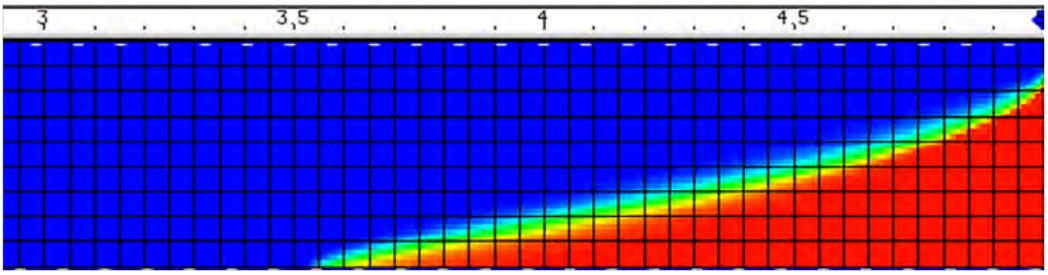

Figure 8.51. Upward level = 41 cm; freshwater recharge forced to infiltrate through the last 2.5 m of the top boundary

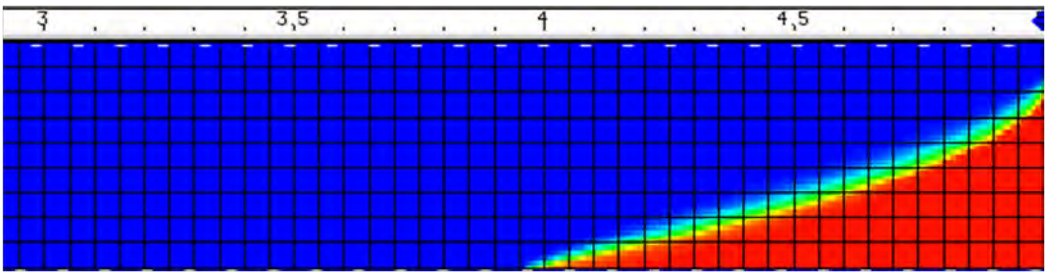

Figure 8.52. Upward level = 42 cm; freshwater recharge forced to infiltrate through the last 2.5 m of the top boundary

Legend for concentration values is reported in Figure 8.6

8.9 Effects of a non-uniform soil

These simulations aimed to study the effects caused by an intermediate layer of soil with different characteristics respect to sand. 2 cases are reported.

In the first one a layer of coarse sand (hydraulic conductivity = 10^{-1} m/s, porosity = 0.4) with a lenght equal to 1.5 m and a thickness equal to 5 cm was interposed through the soil.

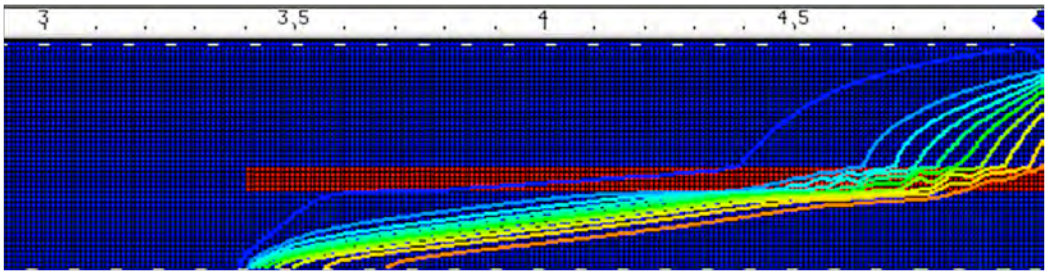

Figure 8.53. Effect on the saltwater intrusion due to an intermediate layer of coarse sand

In the second case a layer of clay (hydraulic conductivity = 10^{-8} m/s, porosity = 0.15) with a lenght equal to 1.5 m and a thickness equal to 5 cm was interposed through the soil.

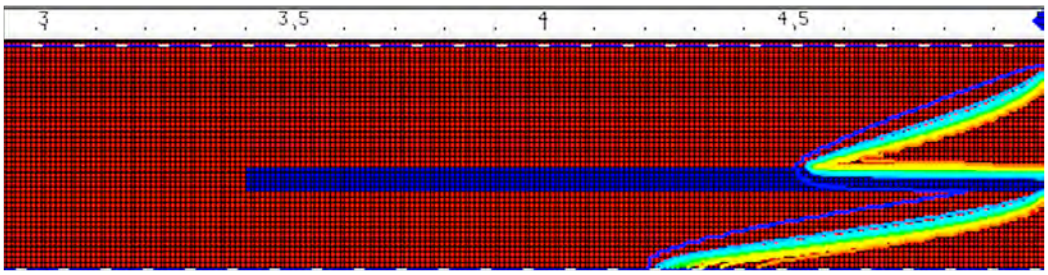

Figure 8.54. Effect on the saltwater intrusion due to an intermediate layer of clay

Figures 8.55, 8.56, 8.57 report the comparison between the standard situation with a uniform soil and the non-uniform soil cases

From the results it is evident that a strong increment in saltwater intrusion occurs when an intermediate layer of coarse sand is present. This is due to the higher hydraulic condutivity of the interposed soil.

The interposed layer of clay results instead in a strong reduction in saltwater intrusion, but this happens only if the layer of clay is long enough to change the pressure distribution. If the lenght of the layer is reduced no significant changes in saltwater intrusion occur.

Legend for concentration values is reported in Figure 8.6

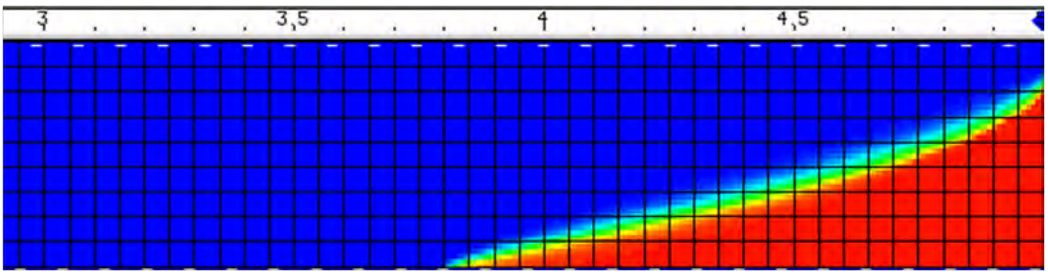

Figure 8.55. Standard situation with uniform soil

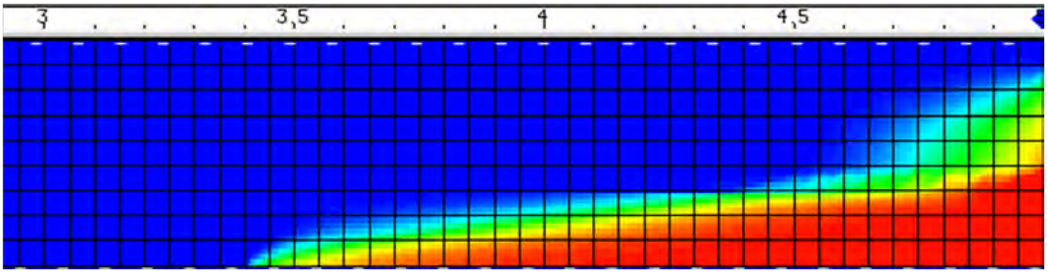

Figure 8.56. Effect of an intermediate layer of coarse sand

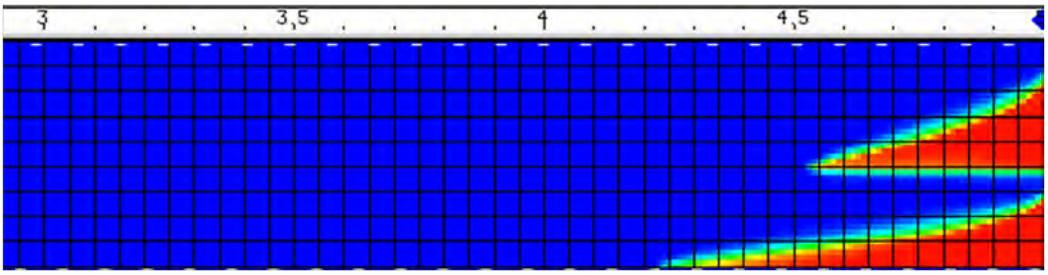

Figure 8.57. Effect of an intermediate layer of clay

Legend for concentration values is reported in Figure 8.6

Part IV

Laboratory experiment

Chapter 9

Results of the physical model

9.1 Experimental set-up

The sand-box was filled using 1125 kg of glass beads to reach an height equal to 45-46 cm. The material was positioned dropping it from a sieve layed above the device, as shown in Figure 9.1. This procedure intended to reduce dishomogeneities. The sand was moistened while falling, in order to lubricate it and facilitate the compaction procedure.

Figure 9.1. Positioning of glass beads in the sand-box device

Glass beads were compacted every 5 cm with a device composed by a weight of 4 kg that fell from 20 cm, packing them.

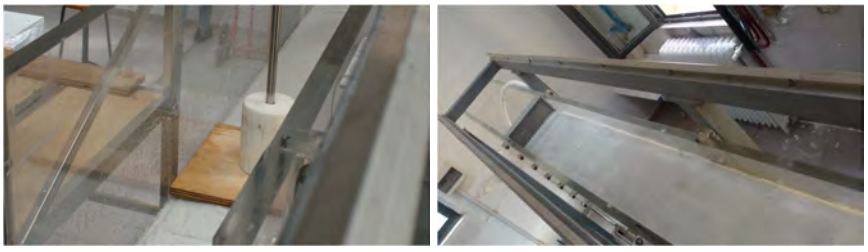

(a) (b)

Figure 9.2. Compaction of glass beads in the sand-box

The estimated porosity, considering that the volume filled with the glass beads is 0.69 m^3, is 0.347, lower than the porosity found with the preliminary tests. The expected variation of porosity, taking into account an underestimation of 25 kg or 50 kg in the used quantity of sand (that may have been lost, for example, because of the breakage of the glass beads bags), is respectively 0.362 and 0.377. However these hypothetical errors do not influence so much the volume of voids, equal respetively to 239 l (for a porosity of 0.347), 250 l (for a porosity of 0.362) and 260 l (for a porosity of 0.377).

The sand was then saturated increasing the hydraulic heads of 5 cm every 40 minutes. This saturation procedure intended to fill all the voids with water, removing the air entrapped into the sand. Saturation continued for 10 days.

(a) (b)

(c) (d)

Figure 9.3. Saturation of glass beads in the sand-box

9.2 Hydraulic conductivity estimation

Three constant head tests were done in order to estimate the effective hydraulic conductivity of the porous media. Hydraulic gradient was changed for every test and water spilled dowstream was weighed with a precision balance (Figure 9.4). In this way it was possible to estimate the infiltration discharge and, consequentely, hydraulic conductivity according to the Dupuit relationship.

(a) (b)

Figure 9.4. Precision balance used to measure spilled water

9.2.1 First conductivity test

In the first test the hydraulic gradient was set equal to 0.046 (H upstream = 44.6 cm, H downstream = 42.3 cm, Δh = 2.3 cm) but some errors were done in the measurement of the upstream and downstream levels, due to the fact that the sand-box facility is not perfectly aligned. Moreover times were not measured in a continued way because the chronometer was reset every time the tank under the spillway was filled.

Despite the fact that this test was not precise, an asymptotic trend in the test result can be pointed out, as shown in Figure 9.5. Hydraulic conductivity settles around a value equal to 1.81-1.82 $\cdot$ 10^{-3} m/s.

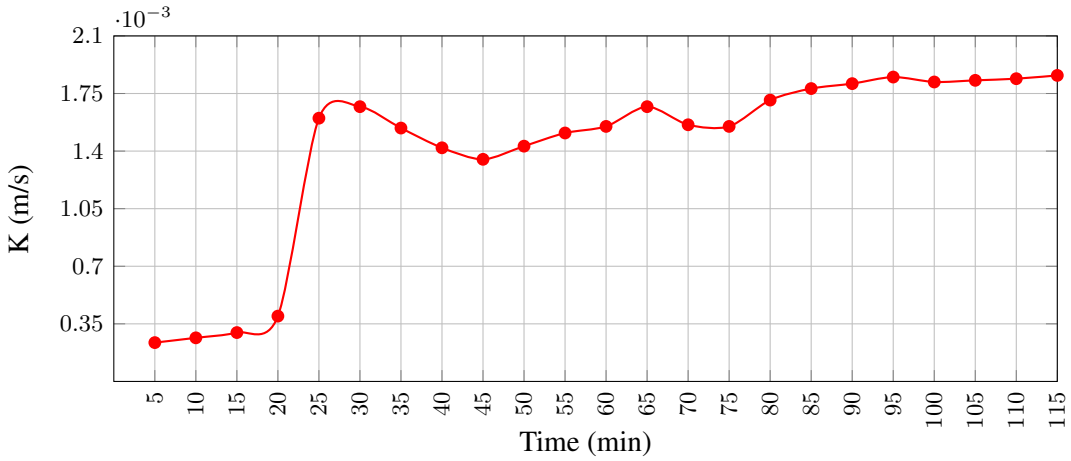

Figure 9.5. Hydraulic conductivity trend in the first constant head test

9.2.2 Second conductivity test

In the second conductivity test the hydraulic gradient was set equal to 0.0112 (Δh = 5.7 cm). The real hydraulic gradient was calculated starting from a straight line drawn manually in the

device, obtained filling the sand-box with water up to the height of the glass beads, and creating then a sort a liquid spirit level. This was done to overcome the problems deriving from the fact that the device is not aligned. Δh calculated from the spirit level is not perfectly coincident with the difference between the levels upstream and dowstream (equal respectively to 44.9 cm and 39.2 cm).

In this test the asymptotic behaviour of hydraulic conductivity in time is much more evident. The system reached the steady-state after about 1.5 h (considering as the starting time the time when the spillway began to drop). According to Figure 9.6, the hydraulic conductivity, calculated with Dupuit relationship, is about $1.81 \cdot 10^{-3}$ m/s when the steady-state was reached. The discontinuity at 80 minutes in the plot is due to an error committed by the operator while taking the measurements.

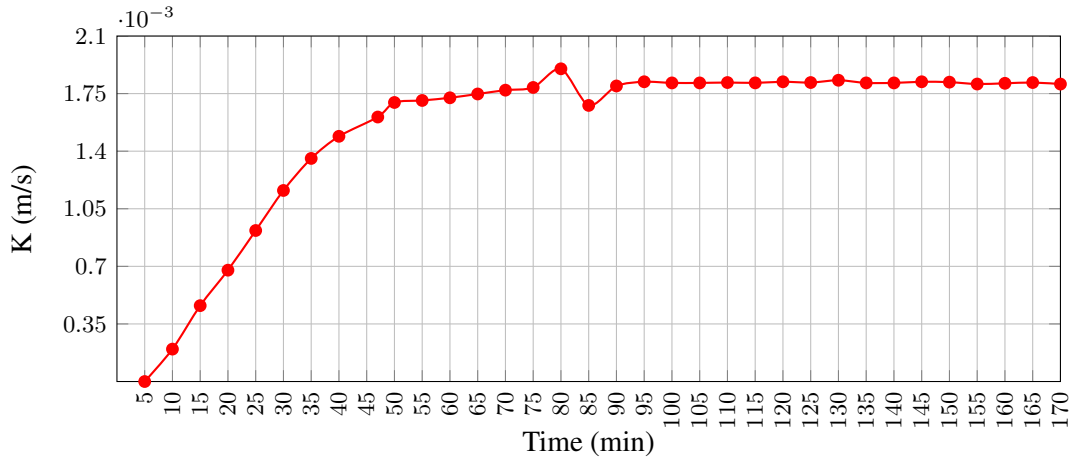

Figure 9.6. Hydraulic conductivity trend in the second constant-head test

9.2.3 Third conductivity test

In this test the hydraulic gradient was further increased and set equal to 0.0164. Upstream and downstream levels were set equal to 45.3 cm and 37.1 cm (Δh = 8.2 cm). The result is reported in Figure 9.7.

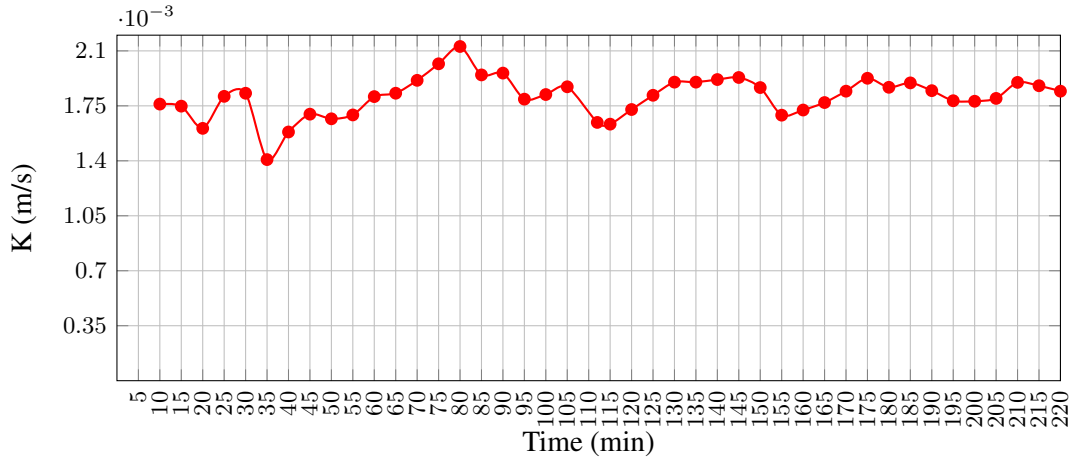

Figure 9.7. Hydraulic conductivity trend in the third constant head test

From the graph reported in Figure 9.7 it is possible to see that a stable steady-state was never reached in this case. Hydraulic conductivity continued to oscillate and never reached an asymptotic behaviour. This was probably due to the presence of a vortex above the upstream spillway (caused by the excessive hydraulic head above the bellmouth spillway) that caused an oscillation of the upstream water level (Figure 9.8).

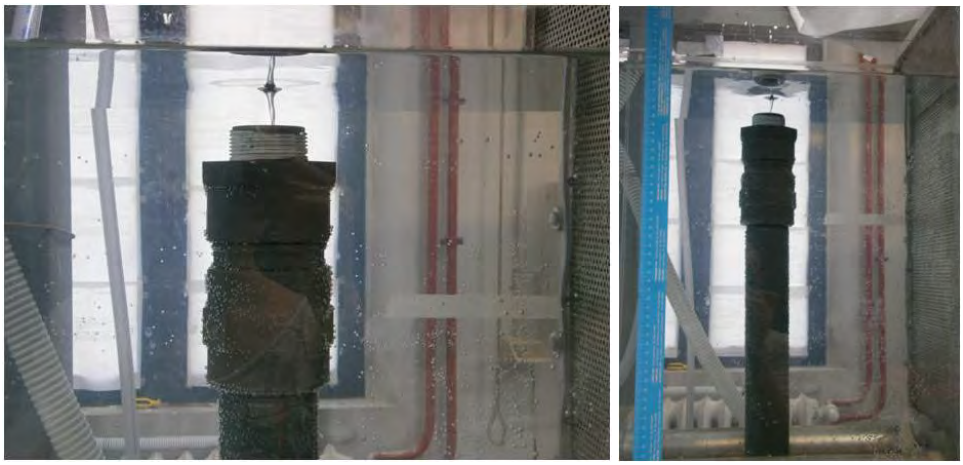

(a) (b)

Figure 9.8. Uptream hydraulic heads during the third load test

However the mobile average pointed out that hydraulic conductivity oscillates around a constant value that is equal to the hydraulic conductivity calculated in the previous tests (1.80-1.81 $\cdot 10^{-3}$ m/s), as reported in Figure 9.9.

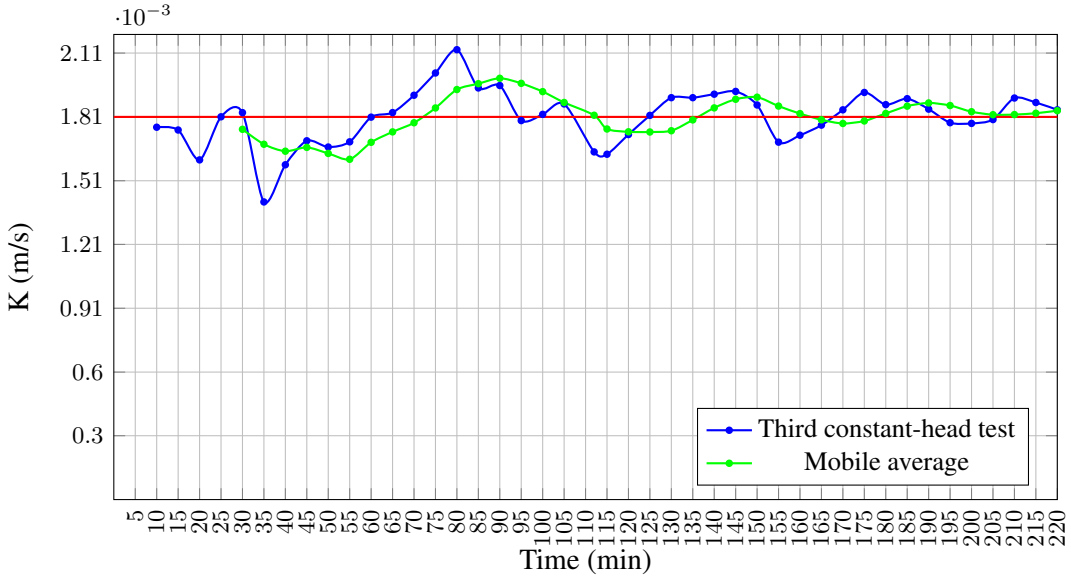

Figure 9.9. Mobile average trend of the third constant-head test

9.3 Saltwater preparation and measure of density

The volume of the smaller tank used to prepare saltwater was equal to 325 l, 4.85 smaller than the tank of the sand-box (=1575 l). 17.5 kg of salt was added in this smaller tank at the beginning. The density calculated with a graduated column (= net weight of the column divided by its volume) was equal to 1025.25 kg/m^3. This implies that 84.8 kg of salt were needed to be added in the tank ($17.5 \cdot 4.85$) in order to reach the same density in the sand-box. Since solubility of NaCl in water is 36 g of solute in 0.1 l of water, all the required quantity of salt could be dissolved in the smaller tank. It was decided to add in this tank a minor quantity of salt (75 kg) and to correct it afterwards in the bigger tank.

In Table 9.1 the densities measures taken with the graduated column are reported (as already said in Section 5.4, the measures taken with the densimeter were not reliable, so a graduated column was used to compare densities and build a calibration line).

Table 9.1. Densities of saltwater for different quantities of dissolved salt

kg of salt	Density from the graduated column [kg/m^3]
17.5	1025.5
25	1036.35
38	1058.58
50	1078.79
75	1115.71

5 kg of red food dye was then added in 325 l of saltwater. The quantity of food dye was doubled respect to that of the preliminary tests in order to increase the colour of saltwater and make more evident the transition zone.

(a) (b)

Figure 9.10. Saltwater used for the experiment prepared in the smaller tank

9.4 Results of the experiment

Hydraulic heads were set equal to 42 cm and 39.8 cm for the final experiment. According to the Dupuit equation, and assuming the hydraulic conductivity equal to $1.81 \cdot 10^{-3}$ m/s, the

expected infiltration discharge should be equal to $1 \cdot 10^{-3}$ l/s (= 3.5 l/h).

During the preparation of the sand-box experiment, the following operations were carried out:

- a sluice gate was inserted downward in order to separate the porous media and the downstream tank; this was done keeping the upstream pump turned on (during the preparation phases, no visible variations of the water level in the upstream tank were observed);
- the downstream tank was emptied of just about 475 l, that corresponded to the volume of the smaller tank that contained the brine ($\simeq$ 325 l) plus a safety threshold volume ($\simeq$ 150 l);
- saltwater previouosly prepared was pumped into the tank that was already filled with about 1100 l of freshwater;
- when all saltwater was pumped, the downstream tank was further filled with freshwater until the level of the spillway was reached;
- 10 kg of salt were added in the saltwater tank in order to obtain the desired density, continously monitored through the densimeter.

These initial preparation phases had a duration of about 50 min. The experiment, i.e. the time of saltwater intrusion, was considered to start at the moment of the remotion of the sluice gate, that divided salty water from the glass beads. Downward spillway began to drop 116 min after the remotion of the sluice gate. Spilled discharge was initially too small to be measured, so it began to be weighed only after around 10-15 minutes from this time.

During the test photos were taken every 15 minutes and the experiment was filmed for 8 hours. Saltwater intrusion, with a time step of 2 hours, is reported from Figure 9.11 to Figure 9.22. The grid, overlapped to the photos, has a size of 5 cm by 5 cm.

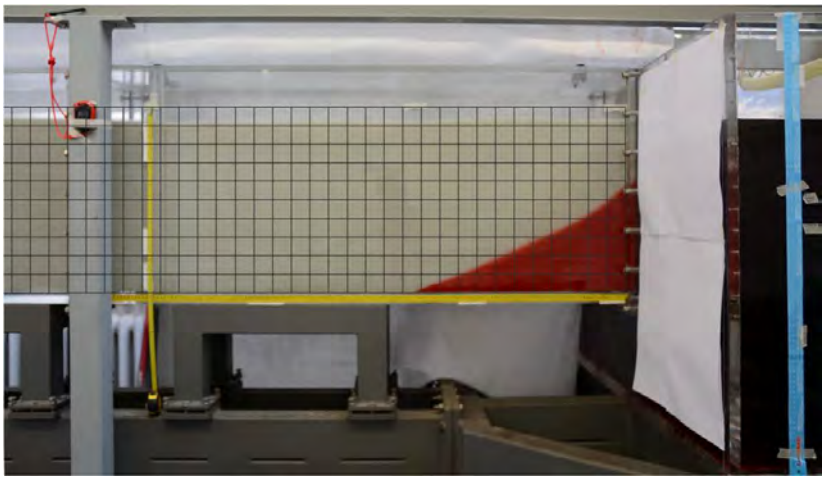

Figure 9.11. Saltwater intrusion after 2 hours

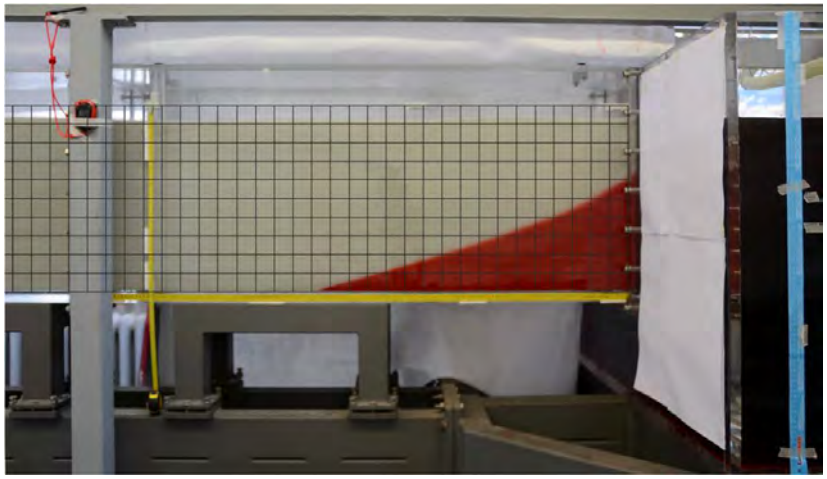

Figure 9.12. Saltwater intrusion after 4 hours

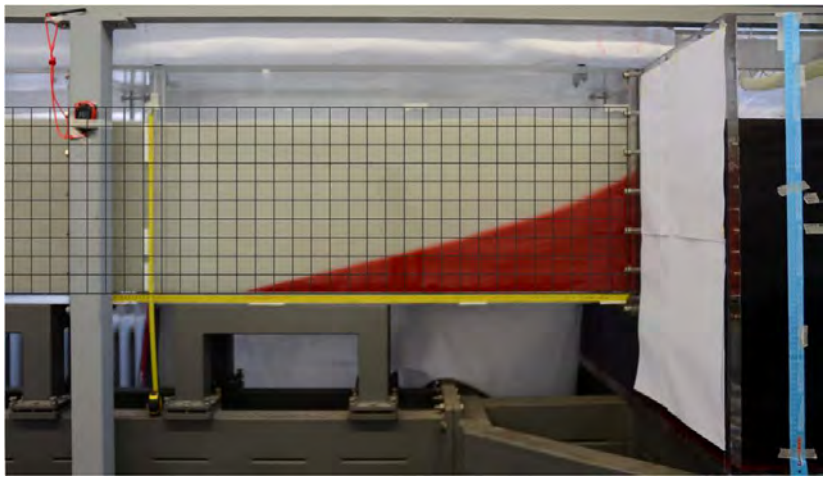

Figure 9.13. Saltwater intrusion after 6 hours

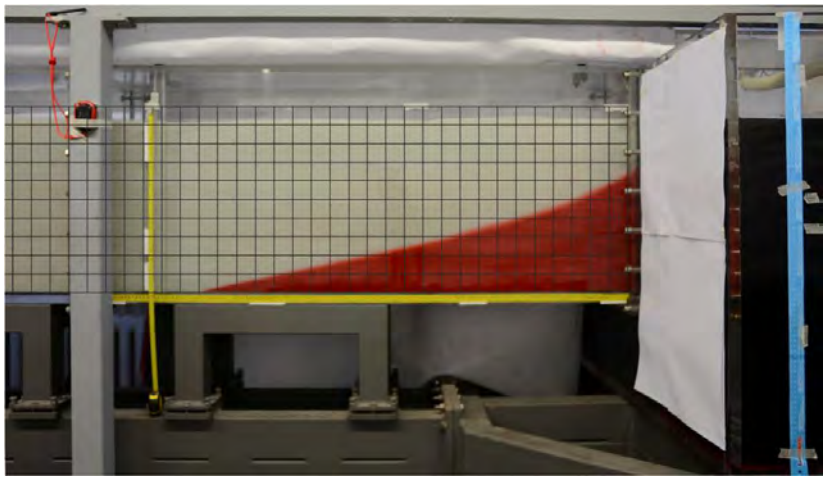

Figure 9.14. Saltwater intrusion after 8 hours

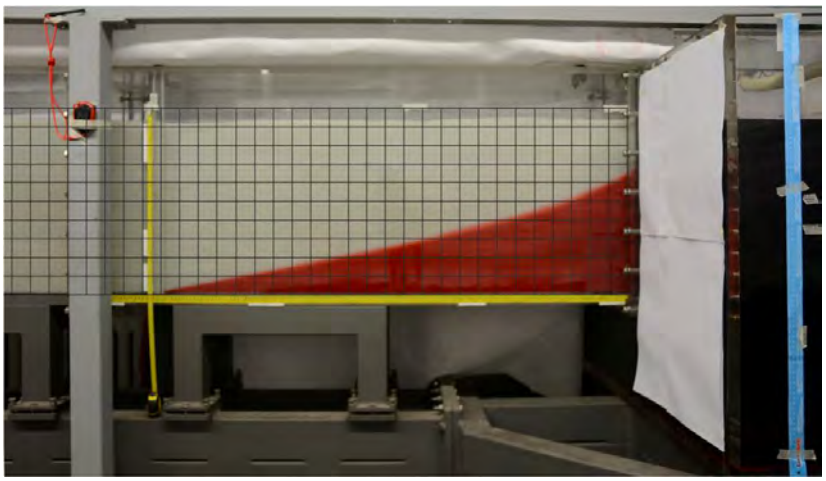

Figure 9.15. Saltwater intrusion after 10 hours

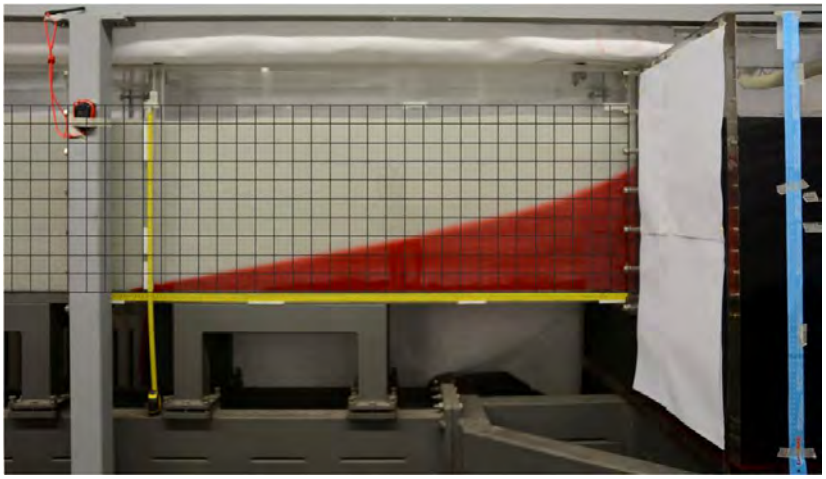

Figure 9.16. Saltwater intrusion after 12 hours

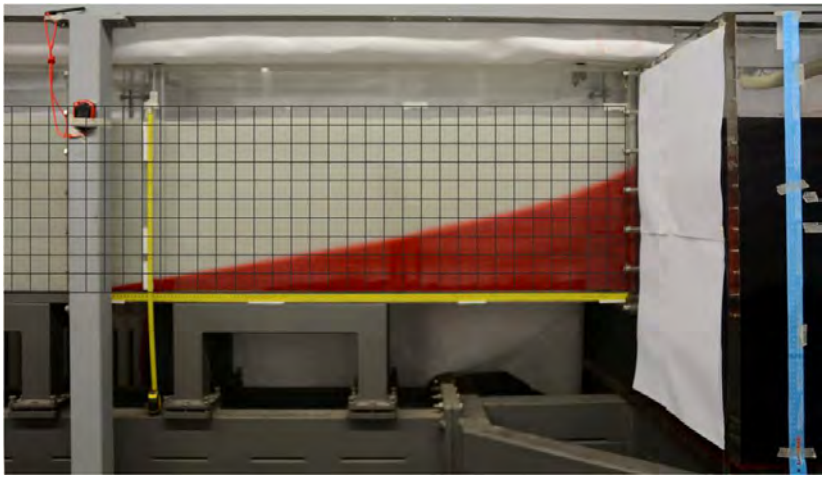

Figure 9.17. Saltwater intrusion after 14 hours

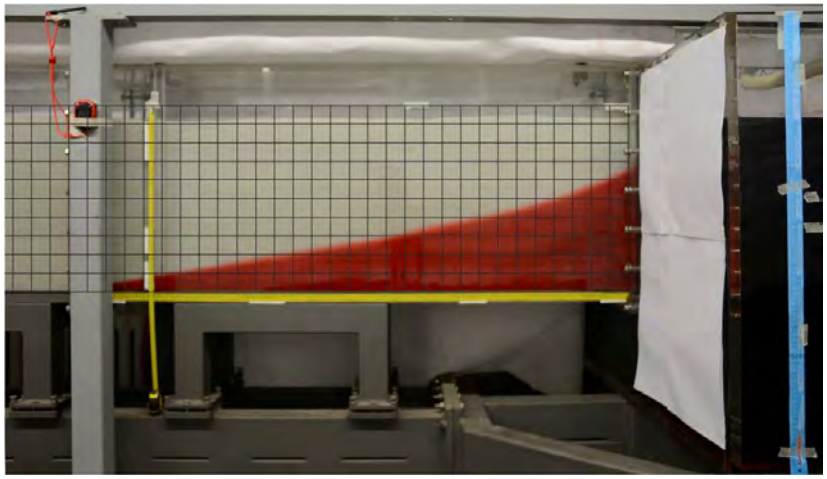

Figure 9.18. Saltwater intrusion after 16 hours

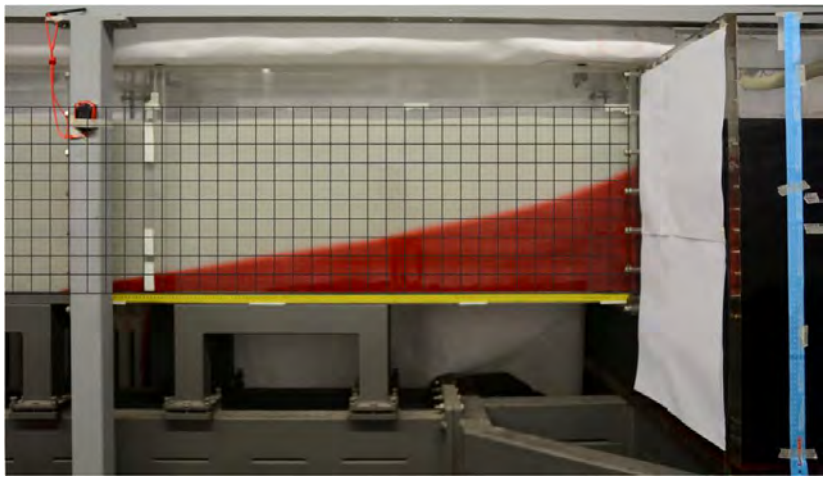

Figure 9.19. Saltwater intrusion after 18 hours

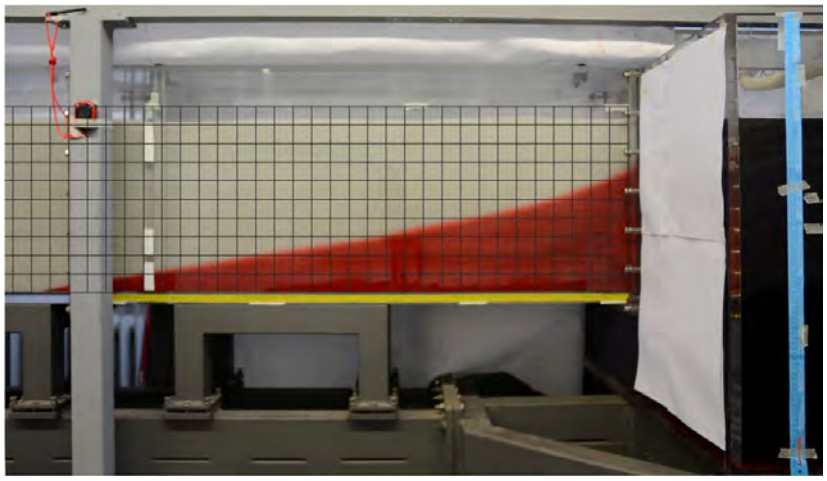

Figure 9.20. Saltwater intrusion after 20 hours

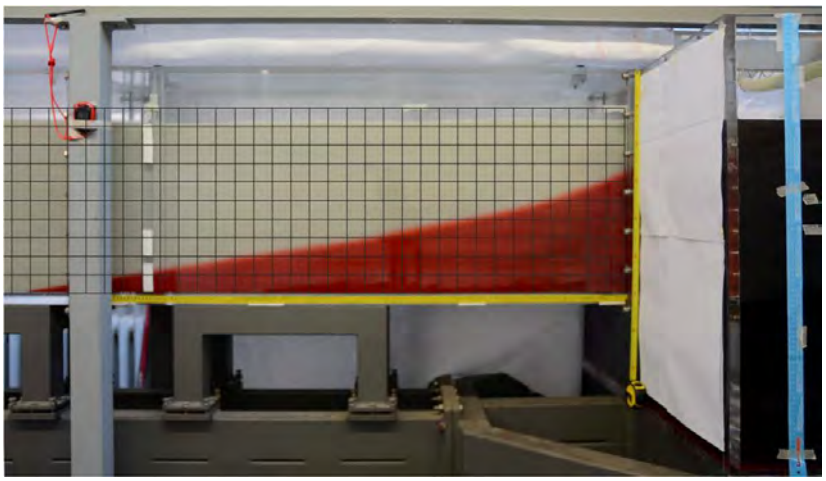

Figure 9.21. Saltwater intrusion after 22 hours

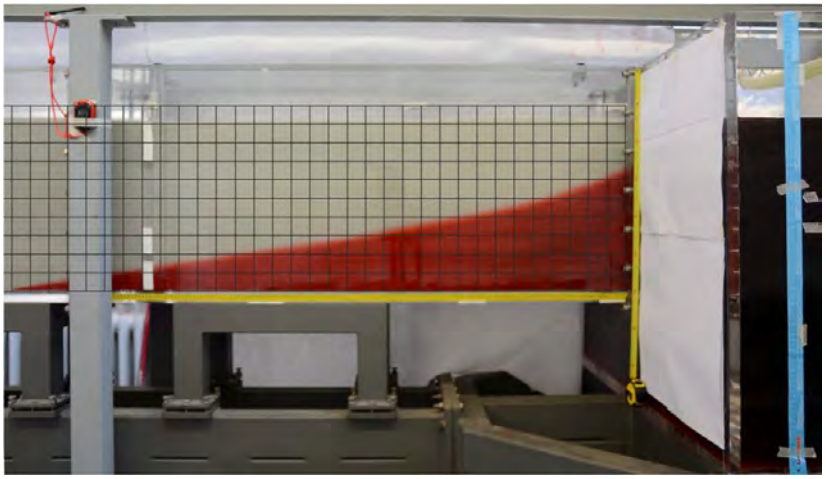

Figure 9.22. Saltwater intrusion after 24 hours

Figure 9.23 reports the spilled water weights measured every 30 minutes.

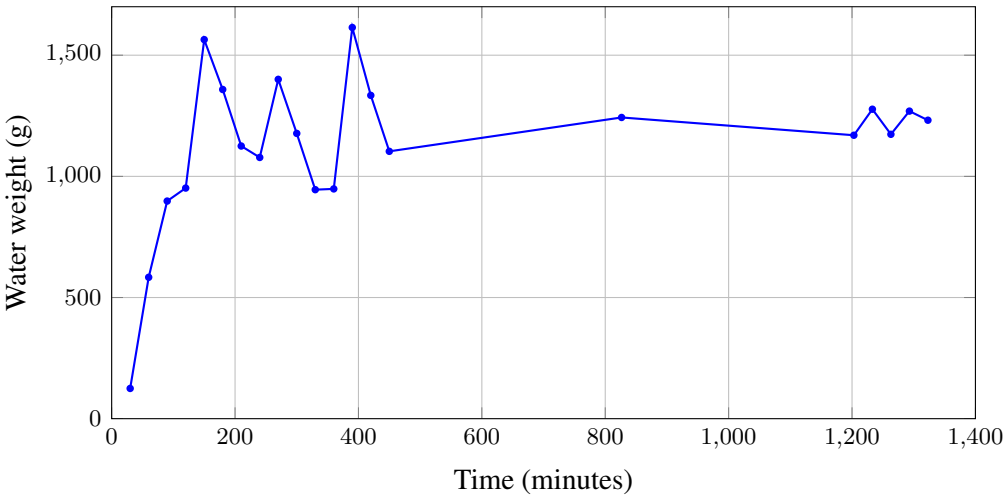

Figure 9.23. Spilled water weights in time

The net weight corresponding at the time equal to 826.5 minutes was calculated as an average value of the total spilled water during the night time (31.2 kg in 12.55 hours). Figure 9.23 points out a continuous oscillation of the spilled water weights, that reduced with time due to the fact that the system approaches the steady-state. The average value of the spilled water, that oscillated around 1.25 l/30 min, is different from the expected one calculated with the Dupuit relationship and equal to 1.75 l/30 min (about 30 % less). This is probably because, when saltwater intrusion is present, the Dupuit integration is no longer valid.

Table 9.2 reports the velocity of the moving edge (the measurements were taken from physical observations during the experiments). Velocity oscillated in time but decreased progressively approaching the steady-state.

Table 9.2. Velocity of the moving edge

Time [min]	Saltwater intrusion [cm]	Velocity of the moving edge [cm/min]
51	38	-
145	80.5	0.452
151	83	0.417
224	91	0.109
287	94.5	0.055
331	102	0.170
347	104	0.125
380	107	0.091
402	111	0.182
498	120.5	0.099
518	123	0.125
539	125	0.095
598	128.5	0.059
1300	167	0.055
1413	171	0.035

Figure 9.24 reports the lenght of the moving edge position. The trend is well approximated by the logarithmic function Y = 37.49 ln(X) - 111.28.

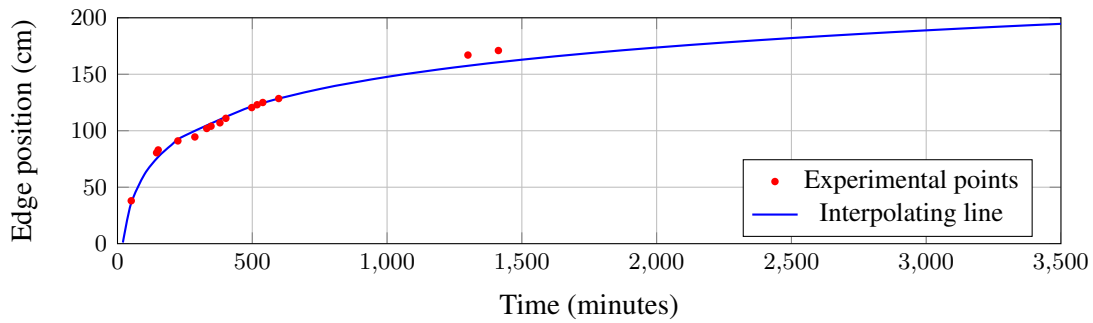

Figure 9.24. Saltwater intrusion in time

During the test some density measurements made on spilled water gave a value close to that of freshwater. Because of this some samples at different depths were taken in the saltwater tank after the experiment in order to point out the water density values along the vertical. The results, reported in Table 9.3, showed an evident increase in the saltwater density with the increase of water depth, that was probably due to a improper mixing of the salty water in the downstream tank during the preparation phases of the experiment. What may be happened is that the last freshwater used to fill the tank up to the spillway level remained above saltwater, without mixing with it, or that the saltwater pumped from the smaller tank (that, as already said, was over-salty and with a density of about 1115.71 kg/m^3), remained below freshwater that was already in the tank.

Table 9.3. Density values measured at different depths

Depth from the water surface [cm]	Density [kg/m^3]
13	1020
26	1023.18
39	1032

The values reported in Table 9.3 are probably affected by a significant error (due for example to: imprecisions of the depth value at which the samples were taken, mixing of the water due to the sampling, imprecise estimation of the volume that was weighed, the fact that the sampler was washed after every withdrawal and was not dry) but are significant in showing that there was a density gradient in the "sea" and that an unappropriate mixing occured. Note also that the densimeter measure at about 15 cm from the water surface a density equal to 1028-1029 kg/m^3.

Stratification between saltwater and freshwater was supported from the fact that the salt wedge started from about 7 cm below the level of the saltwater tank, as shown in Figure 9.4.

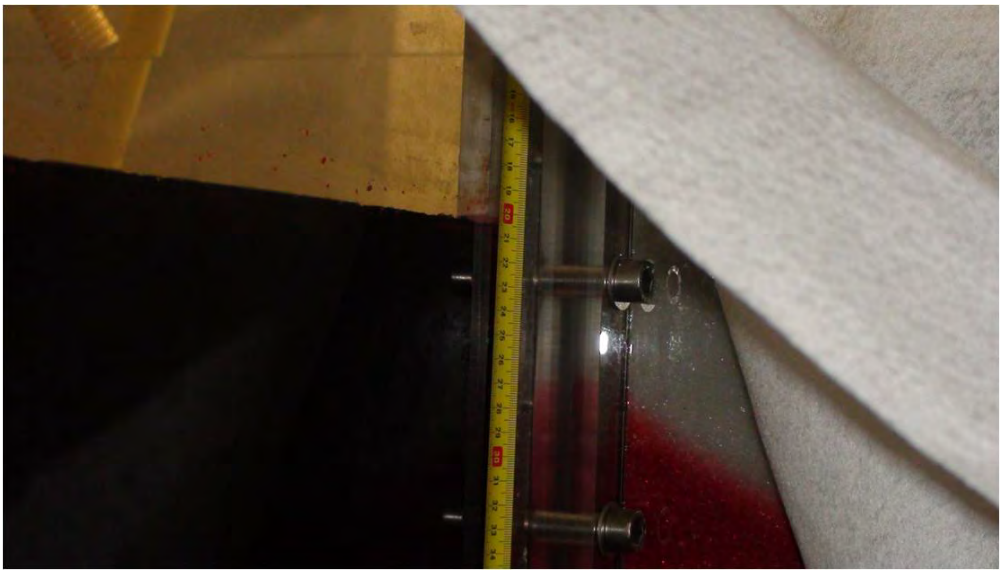

Figure 9.25. Initial part of the salt wedge, starting below the downstream level

9.5 Comparison with the numerical model

Numerical simulations were implemented in order to compare experimental and numerical results. Three sensitivity analysis were developed varying the parameters on which there was a measure uncertainty: the downward water level, the saltwater density and the position of freshwater outflow. In the first sensitivity analysis, concerning the downward water level, the pressure distribution required by the model was fixed and it was calculated by interpolation of the pressure values that derived from the densities reported in Table 9.3. A constant consistent concentration, equal to 40.78 g/l, was assumed for saltwater.

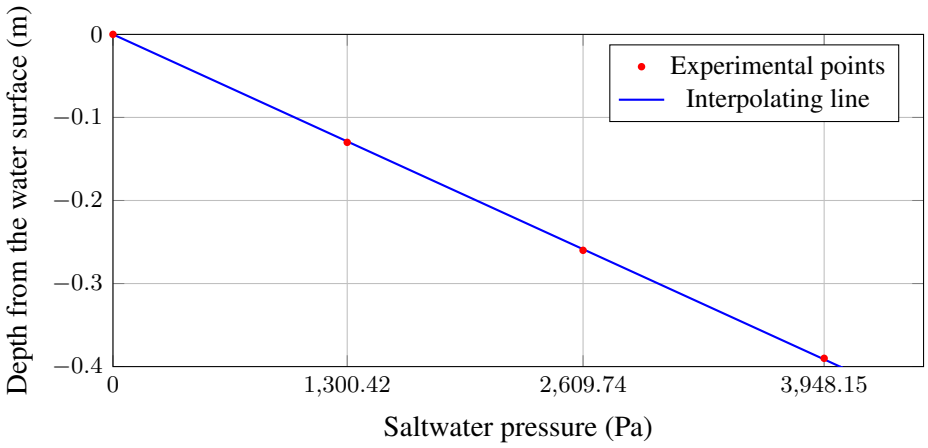

Figure 9.26. Interpolated downstream pressure distribution. Equation of the interpolating line: y = -(1/10090) · x

Since from the experimental results it was evident that the transition zone was very narrow, in the numerical model the smallest dispersivity values supported by the code, respect to the grid discretization, were set. The longitudinal dispersivity was set equal to $7.5 \cdot 10^{-4}$ m, while the transverse one was set equal to $3.75 \cdot 10^{-4}$ m. These values fall within the range suggested by Abarca and Clement (2009) [1]. The numerical instability is not eliminated at all (the error in the concentration values reached at least 2 %, that means that the code returned concentration values 2% higher respect to the maximum set) due to the fact that the mesh Peclet number criterion, reported in Section 6.3.3, is not respected (the mesh elements size is equal to 0.5 · 0.5 cm). However a further vertical discretization would imply an excessive computational time. Consequentely it was necessary to reach a compromise between low dispersivities values comparable with literature and the error committed by the code that is still accettable. Results after 24 h of simulation are reported from Figure 9.27 to Figure 9.29.

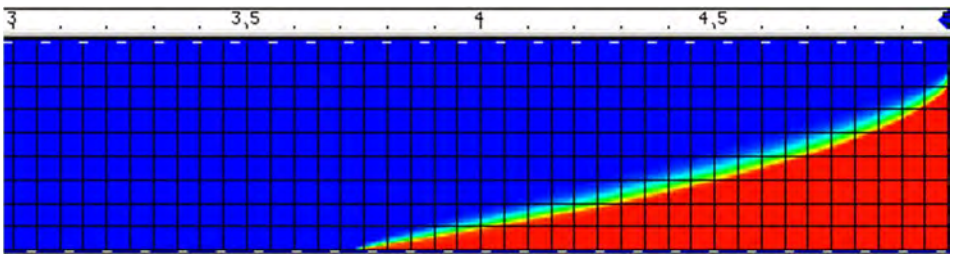

Figure 9.27. Simulation result after 24 h. Downstream level = 0.395 m

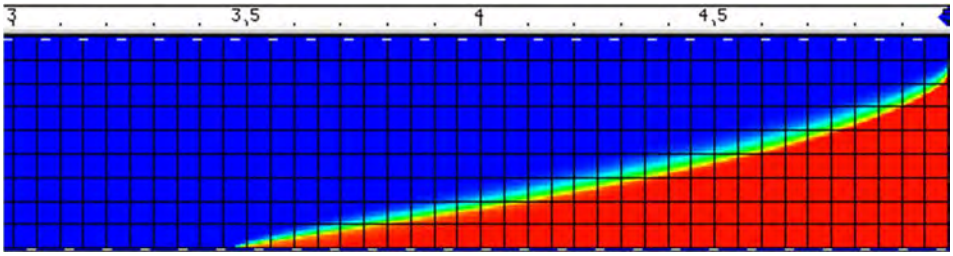

Figure 9.28. Simulation result after 24 h. Downstream level = 0.4 m

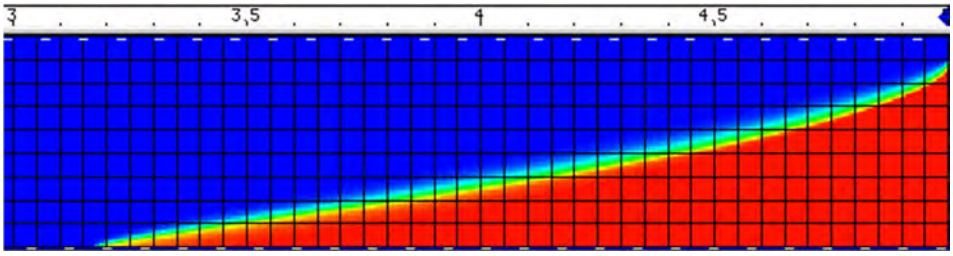

Figure 9.29. Simulation result after 24 h. Downstream level = 0.405 m

From the results of this sensitivity analysis it is evident that saltwater intrusion is strongly influenced from the downward water level. An higher downward saltwater level implies a reduced infiltration discharge and consequentely a greater saltwater intrusion. It is important for a better development of future experiments to install a more precise system of measuring for water levels, which are difficult to read visually due for example to light reflection or the operator point of view.

The second sensitivity analysis concerns saltwater density, and consequently pressure. It was assumed that a underestimation or an overestimation of 0.5 % was comitted by the operator in taking the density measures reported in Table 9.3. This would imply a different downward pressure distribution.

The interpolating line that considers an understestimated pressure is reported in Figure 9.30.

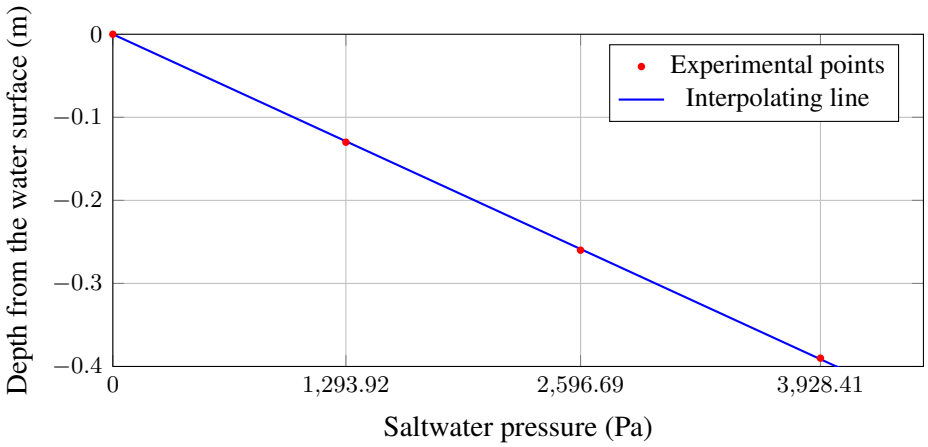

Figure 9.30. Interpolated pressure distribution that considers an underestimation of the 0.5 % in the density experimental values reported in Table 9.3. Equation of the interpolating line: y = -(1/10040) · x

The interpolating line that considers an overestimated pressure is reported in Figure 9.31.

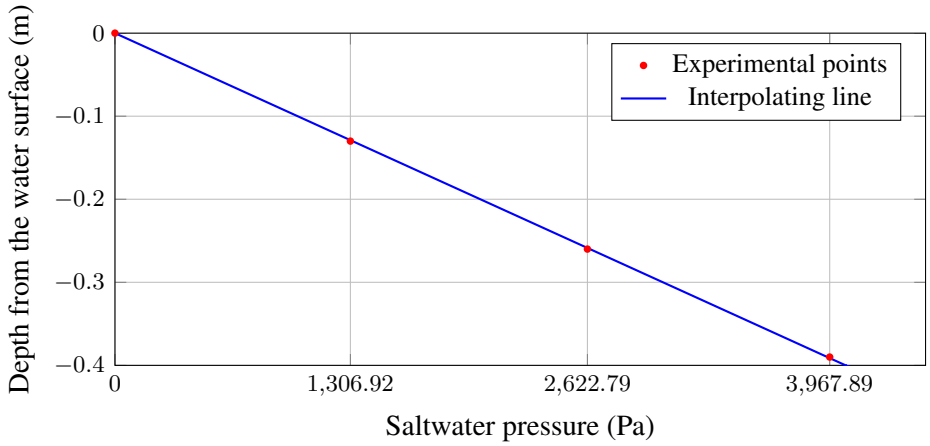

Figure 9.31. Interpolated pressure distribution that considers an overestimation of the 0.5 % in the density experimental values reported in Table 9.3. Equation of the interpolating line: y = -(1/10141) · x

A constant consistent concentration was assumed in the saltwater tank and was set equal to 33.5 g/l in the case in which an underestimated density was supposed, and 48.1 g/l in the other case. The water level downward was fixed at 40 cm.

Results of the simulation are reported in Figures 9.32, 9.33, 9.34. A strong dependence of the saltwater intrusion from the downward concentration and density was pointed out. It is reasonable that some errors could have been comitted in the density measurements reported in Table 9.3, because of the reasons reported in Section 9.4. Consequently it is likely that some dilution of samples was done and that the density was higher than the measured one.

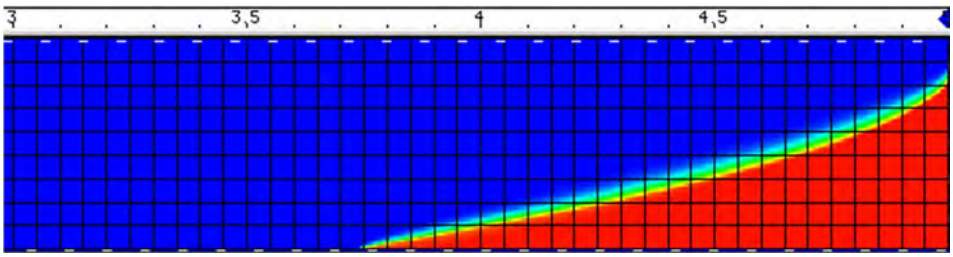

Figure 9.32. Simulation result after 24 h. Downstream level = 0.4 m. Underestimation of 0.5 % in the saltwater density reported in Table 9.3

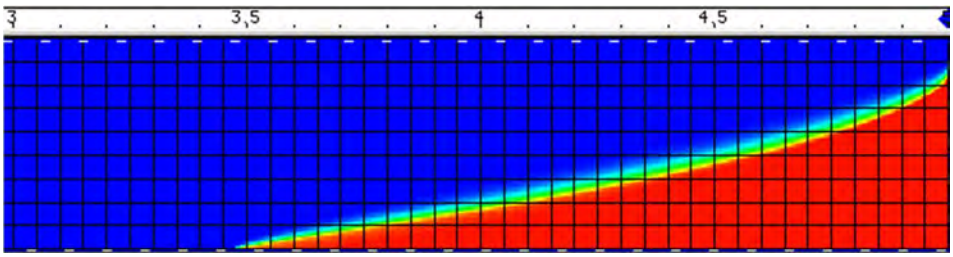

Figure 9.33. Simulation result after 24 h. Downstream level = 0.4 m. Saltwater density measured after the experiment

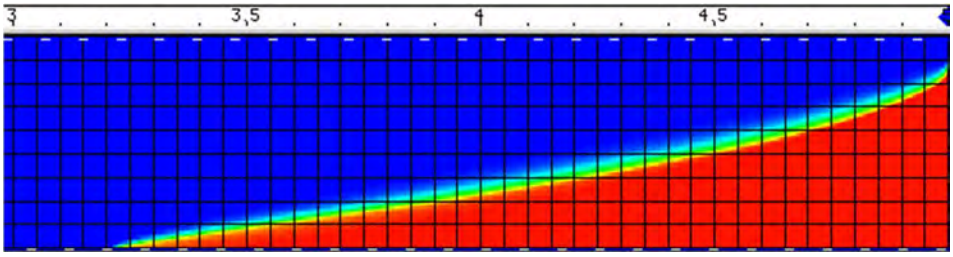

Figure 9.34. Simulation result after 24 h. Downstream level = 0.4 m. Overestimation of 0.5 % in the saltwater density reported in Table 9.3

It is evident that the interpolation of pressure previously reported is a simplification of the downward boundary conditions and implies that saltwater density and concentration are assumed to be constant and equal to an average value. As a consequence there is a significant overestimation in the pressure distribution in the first centimeters below the downward water surface, where, from the experiment, pressure appears to be hydrostatic and concentration equal to 0. Because of this, the initial part of the salt wedge given by the numerical model is not consistent with the experimental result since the salt wedge in the simulations previously reported started from the water level of the dowstream tank. In order to overcome these limitations the density measurements reported in Table 9.3 were interpolated with a polynomial curve. In this way the boundary conditions required by the model (pressure and concentration) are extracted point by point and assigned to each node downward. The equation of the interpolating line is given in terms of x values because, if the two variables are reverted, it is difficult to find a good interpolating polynomial.

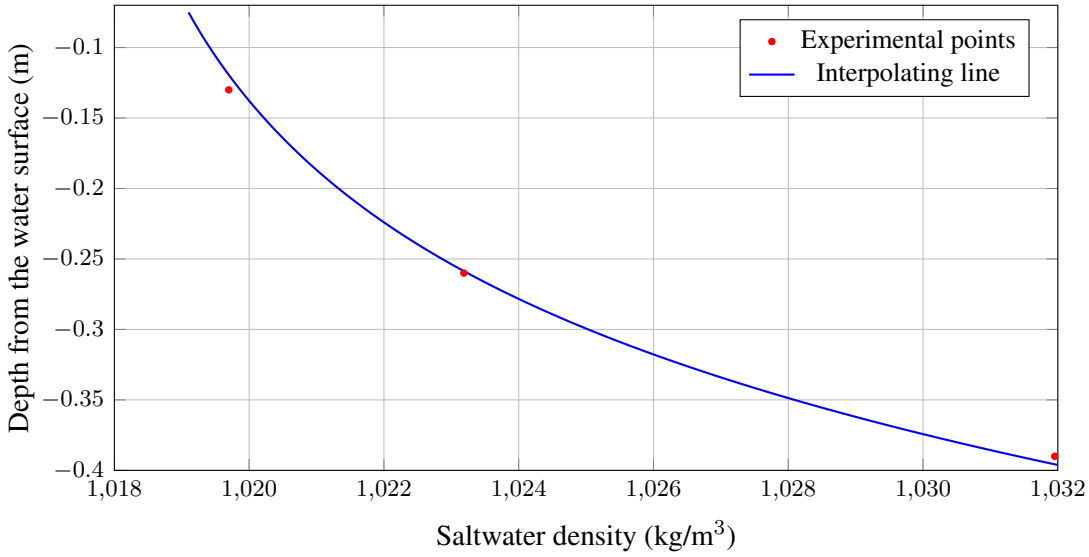

Figure 9.35. Interpolating curve of the density values. Equation of the polynomial interpolating line: x = 437.38 · y^4 +129.27 · y^3 + 57.949 · y^2 - 4.2105 · y + 1018.5

In the first 7 cm below the water level of the dowstream tank the density is assumed to be that of freshwater (1000 kg/m^3) and concentration about 0. From the densities obtained by the plot reported in Figure 9.35 it was possible to calculate the pressures for each node downstream as ($\rho \cdot g \cdot h$) and the saltwater concentration through the relationship:

$$\rho = \rho_0 + 700(C - C_0) \tag{9.1}$$

where ρ_0 and C_0 are the density and concentration of freshwater (see Section 6.1).

The dispersivities values were set equal to 0.009 m (α_L) and 0.0009 m (α_T) to avoid numerical instabilities related to the mesh Peclet number criterion (see Section 6.3.3). This implied a very spread dispersion zone but the simulation was useful in order to check how the numerical model returns the depth from which the salt wedge started.

The result of the model is reported in Figure 9.37.

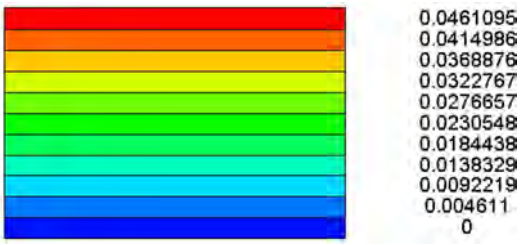

Figure 9.36. Concentration values. Results given in [kg_{solute}/$kg_{seawater}$]

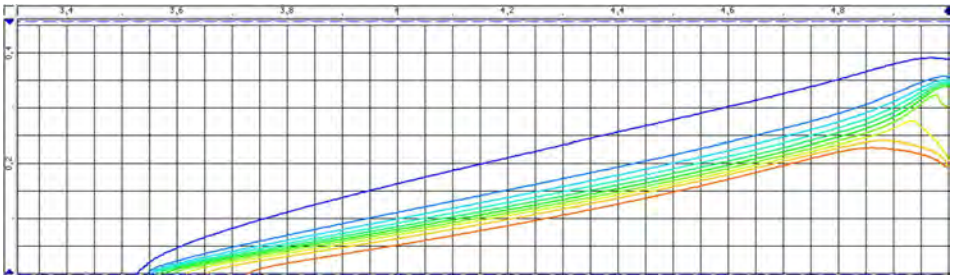

Figure 9.37. Isoconcentration lines resulting from a simulation with variable downward densities and concentrations. Simulation result after 24 h

A similar result is obtained if the downward water density and concentration are kept constant piecewise and increase along the vertical, as shown in Table 9.4 and Figure 9.38. The density value for each step was assumed to be about the average density value taken every 5 cm of depth from Figure 9.35.. In this case the pressure distribution is a non-continuous line increasing its slope as the density increases.

Table 9.4. Saltwater density and concentration kept constant piecewise and increasing along the vertical

Distance from the water surface [cm]	Density [kg/m^3]	C [g/l]
0-7	1000.00	0
7.5-15	1019.70	28.14
15.5-20	1020.70	29.57
20.5-25	1022.00	31.43
25.5-30	1023.80	34
30.5-35	1026.40	37.71
35.5-40	1030.02	42.88

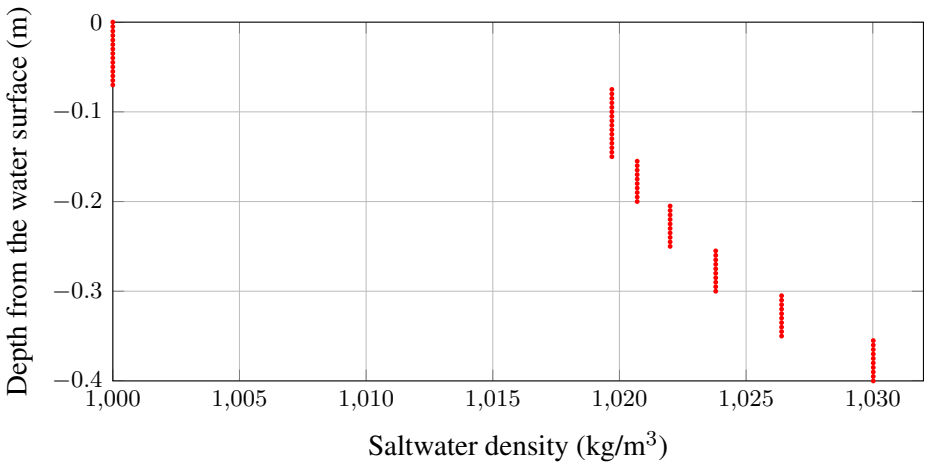

Figure 9.38. Trend of saltwater density kept constant piecewise according to Table 9.4

The numerical result in this case is reported in Figure 9.40.

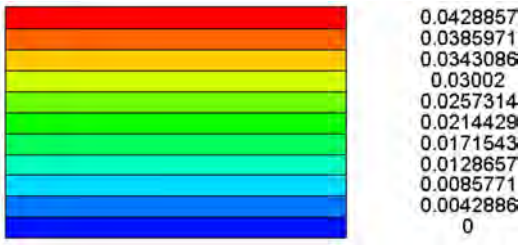

Figure 9.39. Concentration values. Results given in [kg_{solute}/$kg_{seawater}$]

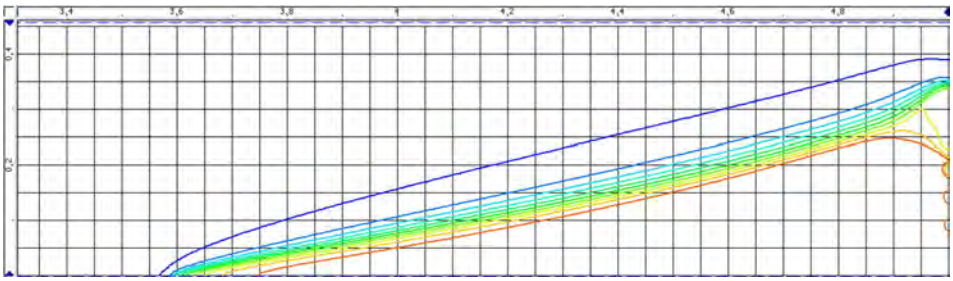

Figure 9.40. Isoconcentration lines resulting from downward densities and concentrations reported in Table 9.4. Simulation result after 24 h

Figures 9.37 and 9.40 show that the initial shape of the salt wedge is comparable with the observed one respect to the initial simulations in which density and concentration were assumed to be constant downward. However the numerical model shows an irregular behaviour in the inlet part due probably to the fact that concentration is not set constant along the vertical downward boundary. The result of the numerical model respects the concentration boundary conditions imposed downward (concentration increases with depth). Neverthless the comparison in terms of concentration with the experimental result can not be done, since the

concentration values were not taken.

A sensitivity analysis was finally performed varying the position of the freshwater outflow, that was collocated at 4.5 cm, 7 cm and 9.5 cm below the water level of the downstream tank. Saltwater density in these simulations was varied according to the curve reported in Figure 9.35. The downstream water level was set equal to 40 cm. Results are reported in Figures 9.41, 9.42, 9.43. The legend for the concentration values is the same of Figure 9.36.

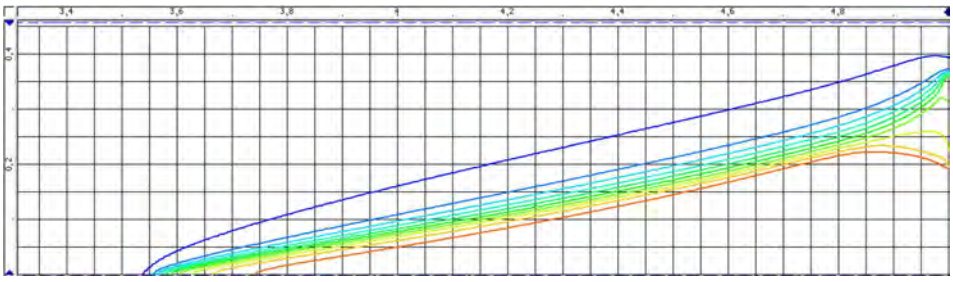

Figure 9.41. Freshwater outflow positioned at 4.5 cm from the downstream water level. Simulation result after 24 h

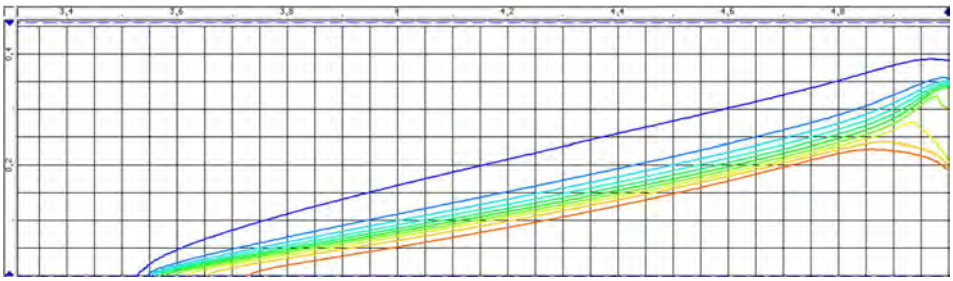

Figure 9.42. Freshwater outflow positioned at 7 cm from the downstream water level. Simulation result after 24 h

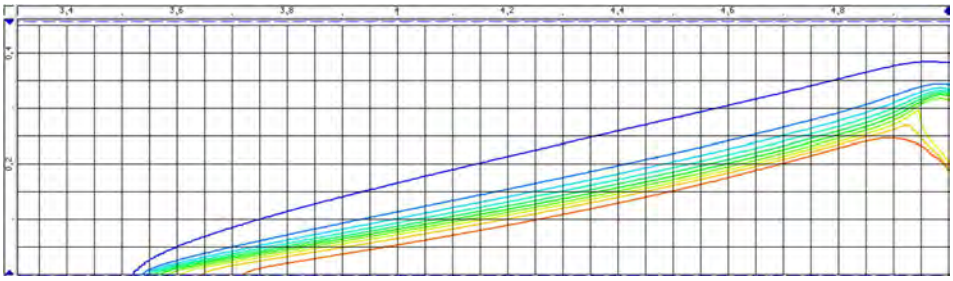

Figure 9.43. Freshwater outflow positioned at 9.5 cm from the downstream water level. Simulation result after 24 h

The results point out that the slope of the isoconcentration lines in the first part of the salt wedge decreases with the increase of the freshwater outflow depth. Anyway an error of about 35 % in the position of the freshwater outflow induces negligeble modification in the long time saltwater spatial behaviour.

9.6 Discussion of the results

The Glover relationship was implemented in order to have an estimation of the outflow face size. With reference to equation 2.11, assuming Δs equal to 0.025 and q_0 equal to the freshwater flow calculated as following:

$$q = \frac{2.5 \cdot 10^{-3}}{3600 \cdot 0.3} = 2.3 \cdot 10^{-6} \frac{m^2}{s} \tag{9.2}$$

the lenght of the discharge zone ξ_0 becomes equal to 5 cm.

Although the geometry of the experiment is not consistent with the Glover solution, the previous result points out that the discharge zone is not negligeble. Therefore the fact that the salt wedge started from below the dowstream water level is probably due not only to the density stratification.

Concerning the numerical model, the result reported in Figure 9.37, that represents the simulation in which the downstream density boundary conditions are closer to the physical experiment, shows that the lenght of the saltwater intrusion given by the model is 20 cm lower than the one measured in laboratory (150 cm versus 170 cm). This difference is surely due to the fact that the dispersivities in the numerical simulations were overstimated in order to avoid numerical instabilities related to the mesh Peclet number (see Section 6.6.3): the longitudinal dispersivity should be of the same order of magnitude of d_{50} (Goswami et al., 2007) [27], that means 0.6 mm in this case, while the dispersivities values in the numerical model were set equal to 0.009 m for α_L, and 0.0009 m for α_T. Dispersivities affect not only the width of the transition zone, but also the lenght of the salt wedge, as was evidenced in Section 8.5.

Another reason for this difference may be that the downward saltwater density was underestimated because of the causes reported in Section 9.4. The sensitivity analysis reported in Figures 9.32, 9.33 and 9.34 highlights that an increment of 0.5 % in the saltwater density implies that the lenght of the salt wedge would be around 27 cm higher (180 cm versus 153 cm, comparing Figure 9.34 with Figure 9.33).

Finally, the last sensitivity analysis highlighted that an error of about 35 % in the position of the freshwater outflow induces negligeble modifications in the long time saltwater spatial behaviour.

It must be said that the comparison between the numerical model and experimental results is hardly feasible, because of the difficulties in properly simulating the density gradient in the "sea" and because of the lack in the concentration values that prevents the comparison with the numerical results.

It is also possible that some local horizontal gradients of concentration occurred in the saltwater tank, due to the freshwater flow above saltwater.

Chapter 10

Conclusions

In many coastal aquifers, seawater intrusion has become one of the major constraints imposed on groundwater utilization. As saltwater intrusion progresses, existing pumping wells, especially those close to the coast, become saline and have to be abandoned. Also the area above the intruding seawater wedge is lost as a source of natural replenishment of the aquifer. Groundwater pollution due to saltwater affects many aquifers in the Italian coasts (i.e. Sardinia, Catania plain, the Tiber Delta, the Versilia coast, the Adriatic coast of the Po plain, the terminal parts of Brenta and Adige Rivers) as well as many other areas including North Africa, the Middle East, China, Mexico, the Atlantic and Gulf Coasts of the United States, and Southern California.

This thesis aims to reproduce an experimental model representing the longitudinal terminal part of an idealized aquifer where the porous media is uniform.

The first part of the thesis introduces the saltwater intrusion process and reports some steady-state analytical solutions useful to estimate the lenght of saltwater intrusion.

In the second part of the study the sand-box device is designed and the characteristics of the porous media used to simulate the sand are pointed out. Glass beads were found to be a good material in order to study saltwater intrusion, since they are not absorbing and allow to perform a colorimetric analysis of the problem. Moreover it was demonstrated that they can be easily washed simply by filtering freshwater.

Special attention was devoted in finding a good tracer for saltwater. Various types of tracers were tested, such as rhodamine, methylene blue, copper sulphate and food dye. Food dye resulted to be the best one since it did not show flocculation processes and allows to solve the problems associated to the coloured water disposal. Consequentely two column tests were performed using food dye and it was verified that conducibility and absorbance have the same trend, that means that the diffusion process is the same for dye and salt.

In the third part of thesis the numerical software SUTRA is applied to preliminary investigate the problem. The code resulted to be a useful tool in order to study saltwater intrusion and the parameters that affect it.

In the fourth part the setting-up (that involves filling, compaction and saturation) of the laboratory sand-box device and the results of the physical experiment are reported.

Three constant head tests in the sand-box were realized to calculate the hydraulic conductivity of the porous media, that was found to be similar to the one obtained from the preliminary tests. An experiment was completed and, after 24 hours, a semi steady-state condition was reached. The results are available in terms of photos, video and discharge measurements. According to these data, the lenght of the salt wedge resulted to be higher than the theoretical one, if compared with preliminary numerical simulations and the analytical solutions. This disagreement is probably due to a density stratification in the downward basin, caused by an improper mixing of saltwater. In fact some samples taken at different

depths in the saltwater tank allowed to point out that there was an increase along the vertical of the saltwater density. The sensitivity analysis performed with the SUTRA code showed that an increase in water density would imply an higher and faster saltwater intrusion. The full comparison between the numerical model and the experimental results is however hardly feasible because of the lack in the physical concentration values. Anyway the agreement between the general space-time behavior of the saltwater edge is consistent with the one predicted by numerical experiments.

The measured spilled discharge resulted to be 30 % lower than the expected theoretical one predicted by the Dupuit solution, maybe due to the fact that the Dupuit integration is not longer valid in the case of saltwater intrusion.

From this first experiment some developments of the sand-box device are found to be necessary for the best outcome of future tests. It was pointed out the need to install an automatic measuring system for upstream and downstream water levels, in order to reduce the uncertainty related to the hydraulic gradient. Furthermore an efficient way to mix saltwater before pumping it in the downstrem tank is necessary to avoid the formation of saltwater density gradients, that would imply uncertainties on pressure and concentration values. Also a device able to measure the spilled downstream water in a continuous way would be useful to limit the errors comitted by the operator when the tank filled with the spilled water is changed and weighed. Since a colorimetric analysis would be difficult to perform due to the light conditions of the area in which the sand-box device is placed, and since the the use of needles to collect water samples would alterate the concentration distribution in the system, a different solution may involve geophysical methods such as the electrical resistivity tomography.

The physical laboratory set-up will be used in future to study saltwater intrusion under a great number of different conditions, for example different combinations of upstream discharges and extracted freshwater, even with the presence of weirs beneath the riverbed.

Bibliography

[1] Abarca E., Clement T. P., *A novel approach for characterizing the mixing zone of saltwater*, Geophysical Research letters, vol. 36, 5 p., 2009.

[2] Ayers R. S., Westcoc D. W., *Water quality for agricolture*, Roma, FAO, 1985.

[3] Alshawabkeh A. N., Reddy K. R., Khire M. V., *Geocongress 2008. Characterization, monitoring and modeling of geosystem*, Virginia, ASCE Publications, 2008.

[4] Barlow P. M., *Groundwater in freshwater-saltwater environments of the Atlantic Coast. Circular 1262*, USGS, 2003.

[5] Barlow P. M., Reichard E. G., *Saltwater intrusion in coastal regions of North America*, Hydrogeology Journal, 18, p. 247-260, 2010.

[6] Bear J., *Dynamics of fluids in porous media*, New York, American Enselvier, 1972.

[7] Bear J., *Hydraulics of groundwater*, New York, McGraw-Hill, 1979.

[8] Benekos I. D., Cirpka O. A., Kitanidis P. K., *Experimental determination of transverse dispersivity in a helix and a cochlea*, Water Resour. Res., 42, 7 p. 2006.

[9] Dam, J. C. van, *Exploitation, restoration and management*, In: Bear J., Cheng A.H.-D., Sorek S., Ouazar D., Heerera I., *Seawater intrusion in coastal aquifers-Concepts, methods and practices*, Netherlands, Kluver Academic Publisher, 1999.

[10] Bear J., Cheng A. H. -D., Sorek S., Ouazar D., Herrera I., *Seawater intrusion in coastal aquifers* In: *Theory and applications of transport in porous media*, Dordrecht/Boston/London, Kluwer Academic Publishers, 1999.

[11] Bogoni M., *Analisi numerica dell' intrusione del cuneo salino alla foce del Fiume Adige con il modello F. V. Shock*, Tesi di Laurea magistrale, Padova, 2013.

[12] Carbognin L., Rizzetto F., Tosi L., Teatini P., Gasparetto Stori G., *L'intrusione salina nel comprensorio lagunare veneziano. Il bacino meridionale*, Giornale di Geologia Applicata 2, p. 119-124, 2005.

[13] Chow V. T., *Handbook of applied hydrology*, New York, McGraw-Hill, 1964.

[14] Cheng A. H.-D., Ouazar D., *Analytical solutions* In: Bear J., Cheng A.H.-D., Sorek S., Ouazar D., Heerera I., *Seawater intrusion in coastal aquifers-Concepts, methods and practices*, Netherlands, Kluver Academic Publisher, 1999.

[15] Consorzio di Bonifica Adige-Euganeo, *Progetti per lo sbarramento antisale sul Fiume Brenta in comune di Chioggia*, 2013.

[16] Consorzio di bonifica Delta-Po-Adige, *Progetto di bacinizzazione dell'ansa di Porta Vaccari, alla foce del Po di Pila, in comune di Porto Tolle (Ro), per la creazione di un invaso di acqua dolce ai fini irrigui da utilizzare nei periodi di forte risalita del cuneo salino*, Taglio di Po, 2008.

[17] D. L. 2 febbraio 2001, nr. 31, *Attuazione della direttiva 98/83/CE relativa alla qualità delle acque destinate al consumo umano*.

[18] D. L. 3 aprile 2006, nr. 152, *Norme in materia ambientale*.

[19] Dagan G., Bear J., *Solving the problem of local interface upconing in a coastal aquifer by the method of small perturbations*, Journal of hydraulic research, vol. 1, p. 15-44, 1968.

[20] Darvini G., *Dispersion phenomena and uncertainty in naturally heterogeneous porous media*, Tesi di Dottorato, Università Politecnica delle Marche, 2004.

[21] Fetter C. W., *Position of the saline water interface beneath oceanic islands*, Water Resour. Res. 8, p. 1307-1314, 1972.

[22] Freeze R. A., Cherry J. A., *Groundwater*, New York, Prentice-Hall, 1979.

[23] Frippiat C. C., Perez P. C., Holeyman A. E., *Estimation of laboratory-scale dispersivities using an anulus-and-core device*, Journal of Hydrology, 362, p. 57-68, 2008.

[24] Gingerich SB, Voss C. I., *Three-dimensional variable-density flow simulation of a coastal aquifer in southern Oahu, Hawaii, USA*, Proceedings of 17th Salt Water Intrusion Meeting (SWIM-17), Delft University of Technology, Delft, The Netherlands, p. 93-103, 2002.

[25] Ghyben H. W., *Nota in verband met de voorgenomen Putboring Naby*, The Hague, Tydyschrift van het Koninkhyk Institute van Ingenieurs, Amsterdam, 21 p., 1888.

[26] Glover R. E., *The pattern of freshwater flow in a coastal aquifer*, Journal of Geophysical Research: 64, p. 457-459, 1959.

[27] Goswami R. R., Clement T. P., *Laboratory scale investigation of saltwater intrusion dynamics*, Water Resour. Res., W04418, doi: 10.1029/2006WR005151, 2007.

[28] Gualbert H.P., *Density Dependent Groundwater Flow*, Utrecht University, Interfaculty Centre of Hydrology Utrecht, Institute of Earth Sciences, Department of Geophysics, online publication, 2001.

[29] Hazen A. *Some physical properties of sands and gravels*, Massachusetts State Board of Health, Annual Report, p. 539-556, 1982.

[30] Herzberg B., *Die Wasserversorgung einiger Nordsubader, Munch*, J. Gasbelenchtung und Wasserversorgung, V. 44, 815 p., 1901.

[31] Hilton H. Cooper, Jr. Francis A. Kohout, Harold R., Henry, Robert E. Glover, *Seawater in coastal aquifers*, Geological Survey water-supply paper 1613-G, USGS, 1964.

[32] Javadi A. A., Abd-Elhamid, *A cost-effective method to control saltwater intrusion in coastal aquifers*, Water Resources Management, 25, p. 2755-2780, 2011.

[33] Koch M., Zhang G., *Numerical simulations of groundwater flow and solute transport by means of the SUTRA model*, report of the Florida Department of Environmental Regulation, 118 p., 1990.

[34] Lusczynski N. J., *Head and flow of groundwater of variable density*, Journal of Geophysical Research: 66, p. 4247-4256, 1961.

[35] Missimer T. M., Ghaffour N., Dehwah A. H. A., Rachman R., Maliva R. G., Amy G., *Subsurface intakes for seawater reverse osmosis facilities: capacity limitation, water quality improvement, and economics*, Journal of Desalination, Vol. 322, p. 37-51, 2013.

[36] Muskat M., *The flow of homogeneous fluids through porous media*, J. W. Edwards, Inc. second edition, p. 480-506, 1946.

[37] Mualem Y., *A new model for predicting the hydraulic conductivity of unsaturated porous media*, Water Resour. Res., 12, p. 513-522, 1976.

[38] Nasab A. A., Boufadel M. C., Li H., Weaver J. W., *Saltwater flushing by freshwater in a laboratory beach*, Journal of Hydrology, 386, p. 1-12, 2009.

[39] Pool M., Carrera J., *A correction factor to account for mixing in Ghyben-Herzberg and critical pumping rate approximations of seawater intrusion in coastal aquifers*, Water Resources Research, Wiley Online Library, 2011.

[40] Provost A. M., Voss C. I., Neuzil C. E., *Glaciation and regional groundwater flow in the Fennoscandian shield*, Swedish nuclear power inspectorate SKI report 96:11, Stockholm, Sweden, 82 p., 1998.

[41] Reilly T. E., Goodman A. S., *Quantitative analysis of saltwater-freshwater relationships in groundwater system - A historical perspective*, J. Hydrol. 80, p. 125-160, 1985.

[42] Salandin P., *Primi risultati di un metodo d'integrazione mista in un modello di filtrazione agli elementi finiti*, Atti del XXI Convegno di Idraulica e Costruzioni idrauliche, p. 461-477, Maggioli Editore, 1988.

[43] Schmorak S. Mercado A.,*Upconing of freshwater-seawater interface below pumping wells, field studies*, Water Resources Res., Vol. 5, no. 6, p. 1290-1311, 1969.

[44] Sriapai T., Walsri C., Phueakphum D., Fuenkajor K., *Physical model simulations of seawater intrusion in unconfined aquifer*, Songklanakarin J. Sci. Technol.: 34, p. 679-687, 2012.

[45] Todd D. K., *Groundwater Hydrology*, New York, John Wiley & Sons Inc., 1976.

[46] Van Genuchten M. T., *A closed-form equation for predicting the hydraulic conductivity of unsaturated soils*, Soil Sci. Soc. Am. J., 44,p. 892-898, 1980.

[47] Voss C. I., *A finite element simulation model for saturated-unsaturated fluid density dependent groundwater flow with energy transport or chemically reactive single species solute tranport*, U. S. Geological Survey Water Resources Investigations Report 84-4368, 409 p., 1984.

[48] Voss C. I., Provost A. M., *Sutra: a model for saturated-unstaturated, variable density groundwater flow with solute or energy transport*, Reston, Virginia, 2010.

[49] Voss C. I., *USGS Sutra code-History, practical use and application in Hawaii*, In: *Theory and applications of transport in porous media*, Dordrecht/Boston/London,Kluwer Academic Publishers, p. 249-313, 1999.

[50] Wagner J., Douglas C. K., *Upconing of saltwater-freshwater interface below a pumping well*, OWRRI technical report, 1982.

[51] Werner A. D., Jakovovic D., Simmons C. T., *Experimental observations of saltwater up-coning*, Journal of Hydrology, 373, p. 230-241, 2009.

[52] Xu M., Eckstein M., *Statistical analysis of the relationsphips between dispersivity and other physical properties of porous media*, Hydrogeology Journal, vol. 5, n. 4, 1997.

[53] www.citywestwater.com

[54] daliformgroup.wordpress.com

[55] desertificazionemediterraneo.wordpress.com

[56] www.jan.ucc.nau.edu

[57] www.vicenzanatura.com

[58] www.image.unipd.it/labidra/